



TECHNISCHE
UNIVERSITÄT
WIEN
Vienna University of Technology

GEOWISSENSCHAFTLICHE MITTEILUNGEN

Heft Nr. 99, 2016

**Influence of GPS satellite orbits and
clock corrections on the estimation of
single difference uncalibrated phase delays**

Fabian Hinterberger

Veröffentlichung des Departments für Geodäsie und Geoinformation
ISSN 1811-8380

Schriftenreihe der Studienrichtung VERMESSUNG UND GEOINFORMATION



TECHNISCHE
UNIVERSITÄT
WIEN
Vienna University of Technology

GEOWISSENSCHAFTLICHE MITTEILUNGEN

Heft Nr. 99, 2016

Influence of GPS satellite orbits and clock corrections on the estimation of single difference uncalibrated phase delays

Fabian Hinterberger

Veröffentlichung des Departments für Geodäsie und Geoinformation
ISSN 1811-8380

Schriftenreihe der Studienrichtung VERMESSUNG UND GEOINFORMATION

2016

Published by the Department of Geodesy and Geoinformation
of the Vienna University of Technology
Gußhausstraße 27-29
1040 Vienna, Austria

Responsible for this issue: Univ.-Prof. Dipl.-Ing. Dr.techn. Johannes Böhm
Printed by: Grafisches Zentrum HTU GmbH

The digital version of the full document with colored figures is available online at:
<http://katalog.ub.tuwien.ac.at/AC13382775>
or
<http://resolver.obvsg.at/urn:nbn:at:at-ubtuw:1-8968>

Die Kosten für den Druck wurden vom Department für Geodäsie und Geoinformation
übernommen.

Diese Arbeit wurde an der Fakultät für Mathematik und Geoinformation der Technischen
Universität Wien zur Erlangung des akademischen Grades eines Doktors der technischen
Wissenschaften eingereicht.

Begutachter:

Ao. Univ. Prof. Dipl.-Ing. Dr. techn. Robert Weber
Department für Geodäsie und Geoinformation der Technischen Universität Wien
Gußhausstraße 27-29, 1040 Wien, Österreich

Univ. Prof. Dipl.-Ing. Dr.techn. Markus Rothacher
Departement Bau, Umwelt und Geomatik der ETH Zürich
Robert-Gnehm-Weg 15, 8093 Zürich, Schweiz

Tag der mündlichen Prüfung: 15.11.2016

Auflage: 20 Stück

ISSN 1811-8380

Prüfungssenat:

**Univ.-Prof. Dipl.-Ing. Dr.techn. Johannes Böhm
Technische Universität Wien**

**Ao. Univ.-Prof. Dipl.-Ing. Dr.techn. Robert Weber
Technische Universität Wien**

**Univ. Prof. Dipl.-Ing. Dr.techn. Markus Rothacher
ETH Zürich**

Danksagung

Zu Beginn dieser Arbeit möchte ich mich besonders bei meinem Betreuer Prof. Dr. Robert Weber bedanken. Er hat mich zu dieser Dissertation motiviert und mir die Zeit und auch den Freiraum gegeben sie nach meinen Vorstellungen zu entwickeln. Dabei ist er mir immer mit seiner freundlichen Art zur Seite gestanden und hat sich stets Zeit für Anregungen und Verbesserungsvorschlägen genommen.

Außerdem möchte ich mich bei Prof. Dr. Markus Rothacher für die Zweitbegutachtung meiner Arbeit bedanken. Ich bin dankbar für das Interesse, sowie die zahlreichen, hilfreichen und präzisen Kommentare zu dieser Arbeit.

Ein großer Dank gilt meinen Kollegen der Forschungsgruppe Höhere Geodäsie für die Hilfsbereitschaft und die tolle Arbeitsatmosphäre. Ein besonderer Dank gilt meinem Zimmerkollegen Dipl. Ing. Gregor Möller. Die zahlreichen anregenden und spannenden Diskussionen dienten mir stets als Inspiration.

Zu guter Letzt möchte ich mich ganz aufrichtig bei meiner Lebensgefährtin Simone, meiner Familie und meinen Freunden für ihre Liebe, Unterstützung und Geduld bedanken. Ein besonderer Dank gilt meiner Tante Hermi für ihren Zuspruch und Hilfe in so manch schwierigen Lebenssituationen.

Abstract

In recent years an increased tendency for using real-time observation data for a precise point positioning by means of global navigation satellite systems has emerged in the field of position and navigation. Especially the principle of Precise Point Positioning (PPP) has become a well established technique for the determination of the position in real-time. By using undifferenced code and phase observations in combination with precise satellite orbits and clock corrections, positions in the range of a couple of centimeters can be obtained. Additional effects which must be considered are the influence of the ionosphere and troposphere, relativistic effects as well as a number of additional effects of small scale. However, despite of these models and corrections, it is still not possible to fix the ambiguities in PPP. This is why the ambiguities are estimated as float values in the conventional approach, which implicates an increased convergence time as well as a decreased position accuracy.

Within the scope of this thesis the conventional PPP error model will be extended by additional fault effects. Fault effects, which have been not taken into account so far, are the so-called UPDs (uncalibrated phase delays), which are the missing link for fixing the ambiguities. In the past years different approaches for the calculation of these UPDs have been developed. In the course of this thesis a software for the calculation of the UPDS from network data was constructed. A primary feature of this software is the possibility to estimate the UPDs in a real-time simulation mode. This mode allows for investigations on the influence of different errors by means of a real-time conformal estimation of the UPDs, which are a main issue of this thesis. It can be proofed that these parameters have significant a influence on the estimation of the UPDs but on the other hand in real-time they are only available with limited accuracy.

Kurzfassung

In den letzten Jahren zeigt sich auf dem Gebiet der Positionierung und Navigation mit Hilfe globaler Satellitennavigationssysteme (GNSS) immer mehr die Tendenz Echtzeitbeobachtungsdaten für die präzise Einzelpunktbestimmung einzusetzen. Dabei hat sich im Speziellen das Prinzip des Precise Point Positioning (PPP) als alternative Technik für die Positionsbestimmung in Echtzeit etabliert. Dabei werden undifferenzierte Code- und Phasenbeobachtungen eines Empfängers in Kombination mit präzisen Satellitenbahnen und -uhrkorrekturen für eine Positionsbestimmung im cm-Bereich verwendet. Weitere zu berücksichtigende Fehler sind der Einfluss der Ionosphäre und der Troposphäre, relativistische Effekte sowie eine Vielzahl weiterer Effekte von geringer Größenordnung. Allerdings ist mit Hilfe der genannten Modelle und Korrekturen eine Fixierung der Mehrdeutigkeiten in PPP nicht möglich. Aus diesem Grund werden in herkömmlichen PPP Ansätzen die Mehrdeutigkeiten als Gleitkommazahlen geschätzt, was eine erhöhte Konvergenzzeit sowie eine reduzierte Positionsgenauigkeit zur Folge hat.

Im Zuge dieser Dissertation wird daher das klassische Fehlermodell von PPP um weitere Fehlerinflüsse erweitert. Eine bisher unberücksichtigte Fehlerquelle sind die sogenannten UPD's (uncalibrated phase delays) welche das fehlende Bindeglied für eine Fixierung der Mehrdeutigkeiten darstellen. In den vergangenen Jahren wurden verschiedene Ansätze für die Berechnung dieser UPDs entwickelt. Im Rahmen dieser Arbeit wurde, basierend auf einem dieser Ansätze, eine Software für die Berechnung der UPDs erstellt. Ein wesentliches Merkmal dieser Software ist die Möglichkeit die UPDs in einem simulierten Echtzeitmodus zu berechnen. Dieser Modus erlaubt den Einfluss verschiedener Fehler an Hand einer Echtzeitgetreuen Berechnung der UPDs zu untersuchen. Neben der Entwicklung der Software stellen detaillierte Untersuchungen über den Einfluss von Satellitenorbit und -uhrkorrekturen einen Schwerpunkt dieser Arbeit dar. Diese Parameter haben einen wesentlichen Einfluss auf die Schätzung der UPDs, stehen in Echtzeit aber nur mit begrenzter Genauigkeit zur Verfügung.

Contents

List of Figures	xv
List of Tables	xxi
Acronyms	xxiii
1 Introduction	1
2 Global Navigation Satellite Systems	3
2.1 Principle of satellite-based positioning	3
2.2 Coordinate systems	4
2.2.1 Conventional celestial reference system	5
2.2.2 Conventional terrestrial reference system	5
2.2.3 The local-level system	6
2.2.4 The satellite-fixed coordinate system	7
2.2.5 Coordinate transformation	7
2.3 Time systems	9
2.4 The Global Positioning System GPS	10
3 The International GNSS Service (IGS)	13
3.1 IGS Real-Time Service	15
3.2 The RTCM Standard	17
4 Precise Point Positioning PPP	19
4.1 Observation model	20
4.2 Integer ambiguity resolution	22
4.2.1 Methods for integer ambiguity resolution in PPP	23
4.2.1.1 Phase recovery from fractional parts	24
5 The software PPP Post	29
5.1 Data source segment	30
5.1.1 Observation data	31
5.1.2 Orbit data	31

5.1.2.1	Broadcast ephemerides and IGS real-time corrections	32
5.1.2.2	Precise ephemerides	34
5.1.3	Additional data sources	35
5.1.3.1	Differential Code Biases DCBs	35
5.1.3.2	Absolute Antenna Offsets	35
5.1.3.3	Station coordinate and information file	36
5.2	Observation segment	36
5.2.1	Application of the DCBs and generation of LCs	37
5.2.2	Cycle slip detection and validation of the satellite eclipse condition	38
5.2.3	Application of required corrections	39
5.2.4	Atmospheric effects	40
5.2.5	Relativistic effects	42
5.2.6	Antenna phase center offset	44
5.2.6.1	Satellite antenna phase center correction	44
5.2.6.2	Receiver antenna phase center correction	46
5.2.7	Phase wind-up effect	46
5.2.8	Noise and quality of the corrected observations	48
5.3	Parameter Segment	50
5.3.1	Station network	51
5.3.2	Determination of the reference satellite	52
5.3.3	Introduction to Kalman Filtering	54
5.3.4	Estimation of the WL UPDs	57
5.3.4.1	Change of the reference satellite	63
5.3.5	Estimation of the NL UPDs	63
5.3.5.1	SD PPP solution	64
5.3.5.2	Fixing of the SD WL ambiguities	70
5.3.5.3	Estimation of the UPDs	71
5.3.6	Application of the UPDs	74
6	Influence of satellite orbits and clock corrections on the estimation of the WL and NL UPDs	77
6.1	Influence of the accuracy and the availability of satellite orbits and clock corrections	77
6.1.1	Stability and availability of the satellite WL UPDs	78
6.1.2	Stability and availability of the satellite NL UPDs	86
6.1.2.1	Quality of the SD PPP solution	86
6.1.2.2	Validation of the fixed SD WL ambiguities	93
6.1.2.3	Satellite NL UPDs	94
6.2	Impact of errors in the satellite orbits and clock corrections	104
6.2.1	Outages of the IGC solution	105
6.2.2	Error simulation and compensation	108

6.2.2.1	Orbit error	108
6.2.2.2	Satellite clock correction error	115
7	Summary and conclusions	123
7.1	Discussion of the influence of satellite orbit and clock corrections on the estimation of WL and NL UPDs	124
7.1.1	Stability and availability of the UPDs	124
7.1.2	Impact on the estimation and the numerical results of the NL UPDs	125
7.2	Outlook	126
	Appendix A	129
	Bibliography	131
	Curriculum vitae	134

List of Figures

2.1	Principle of satellite positioning	3
2.2	Definition of the GCRS	5
2.3	Definition of the TRS	6
2.4	Global and local-level coordinate system	6
2.5	Satellite-fixed coordinate system	7
2.6	Time systems	10
2.7	GPS satellite constellation (Gov. GPS (2015))	12
3.1	IGS tracking network	14
3.2	IGS01 clock comparison (IGS (2015))	16
3.3	IGS01 orbit comparison (IGS (2015))	16
3.4	IGS01 PPP performance of station FFMJ (Frankfurt Germany) over 24 hours (IGS (2015))	17
3.5	IGS02 PPP performance of station FFMJ (Frankfurt Germany) over 24 hours (IGS (2015))	17
4.1	Float solution of station GRAZ using precise IGS products	22
4.2	Ambiguities of the float solution	23
4.3	Transient behavior of the ambiguity of PRN 15	23
5.1	Structure of PPP Post	30
5.2	Observation segment	37
5.3	Cylinder model for the shadow of the earth	38
5.4	Relativistic clock corrections	43
5.5	Problem of the rotation of the reference frame (Radovanovic (2002))	44
5.6	Shapiro delay correction	45
5.7	Phase wind-up correction	48
5.8	Parameter segment	50
5.9	Used station network for the estimation of the UPDs	52
5.10	Number of Observations	53
5.11	Satellite ground tracks	54

5.12	Change of the reference satellite, Day 1 of GPS week 1783	55
5.13	ZD MW PRN19 LEICA GRX1200PRO	57
5.14	ZD MW PRN8 LEICA GRX1200GGPRO	57
5.15	ZD MW PRN13 TRIMBLE NETR5	57
5.16	ZD MW PRN25 JPS LEGACY	57
5.17	SD WL UPD PRN16 - PRN21	59
5.18	SD WL UPD PRN19 - PRN32	59
5.19	SD WL UPD PRN16 - PRN21	60
5.20	SD WL UPD PRN19 - PRN32	60
5.21	SD WL UPD PRN16 - PRN21	62
5.22	SD WL UPD PRN19 - PRN32	62
5.23	Satellite-to-satellite single difference	64
5.24	Temporal progress of the ZTD at station Belfast	69
5.25	Transient behaviour of the ZTD at station Belfast	69
5.26	Temporal progress of the SD IF ambiguities at station Belfast	69
5.27	Temporal behavior of the SD IF ambiguity parameter at station Belfast	70
5.28	Fixed SD WL ambiguities at station Belfast	71
5.29	SD NL UPD PRN16 - PRN21	73
5.30	SD NL UPD PRN19 - PRN32	73
5.31	PPP solution with ambiguity fixing	74
6.1	SD WL UPDs of six satellite pairs on GPS Week/Day 1783/1 (IGS solution)	79
6.2	Mean values and standard deviations of the SD WL UPDs of the first passes of all satellite pairs related to reference satellite PRN15 on GPS Week/Day 1783/1	79
6.3	Mean values and standard deviations of the SD WL UPDs of the first passes of all satellite pairs related to reference satellite PRN12 on GPS Week/Day 1783/1	79
6.4	Histogram of standard deviations of the WL UPD time series (IGS solution)	81
6.5	Mean values of WL UPD passes during the investigation period (IGS solution)	81
6.6	Slopes of the regression lines of the SD WL UPD series (IGS solution)	82
6.7	Histogram of the absolute WL UPD residuals (IGS solution)	82
6.8	WL UPDs on GPS Week/Day 1783/2 (IGS solution)	83
6.9	Histogram of the differences between the WL UPDs of the IGS and IGC solution	84
6.10	Comparison of the number of estimated WL UPDs on GPS Week/Day 1783/2	84
6.11	Availability of the IGS and IGC01 product on GPS Week/Day 1783/2	84
6.12	Availability of the IGS and IGC01 product during the whole investigation period	85
6.13	Comparison of the ZTDs at station MAN2 on GPS Week/Day 1783/2 (IGS solution)	86
6.14	Bias of the ZTD differences between the SD PPP solution (IGS) and the EPN solution at each station	88
6.15	Standard deviation of the ZTD differences between the SD PPP solution (IGS) and the EPN solution at each station	88

6.16 IF code observation residuals of the SD PPP algorithm at station MAN2 on GPS Week/Day 1783/2 (IGS solution)	89
6.17 IF phase observation residuals of the SD PPP algorithm at station MAN2 on GPS Week/Day 1783/2 (IGS solution)	89
6.18 Histogram of the absolute IF code observation residuals on GPS Week/Day 1783/2 (IGS solution)	89
6.19 Histogram of the absolute IF phase observation residuals on GPS Week/Day 1783/2 (IGS solution)	89
6.20 Comparison of the ZTDs at station MAN2 of the IGC solution on GPS Week/Day 1783/2	90
6.21 Bias of the ZTD differences between the SD PPP solution (IGC) and the EPN solution at each station	91
6.22 Standard deviation of the ZTD differences between the SD PPP solution (IGC) and the EPN solution at each station	91
6.23 IF code observation residuals of the SD PPP solution at station MAN2 on GPS Week/Day 1783/2 (IGC solution)	92
6.24 IF phase observation residuals of the SD PPP solution at station MAN2 on GPS Week/Day 1783/2 (IGC solution)	92
6.25 Histogram on the IF code observation residuals of GPS Week/Day 1783/2 (IGC solution)	93
6.26 Histogram of the IF phase observation residuals on GPS Week/Day 1783/2 (IGC solution)	93
6.27 NL UPDs on GPS Week/Day 1783/2 (IGS solution)	96
6.28 Mean values and standard deviations of the NL UPDs of the first passes of all satellite pairs related to reference satellite PRN01 on GPS Week/Day 1783/2	96
6.29 Mean values and standard deviations of the NL UPDs of the first passes of all satellite pairs related to reference satellite PRN29 on GPS Week/Day 1783/2	96
6.30 Histogram of standard deviations of the NL UPD time series (IGS solution)	97
6.31 Mean values of NL UPD passes during the investigation period (IGS solution)	98
6.32 Histogram of the NL UPD residuals (IGS solution)	98
6.33 NL UPDs on GPS Week/Day 1783/2 (IGS solution)	99
6.34 NL UPDs of the IGC solution on GPS Week/Day 1783/2	100
6.35 Mean values and standard deviations of the NL UPDs of the first passes of all satellite pairs related to reference satellite PRN01 on GPS Week/Day 1783/2	101
6.36 Mean values and standard deviations of the NL UPDs of the first passes of all satellite pairs related to reference satellite PRN 29 on GPS Week/Day 1783/2	101
6.37 Histogram of standard deviations of the NL UPD time series of the IGS solution	101
6.38 Histogram of standard deviations of the NL UPD time series of the IGC solution	101
6.39 Mean values of NL UPD passes during the investigation period (IGC solution)	102
6.40 Histogram of the NL UPD residuals (IGC solution)	103

6.41 Availability of the SD NL UPDs during the investigation period	104
6.42 Number of NL UPDs of the IGS and IGC solution on GPS Week/Day 1783/4	105
6.43 Availability of the IGS and IGC product on GPS Week/Day 1783/4	105
6.44 Absolute orbit 3D-differences for all available satellites between the IGS and IGC products on GPS Week/Day 1783/4	106
6.45 Clock correction differences for all available satellites between the IGS and IGC products on GPS Week/Day 1783/4	106
6.46 Absolute differences between the PRN01 satellite orbits of the IGS and the IGC products on GPS Week/Day 1783/4	106
6.47 Differences between the PRN01 satellite clock corrections of the IGS and the IGC products on GPS Week/Day 1783/4	106
6.48 SD IF phase observations at station BELF on GPS Week/Day 1783/4. Outliers of the SD PPP solution are indicated by black lines	107
6.49 SD IF phase observations at station MAN2 on GPS Week/Day 1783/4. Outliers of the SD PPP solution are indicated by black lines	107
6.50 Satellite track of PRN14	109
6.51 Orbit error in radial direction	109
6.52 Differences between the IF phase ranges of the IGS and IGE solution for all stations to the satellite PRN14 on GPS Week/Day 1783/2. Each station is illustrated by a different color	110
6.53 SD NL UPDs PRN19 - PRN14 of the IGS solution on GPS Week/Day 1783/2	110
6.54 SD NL UPDs PRN19 - PRN14 of the IGE solution on GPS Week/Day 1783/2	110
6.55 Satellite track of PRN01	111
6.56 Orbit error in along track direction	111
6.57 Differences between the IF phase ranges of the IGS and IGE solution for all stations to the satellite PRN01 on GPS Week/Day 1783/2. Each station is illustrated by a different color	112
6.58 SD NL UPDs PRN19 - PRN01 of the IGS solution on GPS Week/Day 1783/2	112
6.59 SD NL UPDs PRN19 - PRN01 of the IGE solution on GPS Week/Day 1783/2	112
6.60 Satellite track of PRN03	113
6.61 Orbit error in across track direction	113
6.62 Differences between the IF phase ranges of the IGS and IGE solution for all stations to the satellite PRN03 on GPS Week/Day 1783/2. Each station is illustrated by a different color	114
6.63 SD NL UPDs PRN19 - PRN03 of the IGS solution on GPS Week/Day 1783/2	115
6.64 SD NL UPDs PRN19 - PRN03 of the IGE solution on GPS Week/Day 1783/2	115
6.65 Differences between the IF phase ranges of the IGS and IGE solution for all stations to the satellite PRN14 on GPS Week/Day 1783/2. Each station is illustrated by a different color	116
6.66 SD NL UPDs PRN19 - PRN14 of the IGS solution on GPS Week/Day 1783/2	117

6.67 SD NL UPDs PRN19 - PRN14 of the IGE solution on GPS Week/Day 1783/2 117

6.68 Differences between the IF phase ranges of the IGS and IGE solution of satellite
PRN03 on GPS Week/Day 1783/2. Each station is illustrated by a different color . . 117

6.69 SD NL UPDs PRN19 - PRN03 of the IGS solution on GPS Week/Day 1783/2 118

6.70 SD NL UPDs PRN19 - PRN03 of the IGE solution on GPS Week/Day 1783/2 118

6.71 Differences between the IF phase ranges of the IGS and IGE solution of satellite
PRN01 on GPS Week/Day 1783/2. Each station is illustrated by a different color . . 119

6.72 SD NL UPDs PRN19 - PRN01 of the IGS solution on GPS Week/Day 1783/2 120

6.73 SD NL UPDs PRN19 - PRN01 of the IGE solution on GPS Week/Day 1783/2 120

List of Tables

3.1	GPS orbit and clock products provided by the IGS (IGS (2015))	15
3.2	RTCM Message Types	18
5.1	Broadcast ephemerides (GPS)	32
5.2	Coefficients of the hydrostatic mapping function	41
5.3	Coefficients of the wet mapping function	42
5.4	Examples of APC corrections for GPS satellites	46
5.5	Noise level of different observation types	48
5.6	Noise level of different linear combinations	49
5.7	Number of changes during GPS week 1783	54
5.8	Initial (loose) constraints for the initialization of the SD PPP solution	66
5.9	Variance of the process noise of the SD PPP solution	66
6.1	Fixing rates of the SD WL ambiguities of selected stations of the IGS solution during the investigation period	94
6.2	Fixing rates of the SD WL ambiguities of selected stations during the investigation period using the IGC product	95
6.3	Simulated orbit errors	108
6.4	Simulated clock and orbit errors	115

Acronyms

BKG	Bundesamt für Kartographie und Geodäsie
BNC	BKG NTRIP Client
CODE	Center of Orbit Determination in Europe
DD	Double-Difference
ECEF	Earth-Centered Earth-Fixed
EPN	EUREF Permanent Network
ESOC	European Space Operations Center
GCRS	Geocentric Celestial Reference System
GPST	GPS Time
IAG	International Association of Geodesy
IERS	International Earth Rotation and Reference Systems Service
IF	Ionosphere-Free
ITRF	International Terrestrial Reference Frame
MW	Melbourne Wübbena
NAVSTAR	NAVigation System with Timing And Ranging
NL	Narrow-Lane
NRCan	Natural Resources Canada
PPP	Precise Point Positioning
PRN	Pseudo Random Noise
RINEX	Receiver Independent Exchange Format
RSM	Real-Time Simulation Mode
RTCM-SSR	RTCM State Space Representation
RTM	Real-Time Mode
RTS	Real-Time Service
RTWG	Real-Time Working Group
SD	Single-Difference
TRF	Terrestrial Reference System
TU Graz	Graz University of Technology
UPD	Uncalibrated Phase Delay
UTC	Coordinated Universal Time
UT	Universal Time

List of Tables

WGS84	World Geodetic System 1984
WL	Wide-Lane
ZD	Zero-Difference

Chapter 1

Introduction

In the last years the principle of Precise Point Positioning (PPP) has become a well established technique, especially for real-time applications. Combining precise satellite positions and clocks, derived from global receivers of Global Satellite Navigation System (GNSS), with un-differenced dual-frequency code pseudorange and phase measurements from a single GNSS receiver, PPP is able to provide position solutions at centimeter to decimeter level. PPP requires a precise modeling of errors affecting the signals, as they cannot be eliminated by building observation differences as performed in the well established difference-techniques, like Real-Time Kinematic (RTK) for instance. Therefore the usual practice, when processing dual frequency data, is to build the ionosphere-free observation of the pseudorange and phase observations in order to mitigate the ionospheric effect. The tropospheric influence is divided into a hydrostatic and a wet part. While the hydrostatic part is derived from precise models, the wet part is estimated within the adjustment process. Additional errors which must be taken into account are the satellite and receiver antenna phase center offsets, relativistic effects, the phase wind-up effect and earth-tide and ocean loading effects.

Unfortunately, the application of all these corrections is still not sufficient to allow for integer ambiguity resolution. Therefore, common PPP approaches are based on estimating only real-valued ambiguities. However, the estimation of real-valued ambiguities requires a long convergence period which is the most significant factor limiting wider adoption of PPP. Accordingly, integer ambiguity resolution of undifferenced carrier phase observations is considered as one of the innovative issues for GNSS research and applications in the next years (Rizos (2008)). Therefore this problem is currently a major topic of many scientific investigations.

Motivated by the aforementioned challenge, an Austrian consortium has spent 2 years on the research project PPPserve, which aimed at the development of appropriate algorithms for real-time PPP with special emphasis on the ambiguity resolution of zero-difference observations. A fully functional system was developed that consists of a network-side module, calculating satellite-based GPS wide-lane and narrow-lane phase delays (UPDs) from a regional station network, and a user-software that applies the calculated corrections in a modified PPP algorithm to enable

integer ambiguity resolution on the basis of wide- and narrow-lane observables.

The upcoming sections of this thesis treat the design and functionality of the network-side software PPP Post, from the data preparation to the estimation of the WL and NL UPDs. Additionally, the influence of satellite orbits and satellite clock corrections on the estimation of the UPDs will be treated on basis of the results provided by PPP Post.

Section 2, *Global Navigation Satellite Systems*, provides an overview of the principle of satellite-based positioning. Furthermore, the definition and realization of coordinate and time systems as well as the transformation between coordinate systems which are needed in the context of this thesis, will be treated. Finally an overview about the history, the current status and the modernization of GPS will be given.

Section 3, *The International GNSS Service*, gives an short overview of the International GNSS Service (IGS). It starts with a short historical review of the service, followed by a description of the organizational structure, the station network as well as current available products and services. Especially the tasks and activities of the IGS Real-Time Service will be treated, including an introduction to the RTCM standard.

Section 4, *Precise Point Positioning*, completes the general sections of this thesis and provides the theoretical background of PPP. After the description of the observational model, the issue of integer ambiguity resolution in PPP will be discussed. The section is closed by an overview of methods for integer ambiguity resolution in PPP, including a detailed description of the method “Phase recovery from fractional parts”, which forms the theoretical background of this thesis.

Section 5, *The software PPP Post*, starts with the description of the modular structure of the software. The first module “Data source segment”, serves as interface to external data sources, like GPS satellite orbits and clock corrections, and the PPP Post software. The primary function of the second module the “Observation segment” is the preparation of the GPS observation data for the third module the “Parameter segment”, where the actual estimation of the WL and NL UPDs takes place.

Section 6, *Influence of satellite orbits and clock corrections on the estimation of the WL and NL UPDs*, treats the investigations which have been carried out using the results provided by the PPP Post software. These investigations are basically concentrated on two main points. The first one is the influence of the accuracy and availability of satellite orbits and clock corrections on the stability and availability of UPDs. The second one is the impact of errors in the satellite orbits and clock corrections on the estimation process and their effect on the numerical results of the UPDs. The final remark shows, if and to which extent, these errors can be compensated by the UPDs.

Section 7, *Summary and conclusions*, sums up the results of this thesis and provides a short overview of possible improvements for the PPP Post software as well as other future developments.

Chapter 2

Global Navigation Satellite Systems

2.1 Principle of satellite-based positioning

“Satellite-based positioning is the determination of positions of observing sites on land or at sea, in the air and in space by means of artificial satellites” (Hofmann-Wellenhof et al. (2008)). The three-dimensional position, for example latitude, longitude and height, of a user can be determined by a simple recapture process using ranges measured to satellites. Each range defines the surface of a sphere with the satellite at its center. Using this technique ranges to three satellites are needed since the intersection point of the spheres yields the three unknowns of the position. The interrelationship between the geometric position vector of the satellite r^i and the receiver r_k (see also Fig. 2.1), the receiver and satellite clock errors δt^i and δt_k and the geometric distance range ρ_k^i is given in the following equation

$$\rho_k^i = \| \vec{r}^i + c\delta t^i - \vec{r}_k - c\delta t_k \| = \tau_k^i \cdot c \quad (2.1)$$

The ranges can be accurately measured by recording the travel time τ_k^i (multiplied by the speed of light c) that a signal broadcasted by the satellite needs to reach the receiver on the

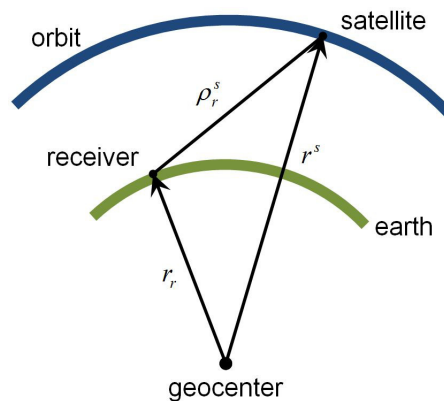


Figure 2.1: Principle of satellite positioning

ground. The time measurement is corrupted by satellite and receiver clock errors and therefore the distance measured differs from the “true” range. As a consequence these distances are called pseudoranges since they represent the geometric range plus a range correction resulting from the receiver and satellite clock error. The positions of the satellites and the satellite clock errors are forecasted and broadcasted along with the GPS signal to the user. The receiver clock error has to be estimated together with the three unknowns of the position (e. g. latitude, longitude and height). Therefore observations to at least four satellites are needed for a successful determination of the position.

2.2 Coordinate systems

Position and navigation applications by means of GNSS require suitable coordinate and time systems for the description of observations (distances) as a function of the satellite position and the station location (Xu (2003)). The definition of a Cartesian coordinate system requires a convention for the orientation of the three axes and for the origin of the system (Hofmann-Wellenhof et al. (2008)). In satellite geodesy equatorial systems with their origin in the earth’s center of mass have been proven to be practical. In principle one can distinguish between a space-fixed or celestial system and an earth-fixed or a terrestrial system. These systems are referred to as Conventional Celestial Reference System and Conventional Terrestrial Reference System. Additional coordinate systems, which are needed in the context of this theses, are a local horizontal system as well as so-called satellite-specific systems. These local systems are needed for the description of diverse receiver- and satellite-specific errors, like absolute antenna offsets. In conclusion coordinate transformation models between these different systems are required as well.

In case of the space-fixed as well as the earth-fixed system the earth’s rotation vector or its unit vector serves as Z-axis¹. The X-axis of the space-fixed system is directed towards the vernal equinox (i.e. the intersection between the equatorial plane and the ecliptic plane). The X-axis of the earth-fixed system is defined as the intersection between the equatorial plane and the Greenwich meridian. In both cases the Y-axis is orthogonal to the respective Z-axis and X-axis, and completes a right-handed coordinate frame. The differential gravitational effect of the sun and moon results in changes of the earth’s rotation vector in terms of orientation and magnitude. In the interest of simplification this effect is partitioned into the secular precession and the periodic nutation. Changes of the earth’s rotation vector with respect to the terrestrial system are referred to as polar motion. The correction for the actual phase of rotation of the earth-fixed system w.r.t. to the space-fixed system completes the effects which are the required parameters for the transformation between the space-fixed and the earth-fixed system.

¹This is not fully true, the Z-axis is defined by the direction of the earth mean rotation pole at J2000.0 and not by the momentary rotation axis of the earth.

2.2.1 Conventional celestial reference system

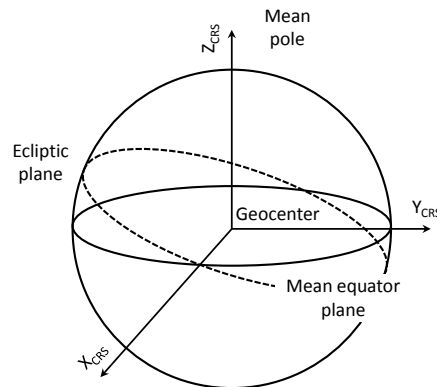


Figure 2.2: Definition of the GCRS

To describe the motion of a satellite a coordinate system, in which the Newtonian mechanics are fully valid, is needed. A system of this kind is denoted as inertial system and is characterized by the fact that it is in an idle state or moves at constant speed. A coordinate system which satisfies these requirements is the aforementioned *Barycentric Celestial Reference System* (BCRS). The origin of the system is located at the barycenter of our Solar system and the Z-axis is by convention identical to the mean position of the earth's rotation axis at a standard epoch denoted by J2000.0. The X-axis is pointing towards the dynamical equinox at J2000.0 and the Y-axis completes a right-handed coordinate system. The orientation of the BCRS coordinate system coincides with that of the *International Celestial Reference System* (ICRS). A realization of the ICRS is the *International Celestial Reference Frame* (ICRF), which is established by the *International Earth Rotation and Reference Systems Service* (IERS). The ICRF is defined by a set of precise positions of extragalactic radio sources, mostly quasars and galactic nuclei.

However, for describing the satellite's motion it is more convenient to use a *Geocentric Celestial Reference System* (GCRS) with the center being located at the earth's center of mass as shown in Fig. 2.2. Because of the accelerated motion of the earth's center around the sun, the system is often referred to as "quasi-inertial" system.

2.2.2 Conventional terrestrial reference system

It is convenient to use a coordinate systems which considers the earth's rotation around its own axis to describe the location of a position. The aforementioned *Terrestrial Reference System* (TRS) is such a system. This reference system is also known as *Earth-Centered, Earth-Fixed* (ECEF) system. The origin of the system is located at the earth's center of mass and the Z-axis is pointing towards the mean position of the earth's rotation axis. This position is called *Conventional International Origin* (CIO) and is by convention an average of the poles from 1900 to 1905. The X-axis is pointing to the intersection point of the equatorial plane with the plane represented by

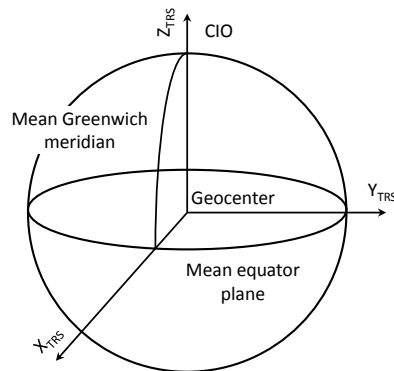


Figure 2.3: Definition of the TRS

the Greenwich meridian and the Y-axis completes a right-handed coordinate system (Fig. 2.3). A realization of such a earth-fixed system is the *International Terrestrial Reference Frame* (ITRF) , which is also provided by the IERS. The ITRF is defined by a set of precise positions of globally distributed monitoring stations of space-geodetic techniques (like *Very Long Baseline Interferometry* (VLBI), *Satellite/Lunar Laser Ranging* (SLR, LLR) and GNSS). In the ITRF temporal effects, which are caused by plate tectonics among others, are also taken into account. The current version is the ITRF2008, whereby the number marks the last year of data used in the formation of the frame. In the near future the ITRF2008 will be substituted by the ITRF2014.

Another example for a terrestrial reference frame is the *World Geodetic System 1984* (WGS84), which is the basic system for the satellite navigation system GPS. After some modifications, the recent realization of the WGS84 is almost identical to the ITRF2008.

2.2.3 The local-level system

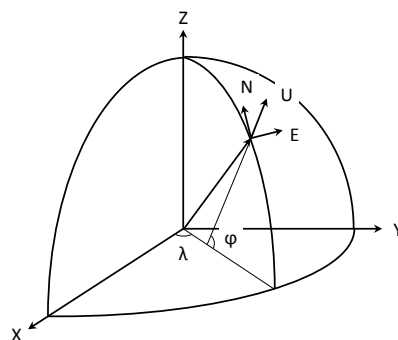


Figure 2.4: Global and local-level coordinate system

For certain receiver specific corrections it is more feasible to use a local-level system instead of a global geocentric system. Such a system can be defined by placing the origin to a local point

P (e. g. the position of a station). The X-axis is pointing towards north, the Y-axis is directing to the east and the Z-axis is pointing to the vertical direction and completes a left-handed Cartesian coordinate system (Fig. 2.4). This system is often referred to as ENU (east,north,up) system and can be used for the characterization of station-specific corrections, like the absolute offset of the antenna phase center or the site eccentricity vector (see Sect. 5.2.6.2).

2.2.4 The satellite-fixed coordinate system

It is convenient to use a satellite-fixed coordinate system for the purpose of the orbit determination and perturbation calculations. One option to establish such a satellite-fixed system is to place the origin to the satellite's center of mass. The X-axis coincides with the radius vector, the Y-axis is pointing into the direction of motion. The Z-axis is placed orthogonal to the X-axis and Y-axis, and completes a right-handed coordinate system (Fig. 2.5). Satellite-fixed coordinate systems of this type are used to describe the deviation of orbital solutions with respect to a reference orbit. Such a system is used for the transmission of orbit corrections with the aid of RTCM standard messages. The deviations in the direction of the X-axis, Y-axis and Z-axis are denoted as radial, along-track and cross-track, respectively.

The characterization of the offset between the satellite's antenna phase center and mass center requires a different satellite-fixed coordinate frame, which can also be used to conveniently model the solar radiation pressure. The origin of the coordinate system is placed to the satellite's center of mass, as before. The Z-axis coincides with the radial vector and is pointing towards the earth, the Y-axis lays in the plane perpendicular to the vector pointing to the sun and the X-axis completes a right-handed coordinate system. A detailed description of the satellite antenna phase center correction is given in Sect. 5.2.6.1.

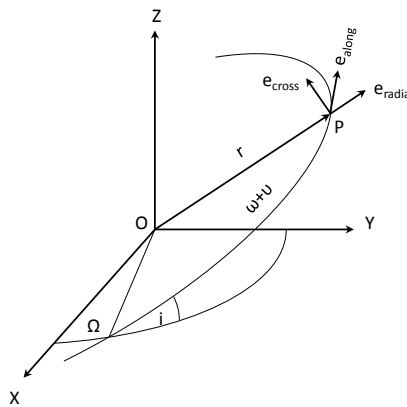


Figure 2.5: Satellite-fixed coordinate system

2.2.5 Coordinate transformation

A variety of geodetic applications require the transformation between different Cartesian coordinate systems. Such a transformation consists of three consecutive rotations, if the origins of

both systems are identical and if they are both right-handed or left-handed coordinate systems. These three rotational matrices are

$$R_1(\alpha_1) = \begin{pmatrix} 1 & 0 & 0 \\ 0 & \cos \alpha_1 & \sin \alpha_1 \\ 0 & -\sin \alpha_1 & \cos \alpha_1 \end{pmatrix} \quad (2.2)$$

$$R_2(\alpha_2) = \begin{pmatrix} \cos \alpha_2 & 0 & -\sin \alpha_2 \\ 0 & 1 & 0 \\ \sin \alpha_2 & 0 & \cos \alpha_2 \end{pmatrix} \quad (2.3)$$

$$R_3(\alpha_3) = \begin{pmatrix} \cos \alpha_3 & \sin \alpha_3 & 0 \\ -\sin \alpha_3 & \cos \alpha_3 & 0 \\ 0 & 0 & 1 \end{pmatrix} \quad (2.4)$$

with α_1 , α_2 , α_3 being the rotation angles and $R_1(\alpha_1)$, $R_2(\alpha_2)$ and $R_3(\alpha_3)$ being the rotating matrices around the X-, Y- and Z-axis, respectively. If the two systems differ in origin and if they also have different scales, the general transformation is provided by the well known Helmert- or 7-parameter transformation

$$\vec{X}_n = \vec{X}_0 + m \cdot R_1(\alpha_1) \cdot R_2(\alpha_2) \cdot R_3(\alpha_3) \cdot \vec{X}_o \quad (2.5)$$

where \vec{X}_n are the coordinates in the target system, \vec{X}_o are the coordinates in the original system, \vec{X}_0 is the translation vector, m is the common scale factor and $R_1(\alpha_1)$, $R_2(\alpha_2)$, $R_3(\alpha_3)$ are the previously defined transformation matrices.

In the following a short overview of the transformations which are needed later in this thesis is given. The transformation from the geocentric earth-fixed system \vec{X}_{ECEF} to the local-fixed system \vec{X}_{ENU} is composed of a shift of the origin and a rotation. The shift is the radius vector of the position given in the earth-fixed system and the rotation is formed by two succeeded rotations according to

$$R = R_1(180^\circ - \varphi) \cdot R_3(180^\circ + \lambda) \quad (2.6)$$

where φ and λ are the geodetic latitude and longitude.

The transformation of the satellite antenna phase center offset, given in the corresponding defined satellite-fixed system, to the geocentric earth-fixed system \vec{X}_{ECEF} is composed of a shift and a rotation as well. The shift is the radius vector of the satellite's position in the earth-fixed system. The rotation matrix R is created by assembling the unit vectors of the satellite-fixed system \vec{e}_x, \vec{e}_y and \vec{e}_z expressed with respect to the ECEF frame as columns in a matrix according to

$$R = \begin{bmatrix} \vec{e}_x & \vec{e}_y & \vec{e}_z \end{bmatrix} \quad (2.7)$$

where \vec{e}_z is the unit vector pointing from the satellite center of mass to the earth's center, the

unit vector \vec{e}_y lays in the plane perpendicular to the vector pointing to the sun and \vec{e}_z completes the right-handed system. A detailed description of the transformation of the satellite antenna phase center correction is given in Sect. 5.2.6.1.

2.3 Time systems

There are several time systems currently in use. These systems are based on different processes, like the rotation of the earth for instance. The following three time systems are of particular importance in satellite geodesy.

1. *Solar Time*, *Sidereal Time* and *Universal Time* (UT) are time systems which are defined by the earth's rotation. These systems are used to relate earth- and space-fixed reference systems.
2. *Barycentric Dynamic Time* (BDT) and *Terrestrial Time* (TT) are time systems which are derived from the motion of the planets of our solar system. TT is used as an independent parameter within the equations of motion of satellites.
3. *International Atomic Time* (TAI) and *Coordinated Universal Time* (UTC) are uniform time systems which are derived from atomic oscillations.

Time systems based on the rotation of the earth can be measured by the angle between an earth-fixed reference meridian (local or Greenwich) and the meridian of a celestial reference. Solar time is defined as Greenwich hour angle of a fictive mean sun uniformly orbiting in the equatorial plane. Sidereal time is the hour angle of the vernal equinox. The difference between a mean sidereal day and a mean solar day is around 4 minutes. Universal Time is defined as the Greenwich hour angle of the mean Sun augmented by 12 hours. In case UT is corrected for polar motion it is referred to as UT1. Due to changes in the polar moment of inertia and the distribution of the mass the rotation of the earth and time systems being derived from the earth's rotation are not uniform. On the contrary the International Atomic Time is a strict uniform time system. This system is realized by a set of globally distributed very precise atomic clocks which are regulated by the International Bureau of Weights and Measures. One second of TAI corresponds to the duration of one ephemeris second and is given by SI (*International System of Units*). The epoch of TAI corresponds by definition to the epoch of UT1 on January 1, 1958. For various applications a uniform time system with the best possible adaption of UT1 is needed. UTC is such a time system and is a compromise between TAI and UT1. This time is also based on an atomic time scale but, to keep it close to UT1 (the difference is always smaller than one second), integer leap seconds are introduced from time to time. Therefore UTC is not a uniform time scale. Since June 30, 2015, the difference between UTC and TAI amounts to 26 seconds.

The different components of GNSS (GPS, GLONASS, Galileo) maintain their own time systems based on atomic clocks at the monitor stations and on board of the satellites. However the evaluation of observations of multiple systems is always referred to *GPS Time* (GPST). The epoch of

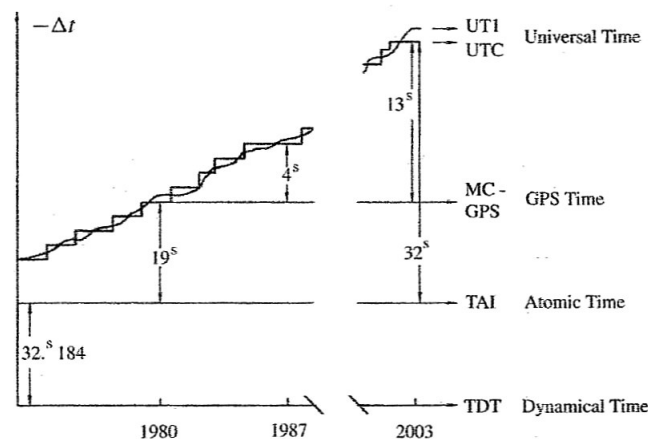


Figure 2.6: Time systems (Seeber (2003))

GPST corresponds to the epoch of UTC at January 5, 1980. Therefore GPST differs by an integer number of seconds from UTC (today 17 seconds) and has a constant offset of 19 seconds to TAI. GPST is synchronized with UTC and the difference is broadcasted within the satellite navigation message.

An overview of the time scales of interest in satellite geodesy is given in Fig. 2.6. More information concerning time scales and standards can be found in, e.g. Hofmann-Wellenhof et al. (2008), Xu (2003) or in the IERS Conventions (2010).

2.4 The Global Positioning System GPS

The satellite-based determination of the positions depends on signals transmitted by one or multiple global navigation satellite systems GNSS. The most well known system is the American GPS. Additional systems are the Russian GLONASS system as well as the new-coming European system Galileo and the Chinese system BeiDou. In the next years a GNSS multiconstellation with over 100 satellites and numerous signals for different levels of services and applications will be available to the users (Karabatić (2011)). Furthermore the existing systems like GPS and GLONASS are modernized in order to improve the performance of their services and to enable interoperability and compatibility between different satellite systems. The industry as well as the scientific community are confronted with the difficult task to develop software and hardware which is capable of using jointly all the different systems and their renewals. Since this thesis solely depends on observations of the GPS system only, a brief overview of the GPS system itself, including the history, the current status as well as modernization plans, will be given. An extensive description of the other systems can be found in the scientific literature, in articles and the internet.

The *NAVigation System with Timing And Ranging* (NAVSTAR) Global Positioning Service is the result of an initial directive of the US *Department of Defense* (DoD) to the *Joint Program Office*

(JPO) in the year 1973 to establish, develop, test, acquire and deploy a space-born positioning system (Hofmann-Wellenhof et al. (2008)). Originally it was designed to serve military purposes only. But as early as 1983 it became open for civil users, however with some limitations. Basically GPS is a navigation system for the determination of a receiver's unknown position, measuring the distance to satellites with known positions. The distance is obtained by means of the measurement of the run time of the electromagnetic signal broadcasted by the satellites.

The GPS system is usually separated into three fundamental segments: a space, a control and a user segment. The space segment, consisting of the satellites, serves for the dissemination of particular radio navigation signals and for storing and retransmitting the navigation message sent by the control segment. The control segment is responsible for the proper operation of the system and consists of a master control station as well as a number of monitoring stations and ground antennas. The measurements recorded by the monitoring stations are used to determine the satellite-specific information (position, clock error and ionospheric model) and to generate the navigation message. These corrections and the navigation message are uploaded to the satellite through the ground antennas. The user segment consists of the GPS receivers which are receiving the signals broadcasted by the satellites to determine the position of the user as well as an accurate time.

The satellite constellation undergoes continuous maintenance and improvements and therefore the constellation changes regularly. The nominal constellation consists of 24 satellites placed on 6 different almost circular orbits with an inclination of 55° . The mean altitude above the earth amounts to 22000 km which results in a revolution period of 12 h sidereal time (11 h 58 m 2 s). A full constellation allows users to observe 4 to 8 satellites at any time on a global scale, with an elevation masking angle of 15° (Subirana et al. (2013)). Nowadays even 28 to 32 satellites of different types are present in the constellation.

The original signal structure of the GPS system consists of two signals, L1 and L2, in the range of the microwaves. The frequency standard is maintained by very accurate and stable clocks which produce the fundamental frequency 10.23 Mhz. The two signals are generated by multiplying the fundamental frequency by 152 and 120. This yields a wavelength of about 19.0 cm for carrier L1 and a wavelength of about 24.4 cm for carrier L2. Onto both of the signals so-called ranging codes are modulated. Each satellite emits a different *Pseudo Random Noise* (PRN) code and therefore each satellite can be unambiguously identified using the *Code Division Multiple Access* (CDMA) principle. Aside from the identification of the satellite, the codes can be used to determine the run time between the satellite and the receiver. The run time is determined by correlating the run time shifted satellite signal and the reference code produced in the receiver. We can distinguish between two types of codes, the *Coarse/Acquisition* (C/A) code also known as civil code and the encrypted P(Y) code (Anti-spoofing) designed exclusively for military use. The C/A code has an effective wavelength of 300 m, is only modulated on the L1 frequency and defines the *Standard Positioning Service* (SPS). The P/Y code has an effective wavelength of 30 m and is modulated onto both frequencies, L1 and L2, and defines the *Precise Positioning Service* (PPS). Additionally

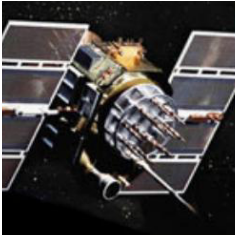
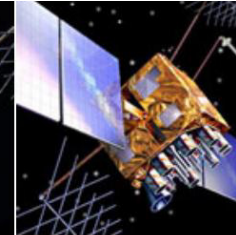
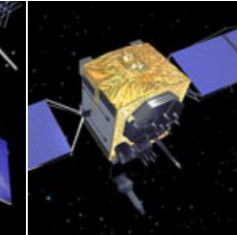
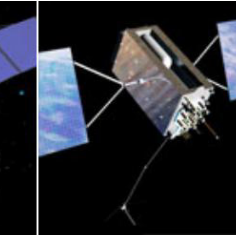
				
BLOCK IIA	BLOCK IIR	BLOCK IIR(M)	BLOCK IIF	GPS III
0 operational	12 operational	7 operational	11 operational	In production
<ul style="list-style-type: none"> ▪ C/A code on L1 ▪ P/Y code on L1 & L2 ▪ Launched in 1990-1997 	<ul style="list-style-type: none"> ▪ C/A code on L1 ▪ P/Y code on L1 & L2 ▪ Launched in 1997-2004 	<ul style="list-style-type: none"> ▪ All legacy signals ▪ 2nd civil signal on L2 (L2C) ▪ New military M code signals for enhanced jam resistance ▪ Launched in 2005-2009 	<ul style="list-style-type: none"> ▪ All Block IIR(M) signals ▪ 3rd civil signal on L5 frequency (L5) ▪ Launched in 2010-2016 	<ul style="list-style-type: none"> ▪ All Block IIF signals ▪ 4th civil signal on L1 (L1C) ▪ Available for launch in 2016

Figure 2.7: GPS satellite constellation (Gov. GPS (2015))

a data or navigation message is modulated onto both of the signals.

The signals described above are still broadcasted by a majority of the satellites (Block IIA and Block IIR, see Fig. 2.7). The Block IIA and Block IIR satellites (A stands for *advanced* and R for *replenish*) have been launched from 1990 to 2004 and mainly served for the maintenance of the system. With the start of the first Block IIR-M satellite in the year 2005 the modernization process of the GPS satellite constellation started. This type of satellite broadcasts, in addition to the already existing signals, another civil code on L2 (L2C) and a new military code M on both of the frequencies. Currently 18 satellites in space are broadcasting these new signals and in the year 2018 the signals shall be emitted from every satellite of the constellation. Additionally a third frequency L5 for civil purposes was added. This new signal is available since the launch of the first Block IIF satellite and offers interesting possibilities in terms of the ionosphere-free (IF) linear combination and the ambiguity resolution. The next generation of GPS satellites (Block III) will provide a fourth civil signal L1C on the frequency L1. This signal shall enable the interoperability with other satellite navigation systems like Galileo.

Chapter 3

The International GNSS Service (IGS)

The International GNSS Service is a federation of about 200 globally distributed agencies that pool resources and permanent GPS & GLONASS station data on a voluntary basis to generate precise GPS & GLONASS products. The aim is to provide highest quality data and products in support of earth science research as well as practical applications. Currently the two satellite navigation systems GPS and GLONASS are supported in regular service, but the IGS intends to incorporate future GNSS (MGEX experiment). In modern geodesy the precise IGS products are used for the improvement and extension of the ITRF, for scientific satellite orbit determination or for observations of the earth's atmosphere (IGS (2015)).

The origin of the IGS goes back the late 80's of the last century. Because of the increasing importance of the U.S Global Positioning System in regional and global studies of the Earth, the scientific community has made an effort to promote international standards for GPS data acquisition and analysis. As part of this effort, the IGS was recognized in 1993 by the *International Association of Geodesy* (IAG), and began routine operations on January 1, 1994. In addition to the development of international GPS data standards and specifications (RINEX, SP3, etc.) the IGS also provides a variety of products based on GNSS observations, like precise orbits and clocks for the GPS and GLONASS constellation, earth orientation parameters, etc.

The IGS global network of permanent tracking stations is the fundamental basis for the operation of the IGS. Currently the IGS network consists of about 350 globally distributed tracking stations (see Fig. 3.1). The Operational Data Centers, which are in direct contact with the tracking sites, collect the raw data (observation data and broadcast ephemerides) and forward it to the Regional or Global Data Centers. In addition to the raw data also the products of the analysis centers are forwarded to the data centers. The users can directly access the data from the ftp-server of the corresponding data centers. The following global data centers are currently available (IGS (2015)):

- *Crustal Dynamics Data Information System* (CDDIS) of the Goddard Space Flight Center
- *Scripps Orbit and Permanent Array Center* (SOPAC) of the University of California in San Diego

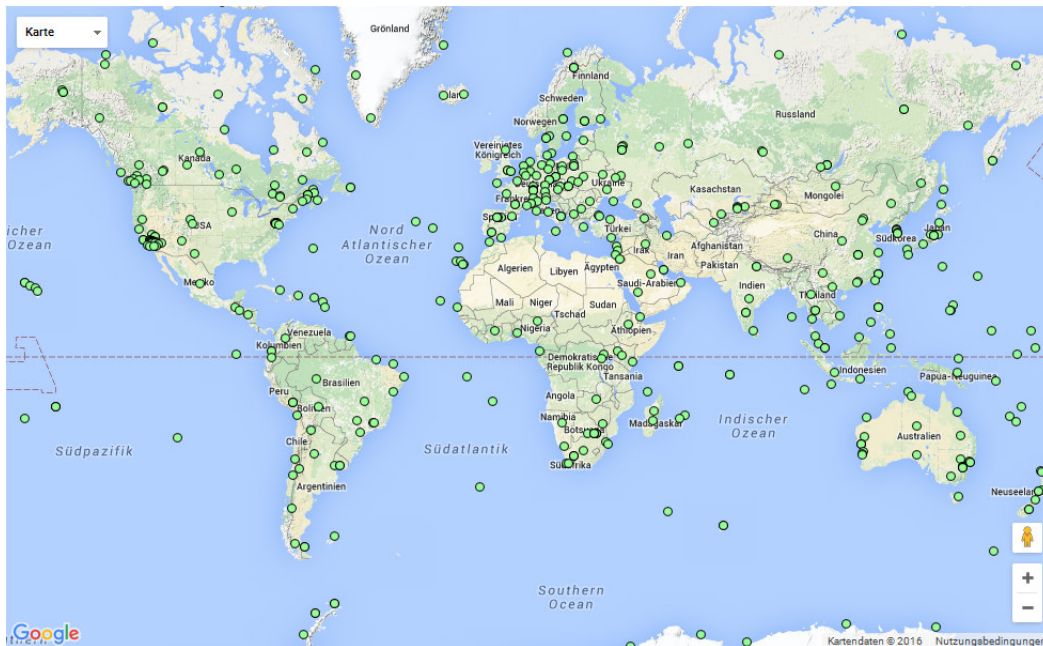


Figure 3.1: IGS tracking network (source: igs.org)

- *Institut Géographique National (IGN)* in Paris, France
- *Korean Astronomy and Space Science Institute (KASI)* in Korea

The IGS analyzes and combines the solutions of the analysis centers (currently thirteen) and provides the following products:

- GPS satellite ephemerides
- GLONASS satellite ephemerides
- Earth rotation parameters
- IGS tracking station coordinates and velocities
- GPS satellite and IGS tracking station clock information
- Zenith tropospheric path delay estimates
- Global ionospheric maps

Four types of solutions are computed for each of the different product group, which differ in regard to quality and latency:

- Ultra-Rapid (predicted half): Prediction of the product parameters based on model assumptions regardless of observation data.
- Ultra-Rapid (observed half): Determination of the product parameters in due consideration of recent observations.

		Accuracy	Latency	Updates	Sample Int.
Broadcast	Orbits	~100 cm	real-time	–	daily
	Sat. clocks	~5 ns RMS ~2.5 ns SDev			
Ultra-Rapid (predicted half)	Orbits	~5 cm	real-time	at 03, 09, 15, 21 UTC	15 min
	Sat. clocks	~3 ns RMS ~1.5 ns SDev			
Ultra-Rapid (observed half)	Orbits	~3 cm	3 - 9 hours	at 03, 09, 15, 21 UTC	15 min
	Sat. clocks	~150 ps RMS ~50 ps SDev			
Rapid	Orbits	~2.5 cm	17 - 41 hours	at 17 UTC daily	15 min
	Sat. clocks	~75 ps RMS ~25 ps SDev			5 min
Final	Orbits	~2.5 cm	12 - 18 days	every Thursday	15 min
	Sat. clocks	~75 ps RMS ~20 ps SDev			Sat.: 30s Stn.: 5 min

Table 3.1: GPS orbit and clock products provided by the IGS (IGS (2015))

- Rapid: Are about equally good as final products and are available on a daily basis.
- Final: Highest quality and accuracy, however highest latency (approximately 2 weeks).

Since the GPS orbit and clock parameters are the only products which are used in the context of this thesis, a detailed list of them is given in Table 3.1. A detailed description of all products can be found on the website of the IGS (2015).

3.1 IGS Real-Time Service

The following section deals with the tasks and activities of the IGS Real-Time Service. Through the *Real-Time Service* (RTS), the IGS provides high-accuracy GPS satellite orbit and clock data as well as 1-Hz data streams of GPS and GLONASS data. The IGS real-time data and orbit and clock products enable precise point positioning and related applications, such as time synchronization and disaster monitoring, at worldwide scales. The RTS is based on the IGS global infrastructure of real-time network stations, data centers and analysis centers and provides data and products openly available to all. Currently the RTS is offered as a GPS-only beta service for the development and testing of applications. The Russian GLONASS is initially provided as an experimental product and will be included within the service, when the RTS reaches its full operating capability. Other GNSS constellations will be added in the near future (IGS (2015)).

The development of the RTS started more than one decade ago with the establishment of the IGS *Real-Time Working Group* (RTWG) in the year 2001. The main task of the RTWG was the design and implementation of a real-time infrastructure and processes for the delivery of real-time data to analysis centers, and the dissemination of real-time products to the users. The design

for a prototype real-time service was adopted at the IGS workshop, “Towards real-time” held in Ottawa in April 2002 (IGS (2002)). In June 2007 the IGS Real-Time Pilot Project started with a three-year target to accomplish its goals. In 2009 the project was extended for three more years and in August 2011 the working group declared that the pilot project reached initial operational capability and recommended to the IGS governing board to launch an official real-time service (Caissy et al. (2012)).

As part of the Real-Time Pilot Project, real-time orbit and clock corrections are generated by 10 *Real-Time Analysis Centers* (RTAC). The role of the *Real-Time Analysis Center Coordinator* (RTACC) is to coordinate the activities of the analysis centers and to generate the combined real-time clock product. Currently the role of the Analysis Coordinator is performed by *European Space Operations Center* (ESOC). Two more combination centers are hosted by *Bundesamt für Kartographie und Geodäsie* (BKG) and *Natural Resources Canada* (NRCan). The quality of the different solutions and the combined products is assessed through the comparison with the precise IGS rapid products. The target of the pilot project was to generate a combined clock product with almost similar quality as the IGS rapid product (accurate within 0.3 nanoseconds). This goal was achieved early on in the project.

The design of the RTS specifies that the RTACS generate their GNSS orbit and clock corrections and transmit them to the combination centers. The combination methods of the RTACC detects and removes outliers that may be present in the individual solutions. In order to generate a combined solution all solutions are aligned to a reference solution by removing a common solution-specific offset from all the satellite clocks. Satellite orbits are combined using solution averages. The orbit corrections are estimated for two reference points, the center of mass and the satellite antenna phase center. The orbit and clock corrections are encoded into RTCM-SSR streams which are then transmitted to two or more data centers. There they become available to the users. In order to ensure robust distribution of the IGS RT products, and to maximize availability, the RTACC and the IGS Working Group designed and implemented a redundancy concept. The concept relies on the parallel generation of each combination product at two or more independent combination centers. In addition, the Analysis Centers themselves make their solutions available at two or more NTRIP casters.

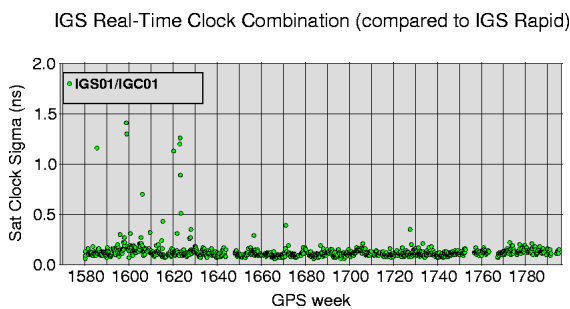


Figure 3.2: IGS01 clock comparison (IGS (2015))

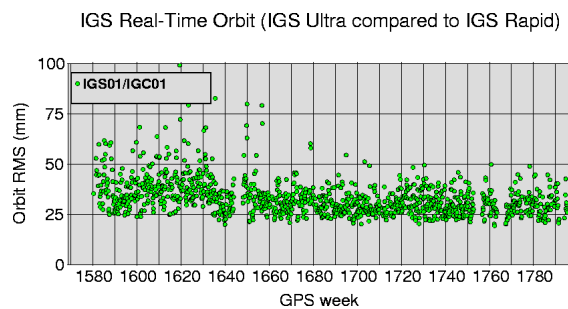


Figure 3.3: IGS01 orbit comparison (IGS (2015))

The performance of the real-time orbit and clock products is monitored mainly through comparisons against the IGS rapid products. The continuous history of the performance of the combined product IGS01 is shown in Figs. 3.2 and 3.3. The clock comparison illustrates that, since GPS week 1630, when a new outlier detection algorithm was implemented, the product has been very stable with clock standard deviations (1-sigma) of 0.1-0.15 ns (IGS (2015)). In addition to the daily comparisons against the IGS rapid solution the real-time corrections are monitored through continuous kinematic *Precise Point Positioning* (PPP) by the BKG. The PPP results using the combination streams IGS01, a single epoch GPS combination, and IGS02, a Kalman filter GPS combination, are displayed in Figs. 3.4 and 3.5, respectively. It can be seen that the horizontal deviation is less than 10 cm for most of the time and that the vertical component is approximately a factor of two larger.

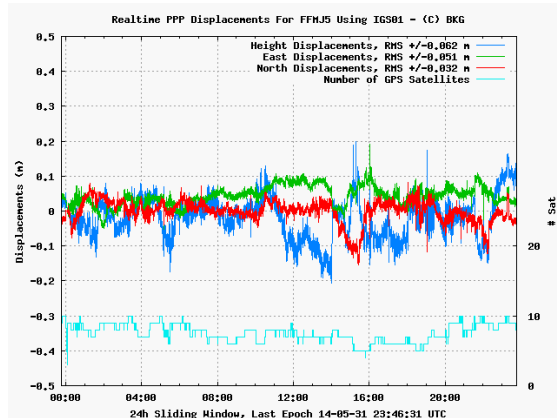


Figure 3.4: IGS01 PPP performance of station FFMJ (Frankfurt Germany) over 24 hours (IGS (2015))

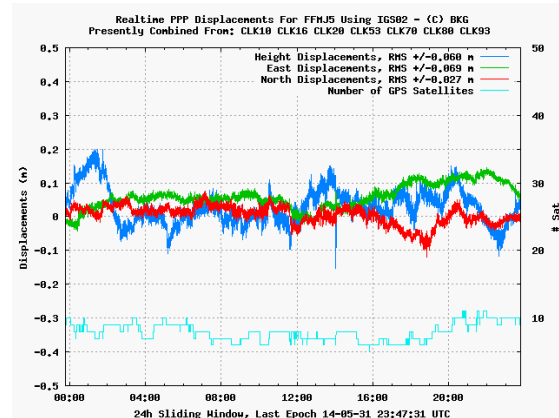


Figure 3.5: IGS02 PPP performance of station FFMJ (Frankfurt Germany) over 24 hours (IGS (2015))

3.2 The RTCM Standard

One of the most important objectives of the IGS is to develop and maintain standards and formats for GNSS data and products. Therefore the IGS joined the RTCM Special Committee 104 in the year 2008. The RTCM is a U.S organization which was established for creating fundamentals and standards for maritime telecommunication. The Special Committee 104, Differential GNSS Service, is responsible for developing standards for the transmission of corrections in GNSS applications. As member of the RTCM-SC104 committee the IGS real-time project adopted the RTCM-3 format (RTCM Special Committee No. 104 (2013)) for observation messages. In the context of the cooperation the *RTCM State Space Representation* (RTCM-SSR) format for orbit and clock correction messages has been developed, which became an official standard in May 2011. A summary of RTCM messages which are of importance in the context of this thesis are provided in Tab. 3.2.

Message Type	Content
1003	GPS L1 and L2 code and phase
1019	GPS ephemeris
1057	GPS orbit corrections to Broadcast Ephemeris
1058	GPS clock corrections to Broadcast Ephemeris
1059	GPS code biases
1060	Combined orbit and clock corrections to GPS Broadcast Ephemeris
1062	High-rate GPS clock corrections to Broadcast Ephemeris

Table 3.2: RTCM Message Types

For the delivery of the real-time observations and products to the user community and for internal operations the IGS-RT uses the *Network Transport of RTCM by Internet Protocol* (NTRIP). NTRIP (RTCM Special Committee No. 104 (2011)) became a RTCM standard in 2004 and provides a robust system for the collection and distribution of GNSS information in real-time. It is the ideal protocol for delivering and receiving RTCM messages. Users must use an NTRIP client application to establish a communication link with the data center that hosts the products of interest. For this purpose the open source software *BKG NTRIP Client* (BNC) was used in the context of this thesis. This software allows for simultaneous retrieval, decoding, converting and processing of real-time GNSS data streams. In addition, BNC also offers the possibility to store the received data in common GNSS data standards. A detailed description of the various features of the BNC software can be found in the software manual (Weber & Mervart (2014)).

Chapter 4

Precise Point Positioning PPP

Precise Point Positioning is a GNSS-based positioning technique that uses un-differenced single- or dual-frequency code pseudorange and/or phase observations from a single GNSS receiver. A precise position can be determined due to the additional compensation for orbit and clock inaccuracies by using precise orbit and clock corrections. The concept of Precise Point Positioning was first introduced in the 1970s by R.R. Anderle, and was characterized as a single station positioning with fixed precise orbit solutions and Doppler satellite observations (cf. Kouba & Héroux (2001)). Nevertheless, GPS data processing was dominated by relative positioning techniques until the late 1990's. First investigations using dual-frequency data from a single GPS receiver data for a few cm-positioning in post-processing mode were published by Zumberge et al. (1997).

Combining the precise satellite positions and clocks with a dual-frequency GNSS receiver (to remove the first-order effect of the ionosphere), PPP is able to provide position solutions at centimeter to decimeter level. The beauty of this zero-difference technique is that it does not require access to observations from one or more close, accurately surveyed, reference stations and that it provides an absolute positioning instead of the location relative to the reference station, as RTK does. Only precise orbit and clock data, based on measurements from reference stations from a relatively sparse station network (thousands of km apart would suffice) are needed. In the last years several PPP post-processing services consolidated (like GAPS from University of New Brunswick (2015) or CSRS-PPP from Natural Resources Canada (2015)) . On the other hand real-time PPP is still not so much consolidated as RTK, since it requires a longer convergence time to achieve maximum performances (in the order of tens of minutes). Therefore, within the last years a handful of services started offering real-time products, as the IGS real-time service for instance.

One of the main challenges with PPP is the integer ambiguity resolution. Simple integer ambiguity fixing of a *zero-difference* (ZD) ambiguity of a satellite-receiver pair or a *single-difference* (SD) ambiguity (in the context of this thesis the difference between two satellites) is prevented by the presence of *Uncalibrated Phase Delays* (UPD) originating from both satellite and receiver

hardware and software. Therefore in PPP usually a real-valued constant is estimated in place of the integer ambiguity. However, the estimation of real-valued ambiguities requires a large convergence period, which is the most significant factor limiting wider adoption of PPP. Furthermore the east-component within float-solutions can be improved by resolving integer phase ambiguities (cf. Ge et al. (2008)). Accordingly, integer ambiguity resolution of undifferenced carrier phase observations is considered as one of the innovative issues for GNSS research and applications in the next years (Rizos (2008)).

In conclusion, the benefits and prospects as well as the challenges of PPP are briefly summarized. Compared to the established relative positioning techniques like DGPS or RTK, PPP has several advantages:

- Contrary to RTK and DGPs only a sparse network of base stations, which is required for the computation of the satellite orbit and clock corrections, is needed and thus PPP reduces the costs,
- no simultaneous observations are necessary,
- state-space-representation of error sources instead of range corrections in observation space,
- no limit of operational range thanks to globally valid corrections and
- no network effects.

But PPP faces several challenges in order to achieve its full potential:

- A difficult observation modeling,
- a long initialization time and
- integer ambiguity resolution.

4.1 Observation model

The PPP algorithm uses as input code $P_{k,m}^i$ and phase $L_{k,m}^i$ observations from a dual-frequency receiver which can be written in the following form

$$P_{k,m}^i = \rho_k^i - c\delta t^i + c\delta t_k + \delta_{ion,m} + \delta_{tro} + \epsilon_{P,m} \quad (4.1)$$

$$L_{k,m}^i = \rho_k^i - c\delta t^i + c\delta t_k - \delta_{ion,m} + \delta_{tro} + \lambda_m B_{k,m}^i + \epsilon_{L,m}. \quad (4.2)$$

The subscript k refers to a receiver, superscript i to a satellite and subscript m to a given frequency. ρ_k^i denotes the geometric distance between the satellite and the receiver, δt^i and δt_k denote the clock errors of satellite and receiver scaled by the speed of light c , $\delta_{ion,m}$ denotes the slant ionospheric delay at the frequency m and δ_{tro} the slant tropospheric delay. $\lambda_m B_{k,m}^i$ is the float

ambiguity at the respective frequency m scaled by the wavelength λ_m and $\epsilon_{P,m}$ and $\epsilon_{L,m}$ denote the remaining errors of the code and phase measurements, respectively.

In PPP, the usual practice, when processing dual-frequency data, is to build the ionosphere-free linear combination of the pseudorange and phase observations in order to mitigate the ionospheric effect, according to

$$P_{k,3}^i = \frac{f_1^2 P_{k,1}^i - f_2^2 P_{k,2}^i}{f_1^2 - f_2^2} = \rho_k^i - c\delta t^i + c\delta t_k + \delta_{tro} + \epsilon_{P,3} \quad (4.3)$$

$$L_{k,3}^i = \frac{f_1^2 L_{k,1}^i - f_2^2 L_{k,2}^i}{f_1^2 - f_2^2} = \rho_k^i - c\delta t^i + c\delta t_k + \delta_{tro} + \lambda_3 B_{k,3}^i + \epsilon_{L,3} \quad (4.4)$$

where f_1 and f_2 denote the frequencies of the code and phase observations. The observations are processed together in a filter that solves for the different unknowns, namely the receiver coordinates, the receiver clock error, the tropospheric delay and the phase ambiguities. Usually sequential filters are used in PPP algorithms. In such a filter the process noise of the coordinates is adjusted depending on the receiver dynamics, the time evolution of the receiver clock is more or less unconstrained (white noise with a high sigma), the process noise of the tropospheric delay is adjusted to standard tropospheric activity and the ambiguities are considered as a constant per pass. Usually the slant tropospheric delay δ_{tro} is expressed as a function of the zenith delay multiplied by a mapping function. The modeling of the observables also considers several additional effects which are not listed at this point. A much more detailed description of all considerable effects will be given in Sec. 5.2.

The accuracy as well as the temporal resolution of the satellite clocks and orbits are the most important factors affecting the quality of PPP. Normally, the precise IGS products are used due to their high accuracy, however the IGS products have a latency of several hours, which makes them improper for real-time PPP. Therefore, for real-time PPP, the precise real-time satellite orbits and clocks of the IGS RTS (see Sect. 3.1) have to be used. Typically, with PPP processing, position, accuracies at the dm-level can be achieved after half an hour of observation. Enhanced accuracies can only be reached after long observation times of two hours and more. Figure 4.1 shows the north, east and up position differences (with respect to the reference position) of a float solution of the IGS station Graz Lustbühel generated using dual-frequency data and the precise IGS products. After some tens of minutes the horizontal position lies within a few cm with respect to the reference, while the height difference is at approximately 1 dm. The solution was generated with a PPP client developed at the *Graz University of Technology* (TU Graz). Detailed information on the PPP client can be found in Huber (2015).

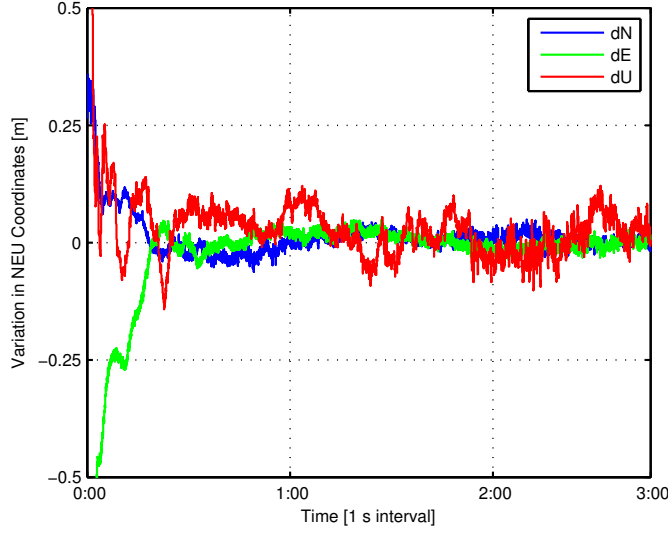


Figure 4.1: Float solution of station GRAZ using precise IGS products

4.2 Integer ambiguity resolution

A key issue in the determination of the precise position based on GNSS phase observations is the estimation of the integer ambiguities of the carrier phase measurements. The carrier phase observations are approximately two orders of magnitude more precise than the pseudorange observations. However, they are ambiguous compared to the pseudoranges by an unknown number of integer cycles. Until recently, integer ambiguities could only be resolved in double difference processing. Thereby the difference of dual-pairs of measurements is built to produce one observable. Building the difference eliminates the UPDs of the transmitter $\Delta\Phi_m^i$ and receiver $\Delta\Phi_{k,m}$ contained in the measurements, with the remaining ambiguities being integer numbers of the wavelengths. With

$$B_{k,m}^i = N_{k,m}^i + \Delta\Phi_m^i - \Delta\Phi_{k,m} \quad (4.5)$$

the *double differences* (DD), between two satellites i, j and two receivers k, l , yield

$$\Delta\nabla B_{k,l,m}^{i,j} = B_{k,m}^i - B_{k,m}^j - (B_{l,m}^i - B_{l,m}^j) = \Delta\nabla N_{k,l,m}^{i,j} \quad (4.6)$$

where the satellite UPD terms ($\Delta\Phi_m^i, \Delta\Phi_m^j$) and receiver UPD terms ($\Delta\Phi_{k,m}, \Delta\Phi_{l,m}$) cancel out.

Usually the UPDs or any linear combination thereof are not integer values, thus preventing the fixing of ambiguities to integers. In order to access the higher precision of the carrier phase using undifferenced measurements, a real-valued constant (therefore the designation float ambiguity) is estimated in place of the integer ambiguity. However, the estimation of such a parameter requires an extended convergence period. In Figure 4.2 the float ambiguities corresponding to the PPP float solution presented before (Fig. 4.1) are shown. As illustrated in the example given in Fig. 4.3 the float ambiguities seem to be quite stable after an initialization time of 3000s.

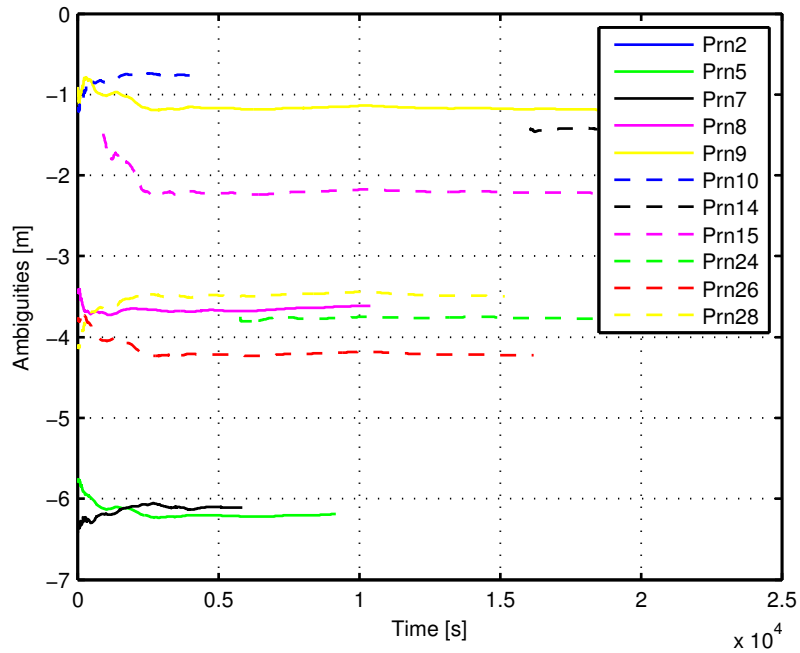


Figure 4.2: Ambiguities of the float solution

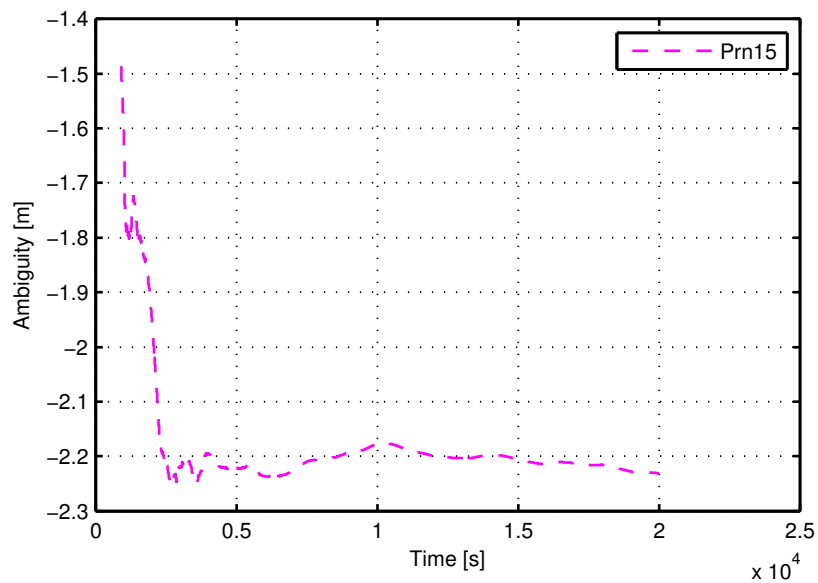


Figure 4.3: Transient behavior of the ambiguity of PRN 15

4.2.1 Methods for integer ambiguity resolution in PPP

During the last years several approaches for recovering the integer nature of zero-difference phase ambiguities, to perform integer PPP, have been developed. Thereby integer resolution is achieved by applying improved satellite products, where the UPDs are separated from the integer

ambiguities. Generally we can distinguish between two approaches, presented in two studies, to enable integer ambiguity resolution on the zero-difference level by applying improved satellite products, where phase biases have been separated from the integer ambiguities.

- On the one hand, Ge et al. (2008) decomposed undifferenced ionosphere-free ambiguities into a *wide-lane* WL and a *narrow-lane* NL part. Thereby satellite-to-satellite single-differences were used to eliminate the receiver-dependent calibration biases. Within a network of reference stations the WL phase biases were determined by averaging the fractional parts of all WL estimates using the Melbourne-Wübbena linear combination of the measurements. These WL phase biases are very stable over several days. The NL phase biases are similarly determined by averaging the fractional parts of all NL ambiguity estimates derived from the WL ambiguities and the IF observables. The NL phase biases do not have a high temporal stability and are proposed to be estimated for 15 minutes intervals. The estimated phase biases can then be used for ambiguity estimates of single receivers to recover their integer nature.
- On the other hand Laurichesse et al. (2009) proposed a quite similar approach, with the difference that the undifferenced ambiguities were directly fixed to integers. To overcome the datum problem they assigned an arbitrary value to the phase bias of a specific receiver in order to determine a first set of satellite phase biases and further the receiver-specific biases of all stations involved. The WL bias determination takes place according to that of Ge et al. (2008). The NL biases, however, are not determined specifically, but assimilated into the clock estimates. Within a network of reference stations NL ambiguities have to be identified and fixed to integers prior to estimating the clocks. Similarly, Collins et al. (2010) developed a concept, where pseudorange clocks differ from phase clocks. Both approaches aim at producing clock corrections that are able to recover the integer nature of NL ambiguities at a single receiver.

A comparison of the aforementioned methods can be found in Geng et al. (2010) and Shi & Gao (2014), which both prove their equivalency.

The method developed and published by Ge et al. (2008) forms the basis of this thesis and will further be referred to as “Phase recovery from fractional parts”. The following section gives a first detailed overview of this method.

4.2.1.1 Phase recovery from fractional parts

The term phase recovery from fractional parts describes an approach to estimate the fractional parts of the SD un-calibrated phase delays between satellites in the wide- and narrow-lane observations from a global or regional network of reference stations. By applying the obtained SD satellite UPDs as corrections to the SD ambiguities at a single station, the corrected SD ambiguities have a naturally integer nature and can therefore be fixed to integer values. In the following the concept of producing such SD UPDs will be described according to Ge et al. (2008).

For PPP in order to eliminate the ionosphere effects, the IF linear combination (see Eq. 4.4) is used, where $B_{k,3}^i$ is the related float ambiguity, which can be decomposed into a WL and NL ambiguity, according to

$$B_{k,3}^i = \frac{f_1}{f_1 + f_2} B_{k,NL}^i + \frac{f_1 f_2}{f_1^2 - f_2^2} B_{k,WL}^i \quad (4.7)$$

where c denotes the speed of light and $B_{k,NL}^i$ and $B_{k,WL}^i$ denote the narrow- and wide-lane float ambiguities, respectively. Introducing

$$B_{k,NL}^i = N_{k,NL}^i + \Delta\Phi_{NL}^i - \Delta\Phi_{k,NL}, \quad (4.8)$$

$$B_{k,WL}^i = N_{k,WL}^i + \Delta\Phi_{WL}^i - \Delta\Phi_{k,WL} \quad (4.9)$$

leads to

$$B_{k,3}^i = \frac{f_1}{f_1 + f_2} (N_{k,NL}^i + \Delta\Phi_{NL}^i - \Delta\Phi_{k,NL}) + \frac{f_1 f_2}{f_1^2 - f_2^2} (N_{k,WL}^i + \Delta\Phi_{WL}^i - \Delta\Phi_{k,WL}) \quad (4.10)$$

where $N_{k,WL}^i$ and $N_{k,NL}^i$ are WL and NL integer ambiguities, $\Delta\Phi_{WL}^i$ and $\Delta\Phi_{k,WL}$ are satellite- and receiver-specific WL UPDs, and $\Delta\Phi_{NL}^i$ and $\Delta\Phi_{k,NL}$ are satellite and receiver specific NL UPDs. In order to eliminate the receiver-dependent UPDs a satellite-to-satellite single-difference is built which can be derived from Equation 4.10 according to

$$\begin{aligned} B_{k,3}^{i,j} &= \frac{f_1}{f_1 + f_2} (N_{k,NL}^{i,j} + \Delta\Phi_{NL}^{i,j}) + \frac{f_1 f_2}{f_1^2 - f_2^2} (N_{k,WL}^{i,j} + \Delta\Phi_{WL}^{i,j}) \\ &= \frac{f_1}{f_1 + f_2} (B_{k,NL}^{i,j}) + \frac{f_1 f_2}{f_1^2 - f_2^2} (B_{k,WL}^{i,j}) \end{aligned} \quad (4.11)$$

where $N_{k,WL}^{i,j}$ and $N_{k,NL}^{i,j}$ are SD integer ambiguities and $\Delta\Phi_{WL}^{i,j}$ and $\Delta\Phi_{NL}^{i,j}$ are SD UPDs between satellites.

Estimation of the Wide-Lane UPDs: The WL and NL ambiguities cannot be estimated simultaneously. Usually, the widelane is fixed using the *Melbourne Wübbena* (MW) linear combination, which is a linear combination of both, carrier phase ($L_{k,1}^i$ and $L_{k,2}^i$) and code ($P_{k,1}^i$ and $P_{k,2}^i$) observables. The MW eliminates the effect of the ionosphere, the geometry, the clocks and the troposphere and is given by

$$L_{k,WL}^i = \frac{1}{f_1 - f_2} (f_1 L_{k,1}^i - f_2 L_{k,2}^i) - \frac{1}{f_1 + f_2} (f_1 P_{k,1}^i + f_2 P_{k,2}^i) = \lambda_{WL} B_{k,WL}^i + \epsilon_{WL} \quad (4.12)$$

where $B_{k,WL}^i$ is the WL ambiguity, which consists of the integer ambiguity and the satellite- and receiver-specific UPDs (see Eq. 4.9), and ϵ_{WL} is the measurement noise, including carrier phase and code multipath. Building the SD of Eq. 4.12, one gets the SD WL ambiguity at each epoch

as:

$$B_{k,WL}^{i,j} = \frac{L_{k,WL}^{i,j}}{\lambda_{WL}}. \quad (4.13)$$

In order to restore the integer nature of the SD WL ambiguity the SD WL UPD must be estimated. Each UPD consists of an integer and a fractional part. For restoring the integer nature only the fractional part must be known, whereas the integer part cannot be separated from the integer ambiguities anyway. The fractional part of the SD WL UPD $\delta\Phi_{WL}^{i,j}$ can be estimated using a network of reference stations. At each station all possible SD WL ambiguities are estimated using Eq. 4.13. Finally the UPD for a specific satellite pair is calculated by averaging the fractional parts of all related SD ambiguities observed at the different stations $\hat{B}_{k,WL}^{i,j}$ according to:

$$\delta\Phi_{WL}^{i,j} = \frac{1}{k} \sum_{i=1}^k \text{Frac}(\hat{B}_{k,WL}^{i,j}) \quad (4.14)$$

where $\text{Frac}()$ is a function to return the fractional part and the sum denotes the average over all stations.

Estimation of the Narrow-Lane UPDs: According to Eq. 4.11 the WL ambiguities must be fixed before the NL ambiguities can be estimated. Therefore we apply the already estimated SD WL UPDs $\delta\Phi_{WL}^{i,j}$ as corrections to the related SD WL ambiguity estimates $\hat{B}_{k,WL}^{i,j}$. The corrected SD WL ambiguity should be an integer number by construction and is derived as:

$$\hat{N}_{k,WL}^{i,j} = \hat{B}_{k,WL}^{i,j} - \delta\Phi_{WL}^{i,j}. \quad (4.15)$$

Instead of directly introducing the fixed SD WL ambiguity $\hat{N}_{k,WL}^{i,j}$ into Eq. 4.11 we reformulate the equation according to:

$$N_{k,NL}^{i,j} + \Delta\Phi_{NL}^{i,j} + \frac{f_2}{f_1 - f_2} (N_{k,WL}^{i,j} + \Delta\Phi_{WL}^{i,j}) = \frac{f_1 + f_2}{f_1} B_{k,3}^{i,j}. \quad (4.16)$$

Introducing the fixed SD WL ambiguity $\hat{N}_{k,WL}^{i,j}$ leads to:

$$N_{k,NL}^{i,j} + \Delta\Phi_{NL}^{i,j} + \frac{f_2}{(f_1 - f_2)} (N_{k,WL}^{i,j} - \hat{N}_{k,WL}^{i,j} + \Delta\Phi_{WL}^{i,j}) = \frac{f_1 + f_2}{f_1} B_{k,3}^{i,j} - \frac{f_2}{f_1 - f_2} \hat{N}_{k,WL}^{i,j}. \quad (4.17)$$

The difference between $N_{k,WL}^{i,j}$ and $\hat{N}_{k,WL}^{i,j}$ must not necessarily be zero. This is mainly caused by the integer part of the SD WL UPD $\Delta\Phi_{WL}^{i,j}$ and biases of the pseudorange which are both constant. Since both, the second and the third term on the left side of Eq. 4.17 are constant, they can be merged into the SD NL UPD according to:

$$\Delta\bar{\Phi}_{NL}^{i,j} = \Delta\Phi_{NL}^{i,j} + \frac{f_2}{f_1 - f_2} (N_{k,WL}^{i,j} - \hat{N}_{k,WL}^{i,j} + \Delta\Phi_{WL}^{i,j}), \quad (4.18)$$

$$B_{k,NL}^{i,j} = N_{k,NL}^{i,j} + \Delta\bar{\Phi}_{NL}^{i,j}. \quad (4.19)$$

In this step one has to keep consistency between the SD NL UPD and the related SD WL UPD. With the definition given in Eq. 4.19, Eq. 4.17 can be rewritten as:

$$B_{k,NL}^{i,j} = \frac{f_1 + f_2}{f_1} B_{k,3}^{i,j} - \frac{f_2}{f_1 - f_2} \hat{N}_{k,WL}^{i,j}. \quad (4.20)$$

Finally the fractional part of the SD NL UPD can be estimated from the network SD NL observations $B_{k,NL}^{i,j}$ using the same principle as for the SD WL UPD.

Chapter 5

The software PPP Post

Within the scope of this thesis the software PPP Post was developed. The source code was written in the coding language C++ and the software is running on common Linux distributions. C++ is a general purpose programming language which was developed by Bjarne Stroustrup starting in 1979 at Bell Labs, adding object-oriented features, such as classes, and other enhancements to the C programming language. General information on the programming language C++ can be found in various technical publications (e. g. Schildt (2004)) or the internet. PPP Post is based on the software RTIGU-Control which was developed at the Vienna University of Technology in the context of the thesis of Thaler (2011). The primary function of RTIGU-Control is the estimation of satellite clock corrections and the monitoring of the predicted IGU products in real-time. Since RTIGU-Control is based on the RTIGS format, that is no longer available, most of the essential parts of the software had to be replaced.

PPP Post is part of a fully functional system for the transmission and application of UPDs, which was developed within the joint project PPPserve of the Vienna University of Technology and the Graz University of Technology. The software is used at the server side and allows for the estimation of UPDs using observations of a regional network (Hinterberger et al. (2015)). The software is based on the concept of a real-time software and can either be used in a *Real-Time Mode* (RTM) or in a *Real-Time Simulation Mode* (RSM). The opportunity to execute the software also in a RSM offers the possibility to investigate the influence of external data sources, different error models and other parameters. The estimation of the UPDs itself is based on the approach of Ge et al. (2008), which was already briefly described in Sect. 4.2. The approach relies on the estimation of the fractional parts of the single-difference uncalibrated phase delays between satellites. The estimated UPDs can be forwarded to a PPP user in the field. By applying the obtained SD UPDs as corrections to the SD ambiguities at the user side, the corrected SD ambiguities have an integer nature and can therefore be fixed to integer values. A much more detailed description of the approach will be given in the remainder of this section.

As it can be gathered from Figure 5.1, PPP Post primarily consists of four segments:

1. Data source segment

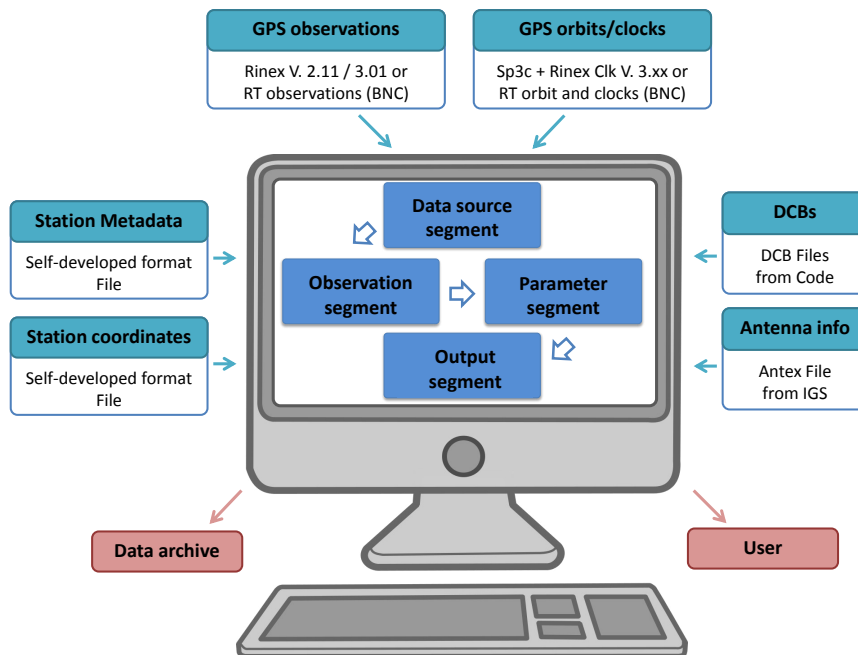


Figure 5.1: Structure of PPP Post

This segment serves as interface between several external data sources of other providers or institutions and the PPP Post software. It contains functions for the real-time as well as the post-processing case of application.

2. Observation segment

This segment serves for processing the observations prior to the parameter estimation.

3. Parameter segment

This segment contains the parameter estimation itself.

4. Output segment

This segment serves as interface between the PPP Post software and the user. Like the data source segment it contains functions for the real-time as well as post-processing applications.

In addition, several auxiliary functions like time conversions (GPS - UTC, GPS - calendar time), coordinate transformations, numerical integration algorithms, to name just a few, exist. In further consequence the functional principle of each individual segment shall be described in detail in the context of this section.

5.1 Data source segment

The data source segment serves as interface between several external data sources of other providers or institutions and the PPP Post software. Concerning the external data one has to

distinguish between the following three fundamental groups of data sources, see also Figure 5.1:

- Observation data: GPS observations from a designated network of reference stations.
- Orbit data: precise satellite orbits and satellite clock corrections.
- Additional data sources: antenna corrections, differential code biases, station information and station coordinates.

The source of the observation and orbit data depends on the used processing mode of the PPP Post software. In case of the RTM the observation as well as the orbit data must be obtained in real-time. The satellite orbits and clock corrections are obtained from the IGS real-time service, see Chap. 3.1. The observations are obtained from stations of a real-time network using the BNC software as interface between the real-time data sources and the PPP Post software. In contrast, using the RSM the observation and orbit data are obtained from ASCII files in the respective formats. Therefore this mode allows for the use of the precise orbit products of the IGS, see Sect. 3. Of course, recorded real-time data can be used as well. The input of all the other data, i.e. station metadata, station coordinates, correction parameters for the code observations and correction parameters for the antenna phase centers are independent of the processing mode used. All data sources are available as ASCII files in the respective formats. The data is obtained at the start of the program and is updated at fixed points in time, depending on the update interval of the data sources itself. By means of the routines of the data source segment, the data is extracted from the ASCII files and stored in the internal data structure of the PPP Post software.

5.1.1 Observation data

In the RTM the observations are obtained from a RTS. By means of the BNC software the real-time observations, of a designated set of stations are gathered, synchronized and forwarded over a TCP/IP port. The PPP Post software accesses the synchronized observations over this specific port and stores the observations station-wise in the internal data structure. In the RSM the observations are read from ASCII files provided in the so-called *Receiver Independent Exchange Format* (RINEX) either in Version 2.11 (Gurtner & Estey (2007)) or Version 3.01 (Gurtner & Estey (2009)). As already mentioned, the PPP Post software is based on the concept of a real-time software. That means that the observations are obtained and processed epoch by epoch, independent of the case of application. Since the software uses GPS observations only, the observations of all the other satellite systems are ignored.

5.1.2 Orbit data

Concerning the ephemerides we have to distinguish between the real-time and post-processing case as well. A proper operation of the PPP Post software requires very precise satellite orbits and clock corrections. In case of the RTM the only products which satisfy these requirements are the

Parameter	Explanation
ID	Satellite identification number
t_e	Reference epoch of the satellite ephemerides
\sqrt{a}	Square root of semi major axis of the orbital ellipse
e	Numerical eccentricity of the ellipse
M_0	Mean anomaly at the reference epoch t_e
ω_0	Argument of the perigee
i_0	Inclination of the orbital plane
Ω_0	Longitude of ascending node at weekly epoch t_0
Δ_n	Mean motion difference
\dot{i}	Rate of inclination angle
$\dot{\Omega}$	Rate of node's right ascension
C_{uc}, C_{us}	Correction coefficients (argument of perigee)
C_{uc}, C_{us}	Correction coefficients (geometric distance)
C_{ic}, C_{is}	Correction coefficients (inclination)
<i>IODE</i>	Issue of Data, Ephemerides
t_e	Reference epoch of the satellite clock
a_0, a_1, a_2	Polynomial coefficients of the satellite clock error
<i>IODC</i>	Issue of Data, Clocks

Table 5.1: Broadcast ephemerides (GPS)

products of the IGS real-time service. On the contrary in the RSM it is possible to use precise post processed IGS ephemerides.

5.1.2.1 Broadcast ephemerides and IGS real-time corrections

The products of the IGS real-time service are provided as orbit and clock corrections to the broadcast ephemerides. The ephemerides and the corrections are obtained from the IGS real-time service and are forwarded to the PPP Post software by the aid of the BNC software. The ephemerides are predicted satellite orbits, which are usually transferred from the satellite to the user by means of the navigation message. Due to their low quality of about 1 m they usually cannot be used in precise applications. The ephemerides basically contain records with general information, records with information on the satellite orbits and records with information concerning the satellite clocks. In case of GPS the information about the satellite orbit is provided in terms of Keplerian parameters together with their temporal variations. The satellite clock correction is provided as coefficients of a polynomial of second degree. All parameters are summarized in Table 5.1. The satellite position and clock correction at each epoch t can be computed using the equations given in Appendix A.

The ephemerides are regularly updated. In case of GPS the update rate amounts to approximately two hours. In order to detect any change in the ephemeris representation the issue of data ephemeris (*IODE*) and issue of data clock (*IODC*) are used. Since the orbit and clock information can be updated at different points in time, two separate quantities are used.

As already mentioned, a proper operation of the PPP Post software requires precise satellite orbits and clock corrections. To reach the required accuracy and temporal resolution the orbit and clock corrections of the IGS real-time service are used. The data contained therein must be combined with the corresponding broadcast messages. For the assignment the previously stated identification numbers IODE and IODC are used. The orbit correction consists of parameters that are provided in terms of radial, along-track and cross-track components. These parameters are used to generate a correction vector $\vec{\delta}x$ w.r.t the position calculated using the broadcast ephemerides. According to Eq. 5.1 the resulting orbits are expressed within the current realization of the ITRS, namely the ITRF08 (RTCM Special Committee No. 104 (2013)):

$$\vec{R}_{Orbit} = \vec{R}_{Broadcast} - \vec{\delta}x \quad (5.1)$$

with

\vec{R}_{Orbit}	satellite position corrected by the RT orbit correction message,
$\vec{R}_{Broadcast}$	satellite position computed from the broadcast ephemerides parameter set identified by the IODE in the orbit correction message,
$\vec{\delta}x$	RT satellite position correction.

The satellite position correction is obtained using the following equations:

$$\vec{e}_{along} = \frac{\vec{r}}{|\vec{r}|}, \quad (5.2)$$

$$\vec{e}_{cross} = \frac{\vec{r} \times \dot{\vec{r}}}{|\vec{r} \times \dot{\vec{r}}|}, \quad (5.3)$$

$$\vec{e}_{radial} = \vec{e}_{along} \times \vec{e}_{cross}, \quad (5.4)$$

$$\vec{\delta}x = [\vec{e}_{radial}, \vec{e}_{along}, \vec{e}_{cross}] \vec{\delta}O, \quad (5.5)$$

with

$\vec{r} = \vec{R}_{Broadcast}$	broadcast satellite position vector,
$\dot{\vec{r}} = \dot{\vec{R}}_{Broadcast}$	broadcast satellite velocity vector,
\vec{e}_i	direction unit vector in the ECEF, $i \in \{radial, along, cross\}$,
$\vec{\delta}O$	RT orbit correction vector.

The complete orbit correction $\vec{\delta}O$ is computed from the individual correction terms and their velocities according to

$$\vec{\delta}O = \begin{bmatrix} \delta O_{radial} \\ \delta O_{along} \\ \delta O_{cross} \end{bmatrix} + \begin{bmatrix} \delta \dot{O}_{radial} \\ \delta \dot{O}_{along} \\ \delta \dot{O}_{cross} \end{bmatrix} (t - t_0) \quad (5.6)$$

with

- t time,
- t_0 reference time obtained from the orbit correction message,
- $\delta O_i, \delta \dot{O}_i$ orbit correction terms from the orbit message, $i \in \{radial, along, cross\}$.

The clock message contains parameters to calculate the clock correction, which has to be applied to the broadcast satellite clock correction using

$$t_{Satellite} = t_{Broadcast} - \frac{\delta c}{c} \quad (5.7)$$

where

- $t_{Satellite}$ satellite clock correction corrected by the RT clock correction,
- $t_{Broadcast}$ satellite clock correction computed from the broadcast ephemerides parameter set identified by the IODC in the orbit correction message,
- δc RT satellite clock correction.

The clock correction is calculated according to

$$\delta c = C_0 + C_1(t - t_0) + C_2(t - t_0)^2 \quad (5.8)$$

with

- t time,
- t_0 reference time obtained from the orbit correction message,
- C_i polynomial coefficients from the clock correction message.

5.1.2.2 Precise ephemerides

Operating the PPP Post software in the RSM allows for the use of the precise products of the IGS (see Chap. 3) in addition to the previously mentioned broadcast ephemerides and RT corrections. The precise products can be obtained from one of the IGS data centers (CDDIS, IGN, ...) using anonymous ftp transfer. The products are provided in terms of ASCII Files in the so-called SP3c format¹. The satellite orbits are presented in the form of equidistantly distributed satellite positions (data points). They are expressed in the recent realization of the ITRS (currently the ITRF08) and have a temporal resolution of 15 minutes. The satellite's position for a given point in time is calculated by interpolating the data at the needed epoch. In addition to the positions, the clock error of every satellite available is given as well. However, the temporal resolution of 15 minutes is not enough to reach the requested cm-level accuracy. Therefore the IGS analysis centers provide clock corrections with a temporal resolution of 30 seconds in terms of the so-called clock RINEX format². The satellite clock corrections are also provided in terms of equidistantly distributed data points.

¹<https://igsb.jpl.nasa.gov/igsb/data/format/sp3c.txt>

²https://igsb.jpl.nasa.gov/igsb/data/format/rinex_clock300.txt

5.1.3 Additional data sources

Additional data sources include the input parameters, which undergo no or no significant changes on long time perspectives or are available far in advance. These parameters are available in the form of ASCII files and the following data sources are assigned to this category.

5.1.3.1 Differential Code Biases DCBs

Besides the phase observations, the code observations experience instrumental time delays as well. These delays are denoted as Code Biases. Absolute values of these biases cannot be estimated, but it is possible to estimate differences between them. These differences are denoted as Differential Code Biases. In case of GPS the most important DCBs are those between P1 and C1 (P1 - C1) and between P1 and P2 (P1 - P2). At this point it should be noted that the DCBs are estimated using a globally distributed network based on a zero-mean condition, and therefore they contain an arbitrary offset.

All IGS products, including the ephemerides are, by convention referred to a special linear combination (the IF linear combination, $2.55 * CB(P1) - 1.55 * CB(P2)$) of the Code Biases (CB) CB(P1) and CB(P2) (Kouba (2009)). Nevertheless a wide range of receivers does not provide the required P1 and P2 observations but rather the C1 and P2 observations. Within the PPP Post software the DCBs are used to generate P1 observations at every station collecting C1 data according to the following equation.

$$P1 = C1 + c \cdot DCB_{P1-C1} \quad (5.9)$$

In this way conformity between given code measurements and IGS products can be guaranteed. Detailed information on the usage of the DCBs in the context of all linear combinations can be found in (Schaer & Steigenberger (2006)).

The DCBs reach several nanoseconds and are very stable over longer periods (several weeks). In the context of this work monthly solutions provided by the *Center of Orbit Determination in Europe* (CODE) at the University of Bern are used. Due to the high stability the usage of monthly solutions has no significant effect on the accuracy of the estimated UPDs.

5.1.3.2 Absolute Antenna Offsets

The precise IGS orbit and clock products are referred to the center of mass of the satellites. Since the observations are referred to the antenna phase center, an offset correction has to be applied. Caution should be exercised, if orbit and clock corrections of the IGS real-time service are used. The IGS real-time service usually provides two different versions of the corrections, which differ with respect to the reference point of the satellite's position. Depending on the version, the corrected position is either referred to the center of mass or to the antenna phase center of the satellite.

The absolute antenna offsets are provided by the IGS in terms of the ANTEX¹ file igs08.atx². IGS uses different antenna phase center vectors for every single satellite. In addition to the offsets of the satellite antennas the file also provides offsets for a variety of GNSS receiver antennas available on the market, which are derived from an absolute calibration of the receiver antenna phase center corrections (Navipedia (2013)).

5.1.3.3 Station coordinate and information file

For a lot of corrections, like the mapping functions, the antenna phase center offsets or the phase wind-up effect, reference coordinates of the stations are required. Since the positions are not determined within the parameter estimation, they are obtained from routinely estimated network solutions. Such solutions are provided by various analysis centers for different networks at regular intervals in terms of ASCII Files in the so-called SINEX³ format. The positions of the stations are given, usually daily or weekly, in a designated epoch of the ITRF08. This datum is consistent with the datum of the ephemerides of the IGS which are given w.r.t. to daily solutions of the ITRF08. At program start the station positions of the latest solution available are obtained and fixed as reference coordinates.

In addition to the station coordinate file, a station information file is read at each program start. This file contains all relevant station-related information, like station names, antenna and receiver types as well as antenna eccentricities. This information is required to model station-specific errors. In case of a change of the equipment at one station, the station information file has to be modified manually.

5.2 Observation segment

The primary function of the observation segment is the preparation of the GPS observation data. It works the same way for the RTM and the RSM and consists of a series of functions and algorithms for the manipulation, correction and control of the observation data. Thereby the observations at each station are processed separately and afterwards all information needed for the subsequent processing is stored in the internal data structure. Each group of observations to one satellite, comprising P1/C1, L1, P2 and L2 observations, undergoes a maximum of three steps:

1. Application of the DCBs (see Eq. 5.9) and generation of all required linear combinations (L3, MW, NL).
2. Cycle slip detection and validation of the satellite eclipse condition.
3. Application of all required corrections.

¹<https://igs.cb.jpl.nasa.gov/igs/cb/station/general/antex14.txt>

²<https://igs.cb.jpl.nasa.gov/igs/cb/station/general/igs08.atx>

³<http://www.iers.org/IERS/EN/Organization/AnalysisCoordinator/SinexFormat/sinex.html>

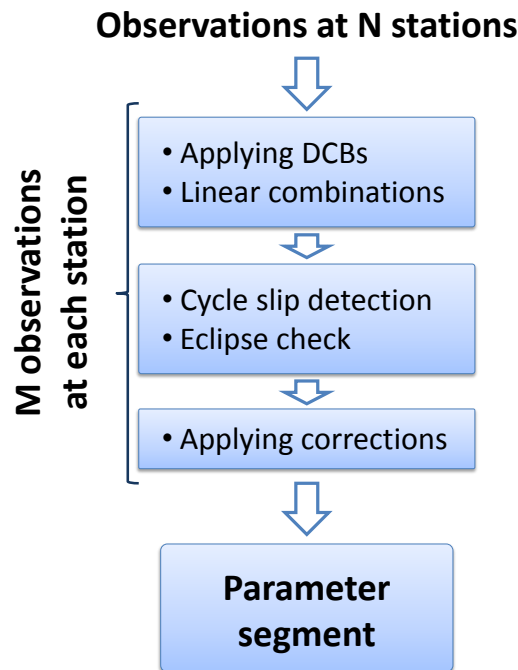


Figure 5.2: Observation segment

5.2.1 Application of the DCBs and generation of LCs

In the first part of the observation segment all given C1 observations are corrected using Eq. 5.9 and the monthly solutions of the DCBs provided by CODE. In this way full consistency between the code measurements and the used IGS orbits (see Sect. 5.1.2) can be achieved. Once all code observations have been corrected, all linear combinations which are requested for the further processing are built. This combinations include the IF linear combination, for both code and phase observations, as well as the Melbourne Wübbena linear combination.

The IF linear combination for code and phase observations is built by means of Eqs. 4.3 and 4.4 and is the essential quantity for the further progress of the calculation. Here the influence of the ionosphere can be eliminated or, more precisely, reduced. The term “ionosphere-free” is not fully correct because only terms up to the first order are eliminated completely. Since these terms correspond to 99.9 % of the total ionospheric time delay, the linear combination satisfies the aimed accuracy. At this point it should be mentioned that building this combination significantly increases the measurement noise.

The second linear combination which is required for the further progress of the calculation is the so-called Melbourne Wübbena linear combination which can be built by means of Eq. 4.12. This combination of both, carrier phase and code observables eliminates the dispersive (ionosphere) as well as the geometric (clocks, troposphere, etc.) influences. The MW LC contains the WL ambiguity plus satellite and receiver instrumental delays and provides a simple option for fixing the WL ambiguity due to the relatively long wavelength. Again it has to be stated that the noise of the MW LC is governed by the introduced code noise and therefore it is significantly

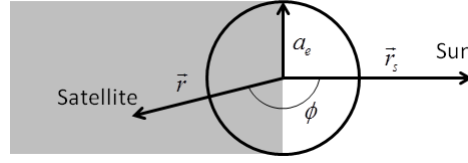


Figure 5.3: Cylinder model for the shadow of the earth

increased compared to the phase noise.

5.2.2 Cycle slip detection and validation of the satellite eclipse condition

Before the observations are further processed it is verified whether jumps occur in the ambiguity term of the phase observations. These jumps are denoted as cycle slips and they can occur for example if the signal from the satellite to the receiver is interrupted by an obstruction or a cycle slip also can be the result of strong ionospheric influences. For the detection of such jumps in the ambiguity term a very simple algorithm based on the already known MW linear combination is used. The algorithm is based on the continuous estimation of the mean $m_{L_{WL}}$ and sigma $s_{L_{WL}}^2$ values of the MW observation L_{WL} (see Eq. 4.12) for each epoch k by means of the following equations:

$$\begin{aligned} m_{L_{k,WL}}(k) &= \frac{k-1}{k} m_{L_{k,WL}}(k-1) + \frac{1}{k} L_{k,WL}(k), \\ s_{L_{k,WL}}^2(k) &= \frac{k-1}{k} s_{L_{k,WL}}^2(k-1) + \frac{1}{k} (L_{k,WL}(k) - m_{L_{k,WL}}(k))^2. \end{aligned} \quad (5.10)$$

A cycle slip is assumed, if a measurement differs from the mean bias value by more than a predefined number of the standard deviation $s_{L_{WL}}^2$ threshold (more details can be found in Blewitt (1990)). The mean bias estimate is highly affected by the noise of the code observations (especially in case of satellites at low elevation) but as the number of averaged samples increases, the estimation becomes more stable and robust. Nevertheless, small jumps can escape the detector, particularly at the beginning of the data series.

In addition to the cycle slip detection it is verified whether a satellite passes into the shadow of the earth. Such a period, each GPS satellite has two periods per year (Mervart (1995)), is denoted as eclipse period and can lead to a degradation of high-precision GNSS positioning. Due to improper modeling of the solar radiation pressure in the dynamics of the satellite orbit errors are introduced into the measurements. Furthermore during eclipse seasons, satellites are subject to rapid rotations, which effects the phase data (Kouba (2009)). As a consequence satellites in an eclipse period can significantly degrade high-precision GNSS positioning. Therefore, observational data of satellites under such conditions are removed using a straightforward algorithm, based on a simple cylinder model for the shadow of the earth. The eclipse condition is defined as follows

$$\cos \phi = \frac{\vec{r} \cdot \vec{r}_S}{|\vec{r} \cdot \vec{r}_S|} < 0 \quad (5.11)$$

and

$$|\vec{r}| \sqrt{1 - \cos^2 \phi} < a_e \quad (5.12)$$

where \vec{r} and \vec{r}_S are the vectors from the geocenter to the satellite and to the sun and a_e is the mean equatorial radius of the earth, respectively.

5.2.3 Application of required corrections

This section covers all additional corrections which must be applied to the previously built ionosphere-free linear combination. It is not necessary to apply the corrections to the MW linear combination since all critical effects are eliminated in this LC. First of all the observation equations already given in Sect. 4.1 have to be adapted. Both, the code and the carrier phase measurements are affected by a variety of systematic errors or biases and a random noise which have been neglected so far. To achieve high accuracy all relevant systematic errors must be carefully modeled. Taking these errors into account the code 4.3 and phase 4.4 observation equations can be completed by

$$P_{k,3}^j = \rho_k^j + c\delta t_k + \delta_{tro} + \delta_{rel} + \delta_{tide} + \epsilon_{P,3}, \quad (5.13)$$

$$L_{k,3}^j = \rho_k^j + c\delta t_k + \delta_{tro} + \delta_{rel} + \delta_{tide} + \lambda_3\omega + \lambda_3 B_{k,3}^j + \epsilon_{L,3} \quad (5.14)$$

where

$P_{k,3}^j$ and $L_{k,3}^{js}$	are the code and phase measurements with 3 denoting the frequency of the IF linear combination,
ρ_k^j	denotes the geometric distance between receiver and satellite,
$c\delta t_k$	is the receiver clock error scaled by the speed of light c ,
δ_{tro}	denotes the tropospheric effect,
δ_{rel}	denotes relativistic effects,
δ_{tide}	denotes the solid Earth tide and ocean loading tide effects,
$\lambda_3\omega$	denotes the phase wind up effect,
$B_{k,3}^j$	is the ambiguity for the respective frequency, where the ambiguity is composed of an integer part plus a receiver and satellite specific UPD (see Eq. 4.5) and
$\epsilon_{P,3}$ and $\epsilon_{L,3}$	are the remaining errors affecting the code and phase measurements.

Both, the satellite clock error and the satellite's position are introduced as known. All the other effects listed above are explained in more detail hereafter.

5.2.4 Atmospheric effects

Electromagnetic waves experience frequency-dependent influences concerning the direction and velocity of propagation, when they pass through the atmosphere of the Earth (Seeber (2003)). With respect to the signal propagation the atmosphere is divided into the neutral atmosphere up to about 100 km and the ionosphere, extending from 60-2000 km depending on time and location (Böhm & Schuh (2013)). The impact on the observed signals is much larger than the accuracy required, therefore both effects must be properly handled. The frequency-dependent (dispersive) ionospheric delay of the first order can be eliminated by forming linear combinations of the emitted carrier signals on (at least) two frequencies. The terms of the second and higher orders are small enough to be neglected. On the contrary, the frequency-independent (non dispersive) tropospheric delay must be modeled or considered within the adjustment process.

In general the total tropospheric delay (assuming azimuthal symmetry) is described as

$$\Delta L(e) = \Delta L_h^z \cdot mf_h(e) + \Delta L_w^z \cdot mf_w(e) \quad (5.15)$$

where ΔL_h^z and ΔL_w^z are the hydrostatic and wet zenith delays, and $mf_h(e)$ and $mf_w(e)$ are the so-called mapping functions, which provide the ratio of the delay in signal direction to the delay in zenith direction. The input parameter of both mapping functions is the elevation angle e of the signal direction from the receiver to the satellite. Currently the best mapping function is the Vienna Mapping Function (Böhm et al. (2009)) which is also recommended in the IERS Conventions (2010). The hydrostatic delay, caused by the dry gases in the troposphere, varies in quite a predictable manner (1% in a few hours) and can be modeled from surface pressure and temperature using the law of ideal gases. The hydrostatic delay amounts to about 2.3 m in zenith direction for stations at sea level and increases for lower elevations, where it can reach up more than a few meters. The wet delay, caused by the water vapor in the atmosphere, varies faster and in a quite unpredictable way, which makes it very difficult to model. Hence for high-precision applications, this delay is estimated. In contrast to the hydrostatic delay the wet delay is small and reaches only some tens of centimeters (Navipedia (2013)).

In the literature (Hofmann-Wellenhof et al. (2008); Xu (2003)) several nominal tropospheric models can be found, which mainly differ regarding the assumptions made on the vertical profiles and mappings. There are two major kinds of models: accurate but generally also more complex models, which need surface meteorological data or less accurate models, where no meteorological data is needed.

Within the framework of this thesis a very simple model (Navipedia (2013)) was implemented into the PPP Post software. This model does not need any surface meteorological data and uses the mapping of niell (Niell (1996)), that considers different obliquity factors for the wet and dry components. The wet component of the tropospheric delay is estimated together with the other

Coefficient ξ	Latitude (ϕ)				
	15°	30°	45°	60°	75°
	Average				
a	1.2769934e-3	1.2683230e-3	1.2465397e-3	1.2196049e-3	1.2045996e-3
b	2.9153695e-3	2.9152299e-3	2.9288445e-3	2.9022565e-3	2.9024912e-3
c	62.610505e-3	62.837393e-3	63.721774e-3	63.824265e-3	64.258455e-3
	Amplitude				
a	0.0	1.2709626e-5	2.6523662e-5	3.4000452e-5	4.1202191e-5
b	0.0	2.1414979e-5	3.0160779e-5	7.2562722e-5	11.723375e-5
c	0.0	9.0128400e-5	4.3497037e-5	84.795348e-5	170.37206e-5
	Height Correction				
a_{ht}	2.53e-5				
b_{ht}	5.49e-3				
c_{ht}	1.14e-3				

Table 5.2: Coefficients of the hydrostatic mapping function

parameters, which allows a huge simplification of the model for the vertical delays:

$$\begin{aligned} L_h^z &= a \cdot e^{-bh}, \\ L_w^z &= L_{w,0}^z + \Delta L_{w,0}^z \end{aligned} \quad (5.16)$$

where $a = 2.3$ m, $b = 0.116 \cdot 10^{-3} \frac{1}{m}$ and h is the height over sea level in meters. $L_{w,0}^z = 0.1$ m and $\Delta L_{w,0}^z$ is estimated as a random-walk process in the Kalman filter together with the other parameters. The factors for the dry and wet component of Niell's mapping function can be computed from the following equations where, e is the elevation angle of the observation to the satellite and h is the receiver height, in kilometer:

Hydrostatic mapping function:

$$\begin{aligned} mf_h(e, h) &= m(e, a_d, b_d, c_d) + \Delta m(e, h) \\ \Delta m(e, h) &= \left[\frac{1}{\sin e} - m(e, a_{ht}, b_{ht}, c_{ht}) \right] \cdot h \end{aligned} \quad (5.17)$$

The parameters a_d, b_d, c_d can be computed according to the following equation, where t is the time from January 0.0 in days and T_0 is taken as DoY 28.

$$\xi(\phi, t) = \xi_{avg}(\phi) - \xi_{amp}(\phi) \cdot \cos\left(2\pi \frac{t - T_0}{365.25}\right) \quad (5.18)$$

where the parameters $\xi_{avg}(\phi)$ and $\xi_{amp}(\phi)$ are linearly interpolated from Table 5.2. a_{ht}, b_{ht}, c_{ht} can be taken directly from Table 5.2

Coefficient ξ	Latitude (ϕ)				
	15°	30°	45°	60°	75°
a	5.8021897e-4	5.6794847e-4	5.8118019e-4	5.9727542e-4	6.1641693e-4
b	1.4275268e-3	1.5138625e-3	1.4572752e-3	1.5007428e-3	1.7599082e-3
c	4.3472961e-2	4.6729510e-2	4.3908931e-2	4.4626982e-2	5.4736038e-2

Table 5.3: Coefficients of the wet mapping function

Wet mapping function:

$$mf_w(e) = m(e, a_w, b_w, c_w)$$

$$m(E, a_w, b_w, c_w) = \frac{1 + \frac{a}{1 + \frac{b}{1+c}}}{\sin e + \frac{a}{\sin e + \frac{b}{\sin e + c}}} \quad (5.19)$$

The a_w, b_w, c_w are latitude dependent and are linearly interpolated from Table 5.3.

5.2.5 Relativistic effects

In the GNSS technology, relativistic effects, which originate from the relative motion of the clock and the potential difference between the satellite and the users, must be taken into account. An overview of these effects is given for example in Ashby (2003).

The major relativistic effects can be captured by a frequency shift of the nominal GPS frequency, which corresponds to $f_0 = 10.23$ MHz. The effect of General Relativity, originating from the difference between the gravitational field at the satellite and the receiver on the earth, causes a faster run of the satellite clocks. The effect of the Special Relativity, originating from the higher velocity of the satellite with respect to the receiver, causes the satellite clocks to run slower than the receiver clocks. To account for these two constant effects the satellite clock frequency is adjusted to the lower frequency of 10.22999999543 MHz.

On top of this constant frequency shift periodic effects are caused by the eccentricity of the satellite orbits and which varies with the satellite position in its plane. The clock correction can be estimated with the help of the Keplerian parameters according to the following formula

$$\delta t_{rel} = \frac{2}{c^2} \sqrt{GM_E a e} \sin E \quad (5.20)$$

where G denotes the gravitational constant, M_E the mass of the earth, a the semi major axis, e the orbital eccentricity and E the eccentric anomaly. Equation 5.20 can also be written as

$$\delta t_{rel} = 2 \frac{\vec{r} \cdot \vec{v}}{c^2} \quad (5.21)$$

where \vec{r} and \vec{v} are the satellite position and velocity vector, respectively. Fig. 5.4 illustrates the variation in range for the satellites in view of a receiver in Belfast. It can be seen, that the variation

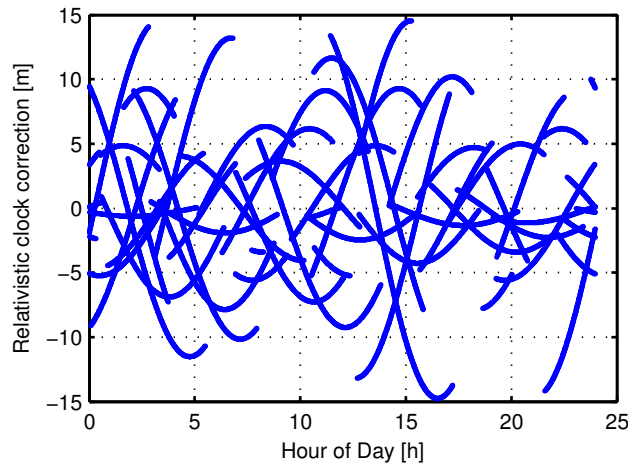


Figure 5.4: Relativistic clock corrections

in range can reach up to 15 meters. Therefore, neglecting this correction results in position errors of several meters.

On the other hand also the earth's oblateness causes a periodic fractional frequency shift with a period of almost 6 hours and an amplitude of about one part in 10^{14} . However, this effect is very small, explaining its effect on the satellite's clock frequency has been neglected until recently (Ashby (2003)).

Another effect which must be accounted for, is the Sagnac effect which can reach up to 30 meters (Xu (2003)). The situation is illustrated in Fig. 5.5. Due to the earth's rotation the earth-fixed system rotates during the signal transmission time, hence the system at the signal emission time t'_s does not coincide with the system at the signal reception time t'_r . In order to correct for this effect the coordinate system at the signal emission time is transformed to the system at the signal reception time by a simple rotation around the z-axis. The required rotation angle is calculated as

$$\omega \cdot \Delta t \quad (5.22)$$

with ω as the rotation rate of the earth and Δt as the signal travel time from the satellite to the receiver.

The so-called Shapiro delay is a secondary relativistic effect that is required for high precision PPP. The gravitational field produces a space-time curvature of the satellite signal and therefore the Euclidean range must be corrected by an amount given by the expression

$$\delta \rho_{rel} = \frac{2GM_E}{c^2} \ln \frac{r^s + r_r + \rho_r^s}{r^s + r_r - \rho_r^s} \quad (5.23)$$

where r^s and r_r are the geocentric distances of the satellite and the receiver and ρ_r^s is the distance between the satellite and the receiver. Fig. 5.6 illustrates the Shapiro signal propagation delays for the satellites in view of a receiver in Belfast. As visible, the values can reach a maximum of

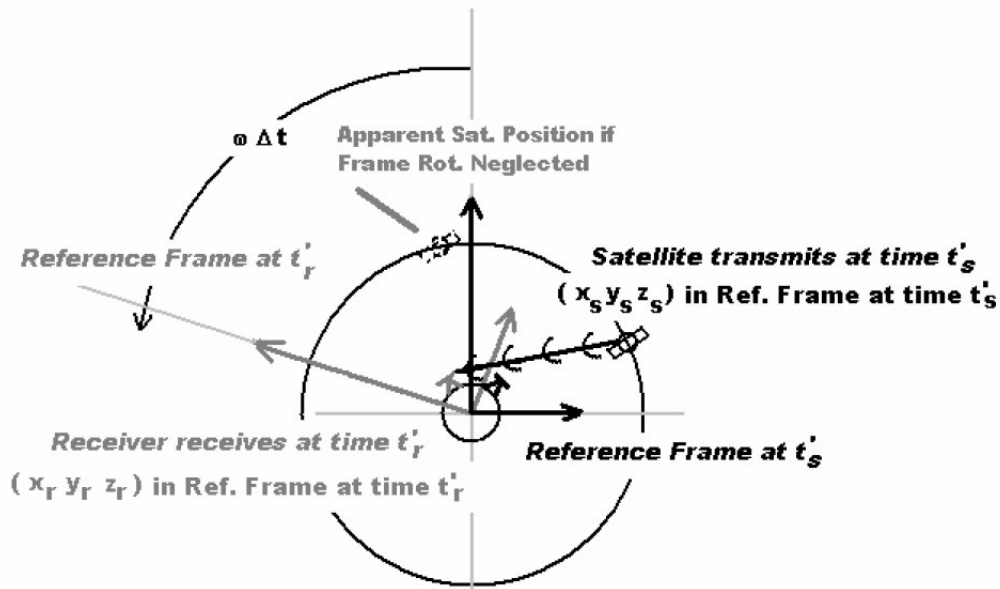


Figure 5.5: Problem of the rotation of the reference frame (Radovanovic (2002))

approximately 2 cm only. However, in case of PPP, it is usually taken into account. A very good review of the relativistic effects on GPS signals in general can be found in Ashby (2003).

5.2.6 Antenna phase center offset

5.2.6.1 Satellite antenna phase center correction

The GNSS measurements between the satellite and the receiver are referred to the phase centers of the two antennas. According to the orbit data used, the position of the satellite is either referred to the antenna phase center (APC) or to the center of mass of the satellite. The broadcast ephemeris and the corresponding real-time orbit and clock corrections are referred to the phase center of the satellite and, therefore, no additional correction is needed. The precise orbits instead are referred to the center of mass of the satellite, which makes it necessary to apply a phase center correction in precise applications.

This phase center offset vector is usually given in a satellite-fixed coordinate system. The origin of the system coincides with the satellite's center of mass, the z-axis is pointing to the earth's center, the y-axis lays in the plane perpendicular to the vector pointing to the sun and the x-axis completes the right-handed coordinate system. Before the correction can be applied, it is necessary to transform the offset vector into the ECEF frame. In order to do this the unitary vectors of the satellite-fixed system ($\vec{e}_x, \vec{e}_y, \vec{e}_z$) are expressed with respect to the ECEF frame

$$\vec{e}_z = -\frac{\vec{r}}{|\vec{r}|}, \quad (5.24)$$

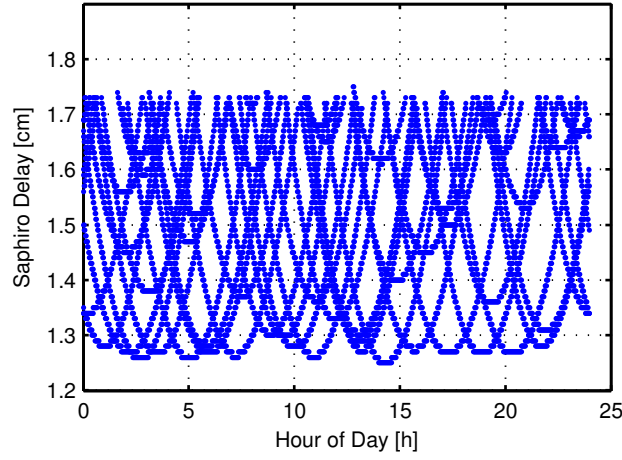


Figure 5.6: Shapiro delay correction

$$\vec{e}_y = \frac{\vec{e}_z \times \vec{n}_{SUN}}{|\vec{e}_z \times \vec{n}_{SUN}|}, \quad (5.25)$$

$$\vec{e}_x = \vec{e}_y \times \vec{e}_z, \quad (5.26)$$

$$\vec{n}_{SUN} = \frac{\vec{r}_S - \vec{r}}{|\vec{r}_S - \vec{r}|}, \quad (5.27)$$

with \vec{r} and \vec{r}_S denoting the position vectors of the satellite and the sun, respectively. With $\vec{\Delta}_{APC}$ being the antenna phase center offset vector in the satellite-fixed coordinate system, the satellite antenna phase center coordinates in the ECEF frame are

$$\vec{r}^{APC} = \vec{r}^{MC} + R\vec{\Delta}_{APC} \quad (5.28)$$

where

$$R = [\vec{e}_x, \vec{e}_y, \vec{e}_z]. \quad (5.29)$$

It should be emphasized that the antenna phase center corrections ($\vec{\Delta}_{APC_{L1}}, \vec{\Delta}_{APC_{L2}}$) are frequency-dependent and that the antenna phase center offset for the IF combination $\vec{\Delta}_{APC_{L3}}$ can be directly estimated using the following equation:

$$\vec{\Delta}_{APC_{L3}} = \frac{f_1^2 \vec{\Delta}_{APC_{L1}} - f_2^2 \vec{\Delta}_{APC_{L2}}}{f_1^2 - f_2^2}. \quad (5.30)$$

In the context of this thesis the publicly available APC correction models provided by the IGS (see Sect. 5.1.3.2) are used. An example of satellite antenna phase center corrections for various types of GPS satellites is given in Tab. 5.4.

For highly precise position solutions also the variations of the satellite antenna phase center should be taken into account. However, common PPP users usually only take care about the offset and therefore the antenna phase center variations are not considered in the PPP Post software.

PRN	Type	\bar{x} [mm]	\bar{y} [mm]	\bar{z} [mm]
G11	IIR-A	0.00	0.00	1141.30
G28	IIR-A	0.00	0.00	1042.80
G04	IIR-M	0.00	0.00	1597.30
G17	IIR-M	0.00	0.00	827.10
G01	IIF	394.00	0.00	1561.30
G25	IIF	394.00	0.00	1600.00

Table 5.4: Examples of APC corrections for GPS satellites

5.2.6.2 Receiver antenna phase center correction

As for the satellite antenna, the measurements are also referred to the phase center of the receiver antenna. Since this location is not a suitable reference, a point tied to the base of the antenna, denoted as antenna reference point (ARP), is used instead. Information on the antenna phase center offset between the APC and ARP should be provided by the manufacturers and can also be obtained from the IGS. Usually the receiver coordinates are referred to a monument marker (MM) or to an external bench mark (BM). The computed coordinates in the IGS SINEX files are referred to the monument marker. The site eccentricity vector between the ARP and the MM is also given in the SINEX file, in up, north and east coordinates. In order to determine the receiver APC position \vec{r} in a ECEF frame the offset vector $\vec{\Delta}_{ARP}$, defining the offset vector between the ARP, and the MM and the $\vec{\Delta}_{APC}$, defining the offset vector between the ARP and the APC, have to be added to the position vector of the MM \vec{r}_{MM} :

$$\vec{r} = \vec{r}_{MM} + \vec{\Delta}_{ARP} + \vec{\Delta}_{APC} \quad (5.31)$$

It should be emphasized that both phase center correction vectors, $\vec{\Delta}_{ARP}$ and $\vec{\Delta}_{APC}$, are usually given in north, east and up components. Thus before they can be added to the position vector of the MM, which is given in the ECEF frame, they have to be transformed using the inverse transformation from the earth-fixed to the local-fixed system given in Sect. 2.2.5. As the receiver antenna phase center corrections are frequency-dependent as well, the antenna phase center offset for the IF combination can be directly estimated using Eq. 5.30.

As in case of the satellite antenna phase center also the variations of the receiver antenna phase center, which are mostly below 10 mm in case of modern antennas (Seeber (2003)), are not taken into account in the PPP Post software.

5.2.7 Phase wind-up effect

The phase wind-up effect affects only the phase measurements and depends on the mutual orientation of the satellite and the receiver antennas. Phase wind-up arises due to the nature of the GPS signals as right-hand circularly polarized (RHCP) radio waves. For a static receiver, like the receivers of a reference network, the wind-up effect is due to the satellite orbital motion.

Usually satellites undergo only slow rotations in order to keep their solar panels pointing to the sun direction. This causes a phase variation, which is misunderstood as a range variation. However, the satellites also undergo rapid rotations in the case of eclipse and noon seasons. During such an event the rotation of the antenna can reach up to one revolution, which corresponds to an increase in the carrier phase measurement of one cycle, within less than half an hour.

For double-difference positioning on distances less than few hundreds of kilometers the carrier phase wind-up effect can be neglected. However, for longer baselines and in undifferenced point-positioning, this effect has to be taken into account. Neglecting the effect and fixing orbits and clocks will lead to positioning errors in the dm-level (Kouba (2009)).

The phase wind-up correction α can be computed according to (Wu et al. (1993)) by

$$\alpha = 2N\pi + \delta\phi \quad (5.32)$$

where $\delta\phi$ denotes the fractional part of a cycle given by

$$\delta\phi = \text{sign}(\zeta) \cdot \arccos\left(\frac{\vec{D}' \cdot \vec{D}}{|\vec{D}'| \cdot |\vec{D}|}\right) \quad (5.33)$$

with

$$\zeta = \vec{k} \cdot (\vec{D}' \times \vec{D}) \quad (5.34)$$

and N is an integer number given by

$$N = \text{nint}\left[\frac{\omega_{prev} - \delta\phi}{2\pi}\right] \quad (5.35)$$

where α_{prev} is the previous value of the phase wind-up correction $\delta\phi$ and nint stands for the nearest integer. \vec{k} is the satellite-to-receiver unit vector and \vec{D}' and \vec{D} denote the effective dipole for the receiver and transmitter antenna, respectively. The two dipole vectors can be computed from the unit vectors of the satellite's $(\vec{x}', \vec{y}', \vec{z}')$ and the receiver's body coordinate system $(\vec{x}, \vec{y}, \vec{z})$, according to:

$$\begin{aligned} \vec{D} &= \vec{x} - \vec{k}(\vec{k} \cdot \vec{x}) + \vec{k} \times \vec{y} \\ \vec{D}' &= \vec{x}' + \vec{k}(\vec{k} \cdot \vec{x}') - \vec{k} \times \vec{y}'. \end{aligned} \quad (5.36)$$

For the unitary vectors of the satellite's body system $\vec{x}', \vec{y}', \vec{z}'$ the same coordinate system as for the satellite antenna phase center is used (see Sect. 5.2.6.1). For the receiver's body coordinate system $\vec{x}, \vec{y}, \vec{z}$ the local ENU coordinate system (see Sect.2.2.3) is applied.

Fig. 5.7 shows the phase wind-up effect for all satellites in view of the receiver located in Belfast over 24 hours. As already mentioned, neglecting the effect leads to positioning errors in the dm-level.

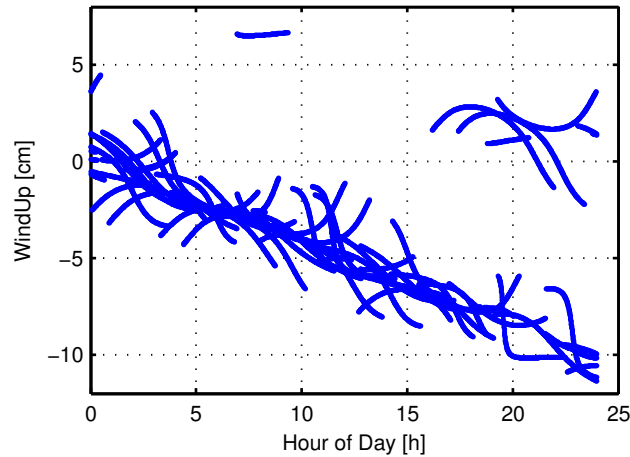


Figure 5.7: Phase wind-up correction

5.2.8 Noise and quality of the corrected observations

For the further calculations (filter process) it is important to evaluate a realistic noise estimate of the preprocessed observations (IF code and phase observations as well as the MW observations). The noise of the observations can be obtained by simply applying the law of error propagation to the linear combinations given in Eqs. 4.3, 4.4 and 4.12 starting from noise estimates for the different basic signals, which are given in Table 5.5. Here it is necessary to stress

Observation Type	Noise
Code-Pseudorange C/A	1.0 m
Code-Pseudorange P-Code	0.2 m
Phase-Pseudorange	0.002 m

Table 5.5: Noise level of different observation types

that realistic numbers do not only differ for the individual signals, but also depend on the receiver. The receivers used in the context of this work are solely precise geodetic receivers and therefore, they all have a very similar noise performance. Since there is a big difference between the noise levels of the C/A-Code and P-Code, one has to distinguish, on which observation types the linear combinations are based. The corresponding noise values for the IF and MW combination can be found in Table 5.6.

For the estimation of the UPDs, observations on the SD level are used most of the time. Building the difference between two observations also increases the measurement noise. According to the law of error propagation building the difference between two observations of the same type increases the noise by a factor of $\sqrt{2}$, if they are uncorrelated.

In order to obtain a first statement on the expected quality of the subsequently estimated UPDs, the previously performed processing steps are considered concerning their accuracy. A

Linear Combination	Noise
IF C/A and P2	~3.0 m
IF P1 and P2	~0.6 m
IF Phase	~0.006 m
MW C/A and P2	~ 0.7 m
MW P1 and P2	~0.15 m

Table 5.6: Noise level of different linear combinations

decisive part is played by the satellite orbits and clock corrections, especially in real-time. As it can be seen from Table 3.1, the accuracy of the satellite positions of the precise IGS products is 2.5 cm and the accuracy of the satellite clock corrections is ~ 75 ps which roughly corresponds to 1.8 cm. Nevertheless, these products are only available for the RSM. In contrast, the products of the IGS RTS are used in the RTM. Regarding the accuracy of the satellite positions there is no appreciable difference between the two products. However, they differ with regard to the satellite clock corrections which cannot be reliably determined in real-time. The accuracy of the satellite clock corrections of the IGS RTS products is specified with 0.1-0.15 ns, which roughly corresponds to 3 cm, which is significantly worse than the accuracy of the precise IGS products. A more detailed investigation on the influence of the different ephemerides on the accuracy of the UPDs will be given in Sect. 6.1.

Aside from the ephemerides also the accuracy of the error modeling plays a major role. Thereby a distinction between the different error sources described in Sect. 5.2.3 must be made:

1. The accuracy of the DCBs, which are applied to the code observations roughly corresponds to 0.005 ns (~ 0.2 cm). This is a relatively small value and therefore has no influence on the accuracy of the code observations. Besides, the code observations play only a minor role in the estimation of the UPDs, since they are weighted significantly less compared to the phase observations due to their high noise.
2. The influence of the ionosphere is largely eliminated by building the IF linear combination. However, only the terms up to the first order are eliminated by means of this linear combination. The influence of the terms of higher order is within the range of 1cm.
3. The accuracy of the correction for the hydrostatic part of the troposphere is around 1-2 cm in the zenith and in the range of a few centimeters at an elevation of 10-15° (the cutoff angle in PPP Post is 10°). Since the wet part is estimated together with the UPDs, the accuracy of the hydrostatic part does not play a significant role either.
4. Concerning the relativistic corrections, a correction due to the ellipticity of the satellite orbit (Eq. 5.20) as well as a correction for the Sagnac effect and the Shapiro delay (Eq. 5.23) are applied. Further relativistic corrections caused by the difference of potential between satellite and receiver for example are already taken into account by the GPS itself or are in the range of some millimeters to centimeters.

5. Range corrections for solid earth tides are directly applied to the coordinates of the reference stations according to the IERS Conventions (2010). Thereby only the terms up to second order are taken into account. The influence of terms of higher order is in the range of some millimeters and therefore they can be neglected. Even though the influence of ocean tides can be up to several cm, at stations which are located close to the ocean, they are not taken into account. At this point it should be stressed, that the station-specific errors will be subsequently wildly eliminated by building observation differences and therefore they also do not significantly effect the accuracy of the observations.

In total this means that, depending on the accuracy of the ephemerides, the accuracy of the modified observations corresponds to about 3 - 5 cm.

5.3 Parameter Segment

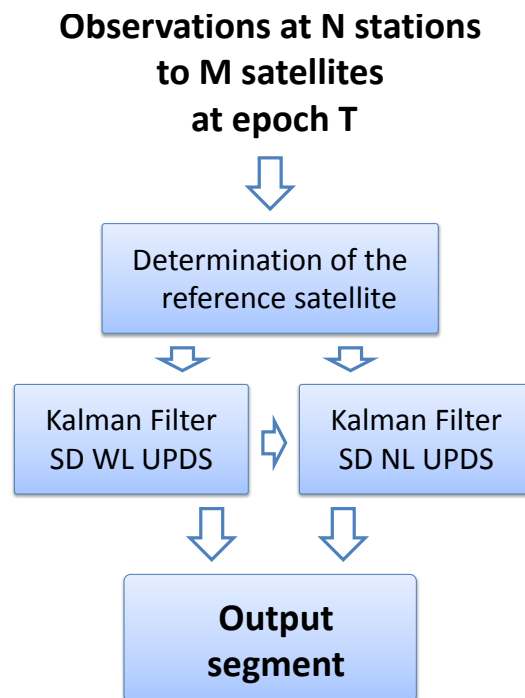


Figure 5.8: Parameter segment

The parameter segment is the centerpiece of PPP Post and deals with the estimation of the satellite-specific UPDs of the WL and NL combination using the preprocessed observations. In addition to that, the wet part of the troposphere at each station of the reference station network is calculated in the course of the parameter estimation as well. The estimation of the WL and NL UPDs is done separately using the principle of the Kalman filtering. Thereby the WL UPDs are estimated in a first step. Based on these results the NL UPDs as well as the wet part of the troposphere at each station are estimated. As it was mentioned in Sect. 4.2.1.1 the parameter estimation process relies on using single difference SD (satellite-to-satellite) observations. Building

these differences requires the determination of a reference satellite. Thus the parameter segment consist of three constituents (see Fig. 5.8):

1. Determination of a reference satellite

As the parameter estimation itself is based on the combination of SD observations of the individual stations a common reference satellite has to be determined

2. Kalman filter for the estimation of the WL UPDs

As a next step, the sliding average of the MW observations is calculated. This reduces the noise of the sliding average that is introduced by the code observations. Afterwards SD observations are built with respect to the previously determined reference satellite. Based on these SD MW observations the SD WL UPDs are estimated at every designated epoch by means of a Kalman filter. Finally the estimated SD WL UPDs are internally stored and forwarded to the output segment for archiving.

3. Kalman filter for the estimation of the NL UPDs

In the last step the estimation of the SD NL UPDs takes place. This step requires the calculation of the SD IF observations at each station, which is accomplished using again the previously determined reference satellite. Based on these SD observations a SD PPP solution is generated at each station, whereby the wet part of the tropospheric delay as well as the IF float ambiguities are estimated as unknown parameters. The station coordinates are fixed and therefore they are not estimated. Following the estimation of the PPP solution, the WL ambiguities are fixed using the SD WL UPDs, which have been estimated before. Afterwards the fixed WL ambiguities are subtracted from the IF ambiguities according to Eq. 4.20. Finally the NL UPDs are estimated at every designated epoch by means of a separate Kalman filter.

In the course of this section the station network used will be shown in the first place. Following this, the determination of the reference satellite will be described. The subsequent section briefly discusses the concept of Kalman filtering, while the last two sections will go into detail with the concept models, approaches and equations of both algorithms used for the estimation of the SD WL and NL UPDs. The section will be concluded by an example of an application of the UPDs.

5.3.1 Station network

For the estimation of the UPDs a regional network was used in the context of this thesis. The main reason for using a regional network is the determination of a common reference satellite for all stations of the network. In case of a global network this is simply not possible. The selected station network consists of 84 stations of the *EUREF Permanent Network* (EPN) which are distributed over Europe. The selection of the stations was done on the basis of the receivers used at the stations. According to Ge et al. (2008) cross-correlation receivers provide pseudorange observations of relatively poor quality and therefore such stations were excluded. Furthermore,

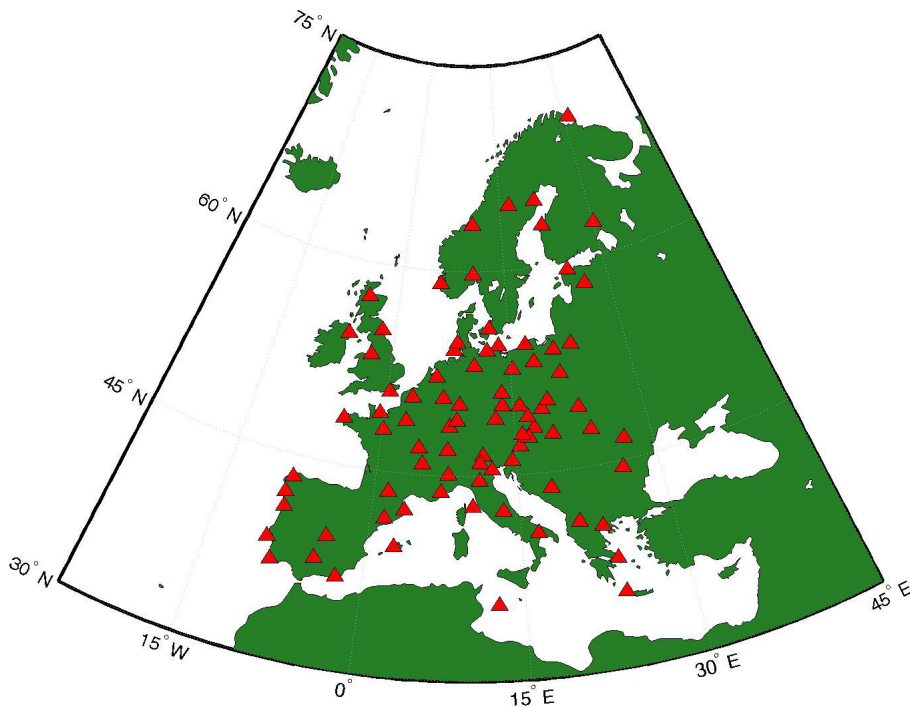


Figure 5.9: Used station network for the estimation of the UPDs

when selecting the stations, emphasis was placed on not having too many different receiver types. The estimation of the UPDs, especially of the NL UPDs suffers from unknown biases in the satellites and receivers. It is believed that receivers of the same type also behave similarly and therefore unknown errors can be treated more effectively.

5.3.2 Determination of the reference satellite

The selection of the reference satellite is based on the visibility of the satellites at the stations of the reference network. Since the network is a regional one, the reference satellite is usually visible at most of the stations. Therefore the satellite, which is visible at most of the stations is chosen as reference satellite. In order to keep the number of changes as low as possible the elevation of the satellite is used as an additional criterion for the selection. This is done in order to exclude those satellites that are visible at many stations but which are going to disappear from the field of view. During the program execution time, the visibility of the reference satellite is reviewed at each epoch. In case the reference satellite becomes visible only at a predefined number of stations (60 stations), a new reference satellite is determined using the aspects mentioned before. A change of the reference satellite also needs to be considered in the parameter estimation. This aspect will be discussed in the appropriate section of the parameter estimation (see Sect. 5.3.4.1).

The following figures illustrate a typical situation during a change of the reference satellite.

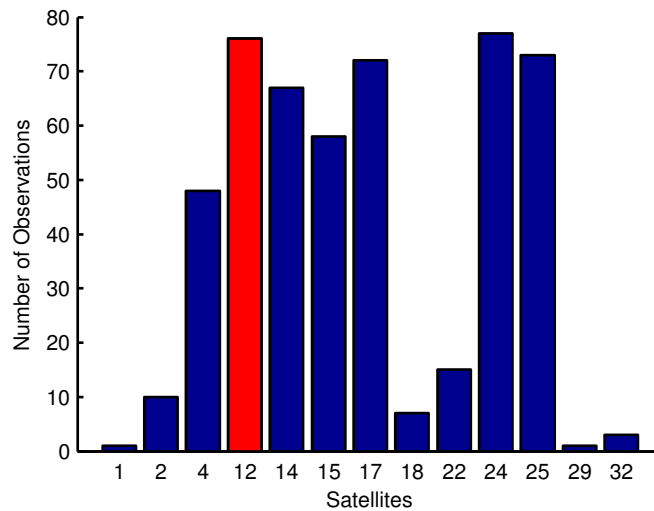


Figure 5.10: Number of Observations

Figure 5.10 is a histogram showing the number of observations at the time of the change, whereby the selected reference satellite is marked in red. As previously mentioned, the choice of the reference satellite occurs based on the number of observations. At the time of the change, there are two satellites which are observed more often compared to the other satellites. These are the satellite 12 with 76 observations and the satellite 24 with 77 observations. Would the choice be solely made on the basis of the observations, satellite 24 would be chosen. The second criterion for the choice of the reference satellite is the elevation. Simply the satellite with the highest elevation for a station located in the center of the network is chosen. This is done in order to prevent a frequent change of the reference satellite. In Fig. 5.11 the satellite ground tracks for a period of one hour before and after the change of the reference satellite are presented, whereby the directions of movement are indicated by circles. Again, the chosen reference satellite is displayed in red. It can be seen, that this satellite is very close to the station network located in Europe at the time of the change, which leads to the satellite being selected as reference satellite.

In order to determine the average number of changes of the reference satellite, one week of observation data (GPS week 1783) has been processed using the PPP Post software. Table 5.7 contains the number of changes of the reference satellite at each single day of the entire week. It can be seen that the reference satellite usually changes 9 to 10 times per day. Only on the fifth day this number increased to 13 events. Figure 5.12 illustrates the course of the change of the reference satellite for the first day of this GPS week. Thereby, the time periods in which the satellites are in view of at least 60 stations are shown. As in the pictures before the reference satellite is shown in red. The number of 60 stations represents the limiting value, that leads to a change of the reference satellite. This limit depends of course on the size of the station network. The network selected for the calculation comprises 84 stations and in this respect a limit of 60 stations has proven to be feasible. The figure shows that seven changes of the reference

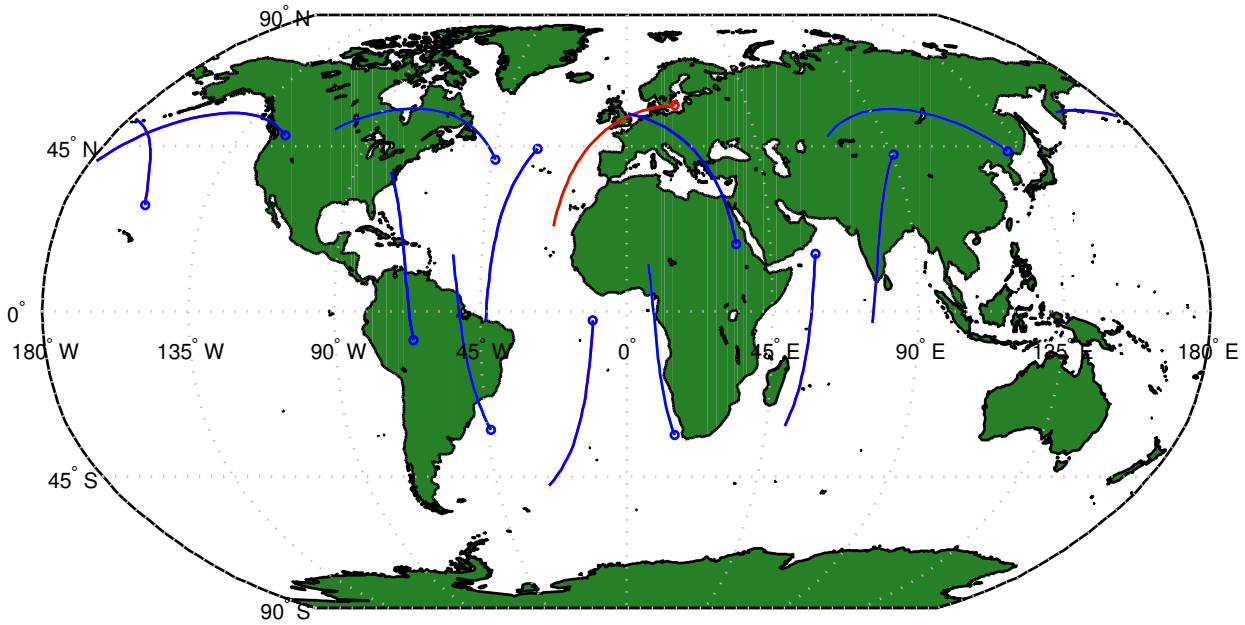


Figure 5.11: Satellite ground tracks

Day	1	2	3	4	5	6	7
Changes	7	10	9	9	13	10	10

Table 5.7: Number of changes during GPS week 1783

satellite occur after the initialization. A closer look at the figure reveals that the algorithm for the determination of the reference satellite could still be improved. In the course of the third exchange for example, it would be possible to immediately switch to the satellite PRN08 instead of the satellite PRN10. This would lead to one change less during that day. As a reduction in the number of changes of the reference satellite would not have a significant influence on the results of the parameter estimation a further optimization has been omitted.

5.3.3 Introduction to Kalman Filtering

The mathematical model for the estimation of the SD WL and NL UPDs is the Kalman filter developed by Rudolf Kalman in the late 1950s. This is an optimal linear estimation method for determining state variables of a dynamic system. In such a system the state variables and their stochastic behavior are functions of time. In contrast to the method of least squares, information about the temporal behavior of the system in the form of a model is used in addition to the measurement used for the estimation of the state variables. The dynamic behavior of such a system is modeled based on the assumption that the state of a system at a time t evolves from the prior state at time $t - 1$ according to the following linear equation

$$\mathbf{x}_k = \mathbf{T}_k \cdot \mathbf{x}_{k-1} + \mathbf{B}_k \cdot \mathbf{u}_k + \mathbf{w}_k \quad (5.37)$$

where the matrix \mathbf{T}_k is the state transition model, which is applied to the previous state \mathbf{x}_{k-1} , the matrix \mathbf{B}_k is the control-input model, which is applied to the control vector \mathbf{u}_k and \mathbf{w}_k is the process noise, which is assumed to be drawn from a zero mean normal distribution with covariance matrix

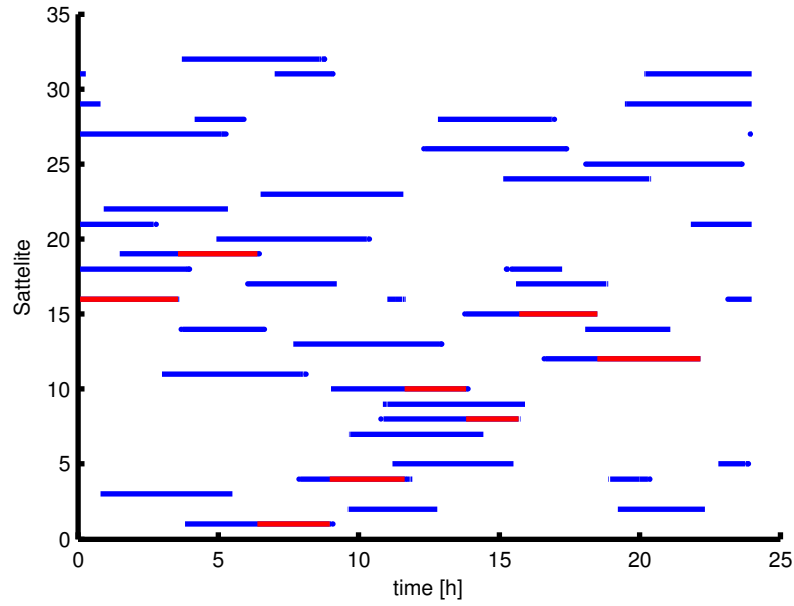


Figure 5.12: Change of the reference satellite, Day 1 of GPS week 1783

\mathbf{Q}_k , briefly $\mathbf{w}_k \sim N(\mathbf{0}, \mathbf{Q}_k)$. The control vector contains parameters which influence the system additionally. These parameters are either measured directly or can be calculated from models. As an example of such a model, the influence of the radiation pressure of the sun can be exemplified. In the specific case of the estimation of the UPDs such disturbances are neglected. An observation (or measurement) \mathbf{z}_k is related with the true state \mathbf{x}_k according to

$$\mathbf{z}_k = \mathbf{H}_k \cdot \mathbf{x}_k + \mathbf{v}_k \quad (5.38)$$

where \mathbf{H}_k is the design matrix which describes the relation between measurements and parameters, and \mathbf{v}_k is the observation noise which is assumed to be zero mean Gaussian white noise with covariance \mathbf{R}_k , briefly $\mathbf{v}_k \sim N(\mathbf{0}, \mathbf{R}_k)$. The design matrix \mathbf{H}_k is obtained by derivation of the observation equations for the unknown model parameters \mathbf{x}_k . Eq. 5.38 forms, together with Eq. 5.37, the basic equations of the discrete Kalman filter.

Usually the Kalman filter is conceptualized as two distinct phases, the "predict" phase and the "update" phase. In the predict phase the state estimate and the associated covariance matrix from the previous time step ($\hat{\mathbf{x}}_{k-1}$ and $\hat{\mathbf{P}}_{k-1}$) are used to produce an estimate of the state and the associated covariance matrix at the current time step ($\bar{\mathbf{x}}_k$ and $\bar{\mathbf{P}}_k$) according to the following equations (\hat{x} means the estimated value, \bar{x} the predicted value)

$$\bar{\mathbf{x}}_k = \mathbf{T}_k \cdot \hat{\mathbf{x}}_{k-1}, \quad (5.39)$$

$$\bar{\mathbf{P}}_k = \mathbf{T}_k \cdot \hat{\mathbf{P}}_{k-1} \cdot \mathbf{T}_k^T + \mathbf{Q}_k. \quad (5.40)$$

This predicted state estimate is also known as the a priori state estimate, because it does not include observation information from the current time step. It should be noted that the process noise is only used for the prediction of the covariance matrix, but it does not enter the prediction of the model parameters itself.

Prior to the update phase the calculation of the so-called gain matrix takes places. The gain matrix is calculated from the covariance matrix $\bar{\mathbf{P}}_k$ of the predicted parameters and the covariance matrix \mathbf{R}_k of the actual observations and determines, whether the prediction of the parameters or the observations are weighted higher. This means that, if the accuracy of the predicted state is very low (e.g. large system noise due to an uncertain model approach) or if the measurements are very accurate ($\mathbf{R}_k \sim \mathbf{0}$), the gain matrix \mathbf{K}_k approximately becomes the unit matrix \mathbf{I} and the measurements are highly weighted compared to the model. On the other hand, if the accuracy of the predicted state is very high (e.g low system noise) or the accuracy of the measurements is low, the gain matrix \mathbf{K}_k approximately becomes the zero matrix $\mathbf{0}$ and the model is highly weighted compared to the measurements. The gain matrix is selected in such a way that the trace of the covariance matrix is minimized. This is achieved by

$$\mathbf{D}_k = \mathbf{R}_k + \mathbf{A}_k \cdot \bar{\mathbf{P}}_k \cdot \mathbf{A}_k^T. \quad (5.41)$$

$$\mathbf{K}_k = \bar{\mathbf{P}}_k \cdot \mathbf{A}_k^T \cdot \mathbf{D}_k^{-1}, \quad (5.42)$$

In the update phase, the a priori prediction is combined with observation information in order to refine the state estimate. The combination of the prediction with the observations is carried out with the help of the previously estimated gain matrix \mathbf{K}_k according to the following equations:

$$\hat{\mathbf{x}}_k = \bar{\mathbf{x}}_k + \mathbf{K}_k \cdot \mathbf{l}_k, \quad (5.43)$$

$$\hat{\mathbf{P}}_k = \bar{\mathbf{P}}_k - \mathbf{K}_k \cdot \mathbf{D}_k \cdot \mathbf{K}_k^T, \quad (5.44)$$

with

$$\mathbf{l}_k = \mathbf{z}_k - \mathbf{H}_k \cdot \bar{\mathbf{x}}_k. \quad (5.45)$$

This improved estimate is termed the a posteriori state estimate and represents an optimal estimation of the parameters. Typically, the predict and the update phase alternate, with the prediction advancing the state until the next scheduled observation, and the update incorporating the observation. As we have already seen, the Kalman filter is a recursive estimator, which means that only the estimated state from the previous time step and the current measurement are needed to compute the estimate for the current state and therefore, it is particularly well suited for applications in real-time. At the beginning initial values for the state variables and covariance matrices are needed. These initial values could be determined from a preceding least-squares adjustment for example. This operation is usually called filter initialization.

5.3.4 Estimation of the WL UPDs

As described earlier in this section, the calculation of the UPDs is divided into two steps, whereby the first step comprises the estimation of the SD WL UPDs. The theoretical background for the estimation was already briefly described in Sect. 4.2.1.1. This section deals with the application of the given theory using some numerical examples. Furthermore upcoming problems are discussed as well as strategies, which have been developed in order to overcome these problems.

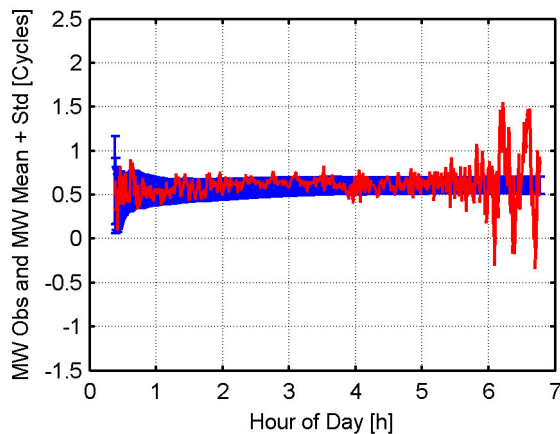


Figure 5.13: ZD MW PRN19
LEICA GRX1200PRO

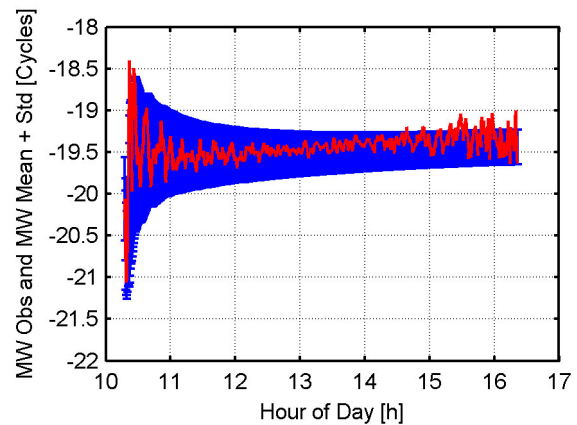


Figure 5.14: ZD MW PRN8
LEICA GRX1200GGPRO

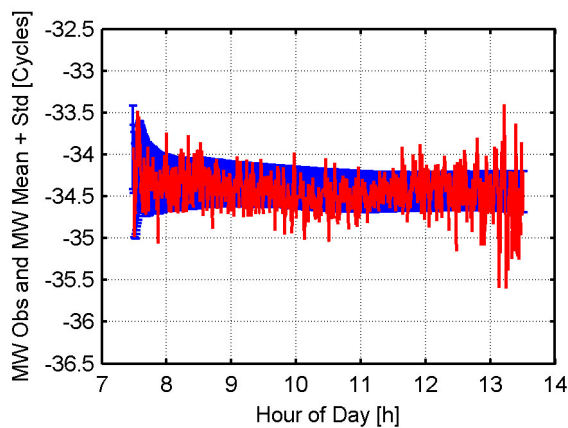


Figure 5.15: ZD MW PRN13
TRIMBLE NETR5

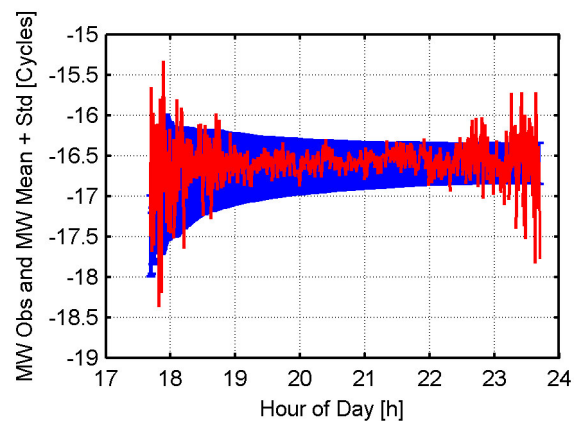


Figure 5.16: ZD MW PRN25
JPS LEGACY

In a first step the so-called Melbourne-Wübbena MW combination is built for each set of observations of every station of the reference station network. According to Eq. 4.12 the MW combination is a linear combination of both, carrier phase and code observables and eliminates the effect of the ionosphere, the geometry, the clocks and the troposphere. It provides an estimation

of the wide-lane ambiguity $N_{k,WL}^i$, according to the following equation:

$$L_{k,WL}^i = \lambda_{WL}(N_{k,WL}^i + \Delta\Phi_{WL}^i - \Delta\Phi_{k,WL}) + \epsilon_{WL} \quad (5.46)$$

where $N_{k,WL}^i$ is the integer wide-lane ambiguity, $\Delta\Phi_{WL}^i$ accounts for the satellite- and $\Delta\Phi_{k,WL}$ for the receiver-specific UPD and ϵ_{WL} is the measurement noise, including carrier phase and code noise. A major disadvantage of the MW combination is the increased observation noise which propagates from the code measurements. Tab.5.6 shows that the measurement noise essentially depends on which code measurements are available at the stations. Most of the receivers in the station network used provide C/A and P2 code measurements resulting in a measurement noise of about 0.7 m. In order to reduce the noise of the MW combination the moving average $m_{L_{k,WL}^i}$ and the corresponding sigma $s_{L_{k,WL}^i}$ values of the MW combination are estimated for each epoch k using the same real-time algorithm as for the cycle slip detection, see Eq. 5.10. To illustrate the influence of the code measurements on the MW combination and to get an idea of the accuracy of the MW combination, some typical examples for different receiver types are given in Figs. 5.13 to 5.16. The red line indicates the zero-difference (ZD) raw MW observation in cycles and the blue line the mean value plus its standard deviation, both given in WL cycles as well. At this point it should be noted that one WL cycle corresponds to approximately 0.86 m.

In the first example (see Fig. 5.13) we see that the noise dramatically increases at the end of the observation interval. Also in the second example the noise is always higher at the beginning and at the end of the observation interval. This indicates that the noise of the MW observations increases for satellites at lower elevations, whereby the strength of the effect seems to depend on the receiver type. In the second example (see Fig 5.14) the noise of the raw MW observations is quite small compared to the other examples. One explanation might be, that the software of the receiver already applies some kind of smoothing to the code observations. In the station network used only two receiver types show such a behavior. All the other receivers show a behavior similar to the last two examples (see Fig. 5.15 and Fig. 5.16). The raw MW observations are quite noisy especially at lower elevations. Despite of the different quality of the raw MW observations, the mean values of the MW observations are rather stable for all receiver types. The variation (standard deviation) of the mean MW observations is smaller than 0.3 cycles in most of the cases. This indicates, that based on MW observations a reliable estimation of the SD WL UPDs is possible.

In the next step the SD observations are built by subtracting the observations of all satellites j in view from the observation of the reference satellite Ref . Building the difference between two ZD MW observations (Eq. 5.46) and dividing the equation by the WL wavelength leads to the following equation with the receiver-specific UPD being eliminated:

$$\frac{L_{WL}^{Ref-j}}{\lambda_{WL}} = N_{WL}^{iRef-j} + \Delta\Phi_{WL}^{Ref-j} + \frac{\Delta\epsilon_{WL}}{\lambda_{WL}} \quad (5.47)$$

where N_{WL}^{iRef-j} is the SD integer wide-lane ambiguity, $\Delta\Phi_{WL}^{Ref-j}$ is the satellite-specific SD UPD and

$\Delta\epsilon_{WL}$ is the measurement noise which is increased by a factor of $\sqrt{2}$ (see Sect. 5.2.8). Each UPD consists of an integer and a fractional part, where the integer part cannot be separated from the integer ambiguities anyway. It is only possible to estimate the fractional part of the UPD. However, this is sufficient to restore the integer nature of the ambiguities.

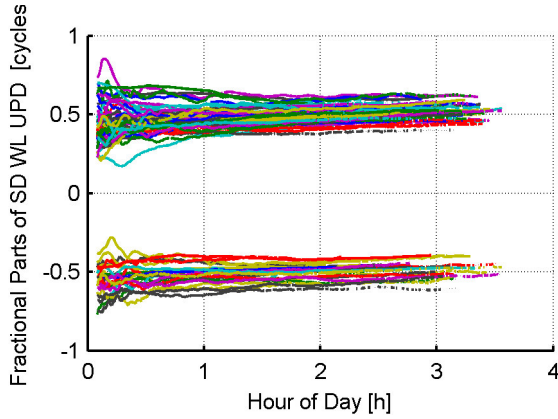


Figure 5.17: SD WL UPD PRN16 - PRN21

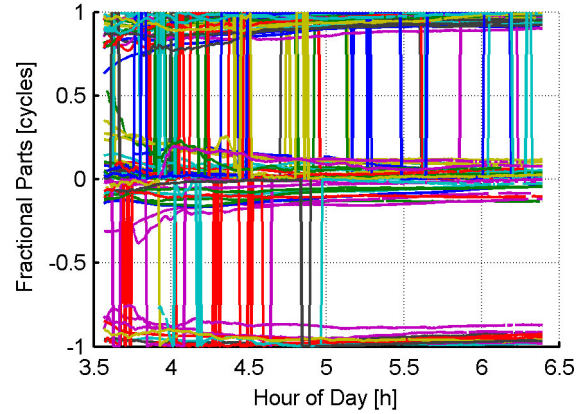


Figure 5.18: SD WL UPD PRN19 - PRN32

At this point the concept of the “fractional part” deserves a closer look. A simple calculation of the fractional part of the SD MW UPD of a specific satellite pair observed at the different stations will result in fractional parts between minus one and plus one cycle. Figures 5.17 and 5.18 show the calculated fractional parts of two satellite pairs, PRN16 - PRN21 and PRN19 - PRN32, whereby the first satellite indicates the reference satellite. Since the satellites cannot be observed continuously due to the used regional station network, the UPDs can only be observed up to a couple of hours. The UPDs observed at the individual stations are illustrated by different colors. Since the network consists of more than 80 stations the same color appears several times. Both examples confirm that a simple estimation of the fractional part results in two different solutions. One in the positive and one in the negative value range. In case of values being near to an integer value the situation is even a little more complex (see Fig. 5.18). Keeping in mind that a shift by an integer number of cycles does not affect the ambiguity resolution, it is possible to shift the fractional parts from the negative to the positive value range. This leads to the so-called “positive” fractional parts (see Fig. 5.19 and Fig. 5.20). Furthermore, it can be seen that the SD WL UPDs observed at the individual stations are very stable after an initialization phase and that the differences are in the range of about 0.3 cycles. This roughly corresponds to the accuracy of the smoothed SD MW observations.

Based on these observations, the estimation of the SD WL UPDs is carried out using a Kalman filter.

$$\mathbf{x}_k = \begin{bmatrix} SD\ WL\ UPD^{Ref-1} \\ \vdots \\ SD\ WL\ UPD^{Ref-n} \end{bmatrix}. \quad (5.48)$$

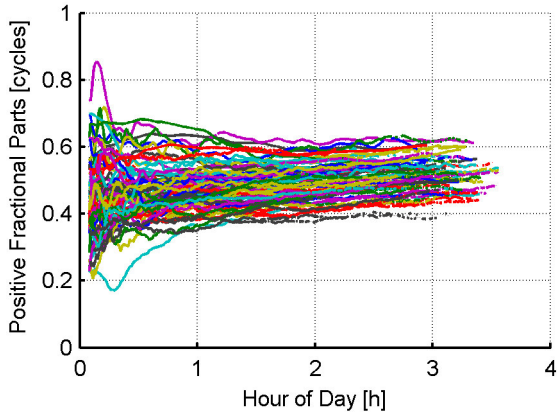


Figure 5.19: SD WL UPD PRN16 - PRN21

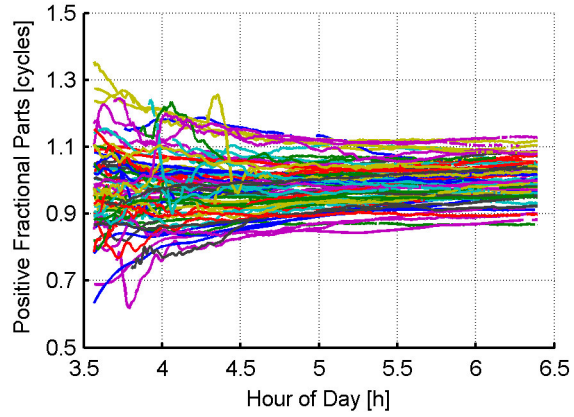


Figure 5.20: SD WL UPD PRN19 - PRN32

Thereby the parameter vector \mathbf{x}_k exclusively contains the SD WL UPDs of the satellites $1 \dots n$ with respect to reference satellite *Ref* that have to be estimated. This means that the parameter vector consists of n parameters. Only those UPDs, which are observed by more than 20 stations, are estimated. This quantity of stations seems quite high but is necessary for a reliable estimation of the UPDs. Due to the regional station network used, the satellites cannot be observed continuously and therefore the number of parameters changes constantly. If a satellite is not visible any more, the corresponding SD WL UPD parameter is removed from the parameter vector and from the covariance matrix. If a new satellite appears and is observed by enough stations, the corresponding SD WL UPD parameter is added to the parameter vector and the covariance matrix and must be initialized subsequently. For the initialization the positive fractional parts of the SD WL UPDs observed at the stations are calculated in the first place. Afterwards the starting value is calculated by building the median solutions of the different stations i (see Fig. 5.19 and 5.20) according to

$$SD\ WL\ UPD = Median\ \{SD\ WL\ UPD_i\}. \quad (5.49)$$

The starting value is applied to the a priori state vector \mathbf{x}_{k-1} . In addition, also the standard deviation in relation to the median is calculated. This value is used as a priori standard deviation of the parameter and is added to the covariance matrix of the a priori states \mathbf{P}_{k-1} .

After the initialization of the filter, the prediction of the parameters and the associated covariance matrix is carried out using Eq. 5.39 and 5.40. The prediction of the SD WL UPDs is done with a simple linear model where predicted value $\overline{SD\ WL\ UPD}_k$ corresponds to the estimated value of the previous epoch $\widehat{SD\ WL\ UPD}_{k-1}$. Thus, the transition matrix results in an $n \times n$ identity matrix ($\mathbf{T}_k = \mathbf{1}$). It is assumed that the UPDs, which are introduced by instrumental errors, are hardly subject to changes and, therefore, remain stable over a prolonged period. Whether this assumption is actually true will be examined later.

The prediction of the covariance matrix of the parameters requires the just determined transition matrix and the estimated covariances of the previous epoch. These are, depending on the

status of the filter, the squared standard deviations of the initialization or the calculated values of the previous epoch. Secondly, one needs information about the stochastic disturbances, which affect the prediction of the covariance matrix in the form of a perturbation matrix. In principle the perturbation matrix describes the shortcomings of the model compared to reality. These shortcomings are represented by normally distributed variables with a zero mean and the covariance matrix \mathbf{Q}_k . As the UPDs are assumed to be stable, the covariance matrix of the disturbances is a $n \times n$ zero matrix ($\mathbf{Q}_k = \mathbf{0}$). Therefore the prediction gets more and more weight compared to the incoming observations during the progress of the filter. If the assumption, that the estimated parameters are constant, is not valid or if some errors are not taken into account properly this would lead to increasing differences between the predicted values and the measured observations. This would ultimately lead to the collapse of the filter. Therefore, it is necessary to examine the stability of the filter in order to detect errors in the prediction or in the processing of the observations.

After the prediction, the measurement equations of the filter are treated. For further calculations, the design matrix \mathbf{H}_k , the covariance matrix of the observations \mathbf{R}_k and the vector \mathbf{l}_k , which is the difference between the observations and the prediction, have to be established. The design matrix is obtained by differentiation of the observation equations with respect to the unknown parameters. In case of the SD WL UPDs the observation equations appear as follows.

$$L_k = SD\ WL\ UPD_k. \quad (5.50)$$

Under consideration of the sequence of the variables within the parameter vector, the differentiation of the observations leads to the design matrix \mathbf{H}_k . For illustration, a simple example based on a fictive situation is given:

- 3 satellites: This leads to 2 SD WL UPDs which must be estimated.
- 3 stations: Station 1 provides observations for both SD WL UPDs, station 2 and 3 an observation for the SD WL UPD of the first satellite pair only.
- Therefore, there are 2 unknown parameters and 4 observations.

$$\mathbf{H}_k = \begin{bmatrix} 1 & 0 \\ 0 & 1 \\ 1 & 0 \\ 1 & 0 \end{bmatrix} \quad (5.51)$$

The number of rows m of the design matrix \mathbf{H}_k is determined by the number of observations, the number of columns by the number of unknown parameters n . The values of the design matrix are obtained by a station-wise differentiation of the observation equations for the SD WL UPDs of both pairs of satellites. The first two lines result from the two observations of station 1. The first observation is related to the SD WL UPD of the first satellite pair and therefore the differentiation gives one. On the contrary the differentiation with respect to the SD WL UPDs of the second pair gives zero. For the second observation of this station the exact opposite is the case. Each of the

other two stations provides an observation of the SD WL UPD of the first satellite pair which result in the entries of the last two rows of the design matrix.

In a next step, the calculation of the observation vector \mathbf{l}_k is carried out. This vector is calculated according to Eq. 5.45 and is therefore nothing more than the difference of the individual observations and the corresponding predicted parameters:

$$\mathbf{l}_k = \begin{bmatrix} L_{1,k} - \overline{SD\ WL\ UPD}_{1,k} \\ L_{2,k} - \overline{SD\ WL\ UPD}_{2,k} \\ \vdots \\ L_{m,k} - \overline{SD\ WL\ UPD}_{m,k} \end{bmatrix}. \quad (5.52)$$

This vector is of crucial importance for the parameter estimation and is often referred to as innovation or innovation vector.

In order to create the covariance matrix of the observations, the standard deviations of the mean values of the ZD MW observations are used (see Eq. 5.10). On top of these standard deviations, an elevation-dependent weight W_e is added, which is calculated according to the following equation:

$$W_e = \begin{cases} 1 & \text{if } e > 30^\circ \\ 2 \cdot \sin(e) & \text{otherwise} \end{cases}. \quad (5.53)$$

In the next step the weighted standard deviations of the zero-difference observations are combined and entered at the corresponding points of the covariance matrix of the observations \mathbf{R}_k .

In the end, the update phase takes place, where the matrices previously created are linked together and deliver as a result an optimal estimation of the unknown parameters. The estimated SD WL UPDs and the corresponding variances are stored internally and transferred to the next part of the program. In addition, the results are written into an ASCII file. In the figures 5.21

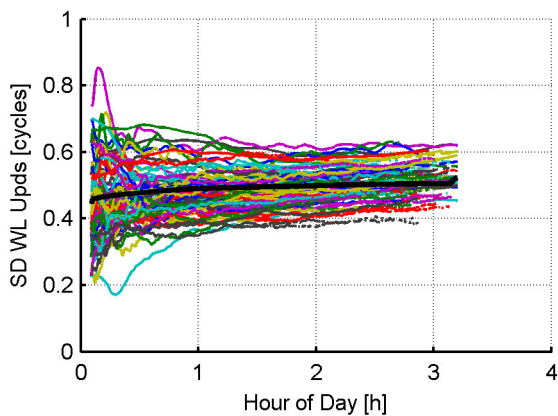


Figure 5.21: SD WL UPD PRN16 - PRN21

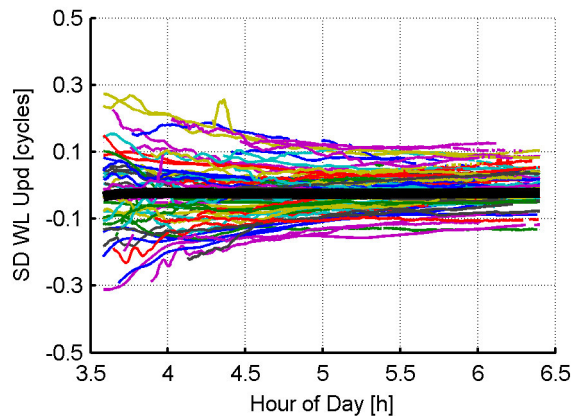


Figure 5.22: SD WL UPD PRN19 - PRN32

and 5.22, the results of the Kalman filter for the already known satellite pairs (PRN16 - PRN21

and PRN19 - PRN32) are shown. As in the previous figures (Fig. 5.19 and 5.20) the observations of the individual stations are illustrated by different colors. In addition to the observations the solution of the Kalman filter is illustrated by a thick black line. It can be seen, that the solution of the Kalman filter corresponds to about the mean value of the observations. Of course the solution can slightly deviate from the mean value since the individual observations are weighted differently.

If one compares Fig. 5.20 with Fig. 5.22, it is obvious that the UPDs differ by one full cycle. Since it would be desirable to have all UPDs in a common range of values, namely 0 to 1, they may be shifted by one cycle. However, in order to keep consistency with the subsequently estimated NL UPDs this reduction is only carried out, if a initialization of a WL UPD parameter takes place. Therefore it may happen that the WL UPDs leave the aforementioned value range in the course of the estimation process, but this has no further consequence for the parameter estimation or for the application at the user side.

5.3.4.1 Change of the reference satellite

During the parameter estimation process the reference satellite changes continuously. Since the SD WL UPDs are referred to the reference satellite, this also leads to a new set of SD WL UPDs every time the reference satellite changes. This circumstance also must be properly taken into account in the Kalman filter. The easiest way would be to restart the filter every time the SD WL UPDs change. Due to the convergence time of the parameter estimation process this would lead to a significant deterioration of the results. Another way to allow for a change of the reference satellite is to combine the corresponding SD WL UPDs according to the following equations

$$\begin{aligned} UPD^{NewRef-j} &= UPD^{NewRef-OldRef} + UPD^{OldRef-j}, \\ UPD^{NewRef-OldRef} &= -UPD^{OldRef-NewRef} \end{aligned} \quad (5.54)$$

with *NewRef* and *OldRef* being the notations for the new and the old reference satellite. Thus according to Eq.5.54 the UPDs can be corrected by simply adding the negative value of the SD UPD related to the difference between the old and the new reference satellite $UPD^{OldRef-NewRef}$. In most of the cases this value is available, since the reference satellites are usually observed by most of the stations. However, if this should not be the case a reset of the Kalman filter is carried out. Of course this correction also affects the accuracy of the UPDs, which can be treated by applying the law of error propagation on the accuracies of the UPDs being combined.

5.3.5 Estimation of the NL UPDs

Following the estimation of the SD WL UPDs the estimation of the SD NL UPDs is carried out. The theoretical background for the estimation of the SD NL UPDs has already been described in Sect. 4.2.1.1 and forms the backbone of this section. Starting point for the estimation of the SD

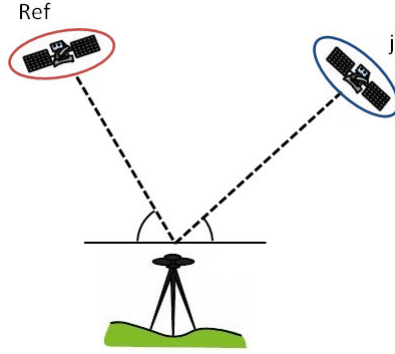


Figure 5.23: Satellite-to-satellite single difference

NL UPDs is Eq. 4.20, which is given again at this point for reasons of clarity.

$$B_{NL}^{Ref-j} = \frac{f_1 + f_2}{f_1} B_3^{Ref-j} - \frac{f_2}{f_1 - f_2} \hat{N}_{WL}^{Ref-j} \quad (5.55)$$

with $B_{NL}^{Ref-j} = N_{NL}^{Ref-j} + \Delta\bar{\Phi}_{NL}^{Ref-j}$ representing the SD NL ambiguity consisting of the integer part N_{NL}^{Ref-j} and the UPD $\Delta\bar{\Phi}_{NL}^{Ref-j}$, B_3^{Ref-j} being the ambiguity of the ionosphere-free linear combination and \hat{N}_{WL}^{Ref-j} being the fixed integer SD WL ambiguity. According to Eq. 5.55 an estimation of the SD NL UPD requires a solution of the ionosphere-free ambiguity B_3^{Ref-j} . For the calculation of this value there are basically two ways, both of them being based on PPP solutions.

5.3.5.1 SD PPP solution

According to Sect. 4.1 a standard PPP solution could be created by processing the zero-difference code and phase observations (Eq. 4.3 and Eq. 4.4, respectively) together in a filter that solves for the different unknowns, namely the receiver coordinates, the receiver clock error, the zenith tropospheric delay and the ambiguities, which are estimated as float values. In order to be able to combine the NL ambiguities with the SD WL ambiguities the NL ambiguities must also be brought on SD level (see Fig. 5.23). This is achieved by calculating the difference between the corresponding IF ambiguities.

A second possibility would be to estimate a PPP solution directly on the SD level. Assuming that the position of the satellite and the satellite clock error are known and all necessary corrections are applied, the SD code P_3^{Ref-j} and phase L_3^{Ref-j} observations can be written as follows

$$P_3^{Ref-j} = \delta_{tro}^{Ref-j} + \sqrt{2} \Delta\epsilon_{P,3}, \quad (5.56)$$

$$L_3^{Ref-j} = \delta_{tro}^{Ref-j} + \lambda_3 B_3^{Ref-j} + \sqrt{2} \Delta\epsilon_{L,3} \quad (5.57)$$

with δ_{tro}^{Ref-j} being the difference of the slant tropospheric delay and B_3^{Ref-j} being the SD ambiguity with respect to the reference satellite. As already described earlier the noise $\Delta\epsilon_{P,3}$ and $\Delta\epsilon_{L,3}$ of

the code and phase observations, respectively, increases by a factor of $\sqrt{2}$ compared to the basic observations. Building SD observations eliminates the receiver clock error and most importantly the receiver-specific UPD. However, the situation is different for the tropospheric delay. This becomes clearer, if the slant delay δ_{tro}^{Ref} is replaced by the zenith tropospheric wet delay L_w^z and the corresponding mapping function $mf_w(e)$, which depends on the elevation angle e (see Sect. 5.2.4) according to

$$\delta_{tro}^{Ref} = L_w^z \cdot mf_w(e^{Ref}). \quad (5.58)$$

Building the difference between the slant tropospheric delays related to two different satellites leads to

$$\begin{aligned} \delta_{tro}^{Ref-j} &= L_w^z \cdot \Delta mf_w, \\ \Delta mf_w &= mf_w(e^{Ref}) - mf_w(e^j). \end{aligned} \quad (5.59)$$

As described in Sect. 5.2.4, the hydrostatic part of the atmosphere can be modeled very precisely, therefore only the wet part of the troposphere plus the error in the hydrostatic model is estimated together with the other unknown parameters. Due to that reason the hydrostatic part has been omitted in the equations above.

In conclusion, forming the difference between two observations at the same site at identical epochs does not only eliminate some station-specific errors but also some station-specific unknowns. As a result, the number of unknown parameters is reduced: this covers the receiver clock error and the receiver-specific UPD. The remaining parameters, which must be estimated, are the zenith tropospheric wet delay and the SD IF ambiguities, i.e. the parameters of interest.

Both approaches result in the same outcome but differ in other aspects. The advantage of the second approach is the reduction of the parameters which offers two benefits. One benefit is that the computing power for the estimation of the parameters is reduced a bit, but in terms of the fast progress in the hardware of modern computers this has no significant impact. The substantial advantage of the reduction of the parameters is the shortening of the convergence time of the PPP solution, due to the reduced number of parameters which are estimated. In order to estimate the SD NL UPDs with sufficient accuracy, an accurate solution of the real-valued ionosphere free ambiguities is required. To achieve this accuracy using a standard ZD PPP solution requires a correspondingly long convergence time. As mentioned in Sect. 4 the convergence time mainly suffers from the necessity of estimating real-valued ambiguities. But also some other factors, such as the number of visible satellites, the geometry as well as the accuracy of the initial values of the unknown parameters influence the convergence time. Anyway, even in the case of reference stations located in very favorable conditions the convergence time may be up to 30 minutes. However, the reduction of the convergence time only has an advantage for the program start, when a new PPP solution is prepared at all stations of the network. During run time, only in rare cases the PPP solutions of individual stations is restarted. This will only happen, if less than four satellites are visible over a certain period, e. g., when it comes to an utter failure of the station.

Due to the decreased number of parameters and the fact that some station-,specific errors are

Parameter	Standard deviation
ZTD	± 0.5 [m]
SD IF Amb.	± 10 [m]

Table 5.8: Initial (loose) constraints for the initialization of the SD PPP solution

Parameter	Process noise
ZTD	$2[\frac{mm^2}{h}] \sim 1e^{-9}[\frac{m^2}{s}]$

Table 5.9: Variance of the process noise of the SD PPP solution

eliminated a SD PPP solution using the principle of a Kalman filter was realized. The developed SD PPP algorithm is carried out for every individual station of the reference network. As a consequence the parameter vector \mathbf{x}_k only contains station-specific parameters. As mentioned before, contrary to a standard PPP solution, the parameter vector only contains the zenith tropospheric wet delay L_w^z and the SD IF ambiguities with respect to the reference satellite $B_3^{Ref-1} \dots B_3^{Ref-n}$. Due to the presence of the UPDs these ambiguities do not have an integer nature and, therefore, they can only be estimated as float values.

$$\mathbf{x}_k = \begin{bmatrix} L_w^z \\ B_3^{Ref-1} \\ \vdots \\ B_3^{Ref-n} \end{bmatrix} \quad (5.60)$$

According to Navipedia (2013) 10 cm is an appropriate initial value for the zenith tropospheric wet delay. The initial values of the SD IF ambiguities are calculated on the basis of Eq. 5.57, by subtracting the zenith tropospheric wet delay from the corresponding SD IF observations. Since the SD IF ambiguities cannot be observed permanently, the parameter vector and the covariance matrix change from time to time, due to geometry changes (rising and setting satellites), in the course of the parameter estimation process. If a satellite is no longer visible, or if a cycle slip is detected the corresponding entry of the parameter vector is removed. In case of a new SD IF ambiguity being observed, an additional entry is added to the parameter vector, which is initialized subsequently. For the initialization, a priori standard deviations for the zenith tropospheric wet delay and the SD IF ambiguities are needed. The chosen values are listed in Tab. 5.8.

Following the initialization the prediction of the parameters and the covariance matrix is carried out. As for the SD WL UPDs, it can be assumed that the parameters do not change between two observation epochs. As a consequence the identity matrix becomes an $n + 1 \times n + 1$ identity matrix ($\mathbf{T}_k = \mathbf{1}$). For the prediction of the covariance matrix, information on the perturbation matrix \mathbf{Q}_k , which describes the shortcomings of the prediction model, is needed. Based on the assumption that the SD IF ambiguities are constant, the corresponding entries of the perturbation matrix are zero. The assumption of a ZTD stable over time is not exactly applicable. This

imperfection of the prediction is taken into consideration by adding a process noise in terms of the perturbation matrix. This leads to the ZTD being estimated as a random walk process. Tab. 5.9 contains the value used for the process noise. This value allows for a variation of 2 mm^2 of the ZTD in the course of one hour. Since the noise depends on the time difference between two consecutive epochs, the perturbation matrix has the following form

$$\mathbf{Q}_k = \begin{bmatrix} 1e^{-9} \cdot \Delta t & 0 & \cdots & 0 \\ 0 & 0 & & \vdots \\ \vdots & & \ddots & \\ 0 & \cdots & & 0 \end{bmatrix} \quad (5.61)$$

with Δt being the time difference in seconds.

Furthermore, the design matrix \mathbf{H}_k , the covariance matrix \mathbf{R}_k and the vector \mathbf{l}_k are needed. The design matrix is obtained by differentiation of the observation equations with respect to the unknown parameters. In case of the SD PPP solution these are the equations of the SD IF code and phase observations (see Eq. 5.56 and Eq. 5.57). Even though the code observations do not provide information on the SD IF ambiguities, they are used as well. The main purpose of the code observations is to provide information on the ZTD parameter, which is highly correlated with the SD IF ambiguities. Taking into account the order of variables within the parameter vector \mathbf{x} , the derivation of the code and phase observation equations results in the following design matrix

$$\mathbf{H}_k = \begin{bmatrix} \Delta m f_{w,1} & 0 & \cdots & 0 \\ \vdots & \vdots & \ddots & \vdots \\ \Delta m f_w^{w,mc} & 0 & \cdots & 0 \\ \Delta m f_{w,1} & 1 & \cdots & 0 \\ \vdots & \vdots & \ddots & \vdots \\ \Delta m f_w^{w,mp} & 0 & \cdots & 1 \end{bmatrix} \quad (5.62)$$

with mc and mp being the number of code and phase observations, respectively. The different number of code and phase observations comes from the fact that phase observations will not be used in case of a cycle slip, while the corresponding code observation can be used. Furthermore, it can happen that code or phase observations are detected as outliers and have to be removed. In order to keep as much observations as possible the code and phase observations related to one satellite pair are treated independent of each other. The number of rows of the design matrix \mathbf{H}_k is defined by the number of observations, namely $m = mc + mp$, and the number of columns by the unknown parameters $n = 1 + mp$. According to what was written at the beginning of this section these parameters are the ZTD and the SD IF ambiguities of the individual phase observations. Both, the code and phase observations contain the ZTD and the differentiation with respect to the ZTD leads to the SD mapping function $\Delta m f_w$. Therefore, the first column contains the SD mapping functions related to the different satellite pairs. Since the code observations do not

provide information on the SD IF ambiguities, the differentiation with respect to the ambiguities is zero. The individual phase observations only provide information on the corresponding ambiguity parameter, which results in an identity matrix in the lower right part of the design matrix \mathbf{H}_k .

In the next step the observation vector is built according to Eq. 5.38. Therefore the difference between the code P_k and phase observations L_k (see Eq. 5.56 and Eq. 5.57) and the predicted observations, \bar{P}_k and \bar{L}_k , is calculated, which leads to the following representation

$$\mathbf{l}_k = \begin{bmatrix} P_{k,1} - \bar{P}_{k,1} \\ \vdots \\ P_{k,mc} - \bar{P}_{k,mc} \\ L_{k,1} - \bar{L}_{k,1} \\ \vdots \\ L_{k,mp} - \bar{L}_{k,mp} \end{bmatrix} \quad (5.63)$$

with the predicted observation calculated by $\mathbf{H}_k \cdot \bar{\mathbf{x}}_k$

$$\bar{P}_k = \bar{L}_{w,k}^z \cdot \Delta m f_{w,k}, \quad (5.64)$$

$$\bar{L}_k = \bar{L}_{w,k}^z \cdot \Delta m f_{w,k} + \lambda_3 \bar{\mathbf{B}}_{3,k}^{Ref-1}. \quad (5.65)$$

Last but not least, the covariance matrix of the observations \mathbf{R}_k has to be established using the noise values for the IF code and phase observations given in Tab. 5.6. These values are modified by applying the already known elevation-dependent weighting function W_e given in Eq. 5.53. Afterwards the weighted standard deviations of the ZD observations in the SD combination are combined and entered at the corresponding place into the covariance matrix \mathbf{R}_k .

In the end, the update phase takes place, which delivers as a result an optimal estimation of the unknown parameters. In order to make the SD PPP solution more robust and reliable, an outlier detection is performed subsequent to the update phase. The detection algorithm is based on a simple screening of the code and phase observation residuals. If the residuals exceed a defined threshold, the corresponding observations are removed and the SD PPP solution is carried out again. This procedure is repeated until no outliers are found anymore.

As in the case of the SD WL UPDs, a change of the reference satellite also needs to be considered in the SD PPP solution. A possible change only affects the ambiguity parameters and not the ZTD, which is a station-specific parameter. For the correction of the SD IF ambiguities the same procedure as for the SD WL UPDs (see Eq. 5.54) can be used. At stations, where the reference satellite is not visible, no correction is applied and the SD PPP solution is simply kept up until a reference satellite becomes visible.

In Figures 5.24 to 5.27 the results of the SD PPP solution for the station in Belfast are shown over the period of the first day of GPS Week 1783. In Fig. 5.24 the temporal progress of the ZTD is shown. The ZTD only needs a couple of periods to settle and afterwards it remains rather

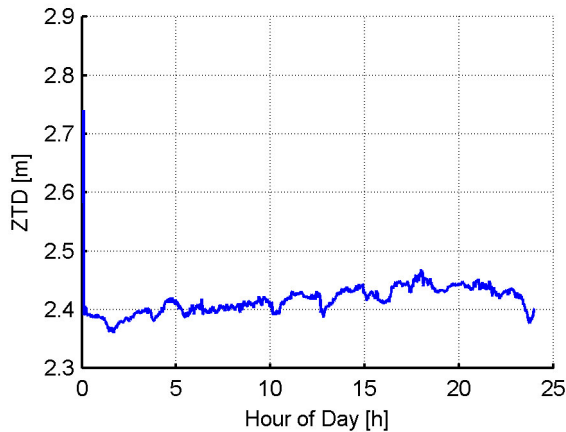


Figure 5.24: Temporal progress of the ZTD at station Belfast

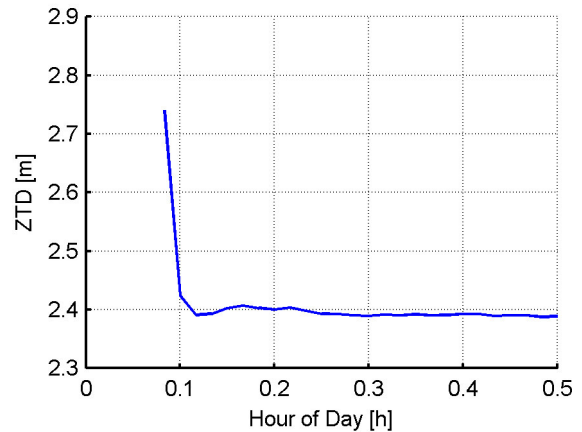


Figure 5.25: Transient behaviour of the ZTD at station Belfast

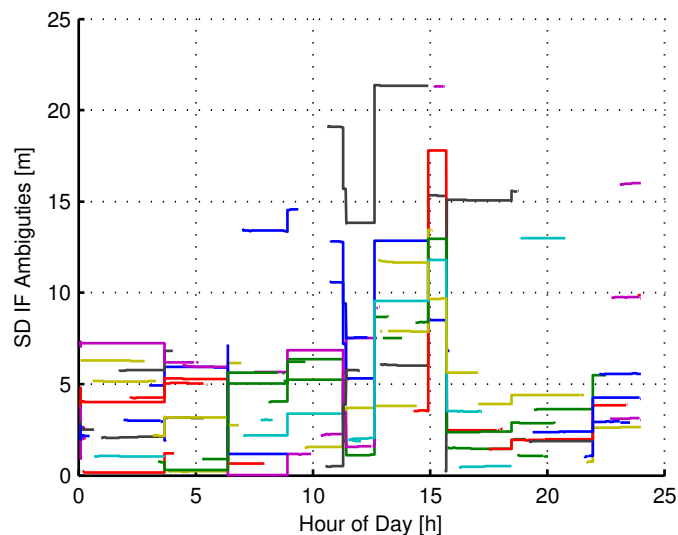


Figure 5.26: Temporal progress of the SD IF ambiguities at station Belfast

stable. The convergence behavior of the ZTD is illustrated in Fig. 5.25 which shows the first half hour of the time series. It can be seen, that the convergence time amounts to only a couple of epochs. In Fig. 5.26 the temporal progress of the SD IF ambiguities is shown. In order to ensure a better overview of the ambiguities, the absolute values of the ambiguities are shown. As for the ZTD, the ambiguities solely need a couple of epochs to settle, see also Fig. 5.27. Furthermore the changes of the reference satellite (see Fig. 5.12) are clearly visible in Fig. 5.26. They lead to the jumps in the values of the SD IF ambiguities. As an aside, note that the SD PPP solution does not start at 00:00. The reason for this is that the initialization of the outlier detection algorithm requires a couple of epochs. During that time no parameter estimation takes place.

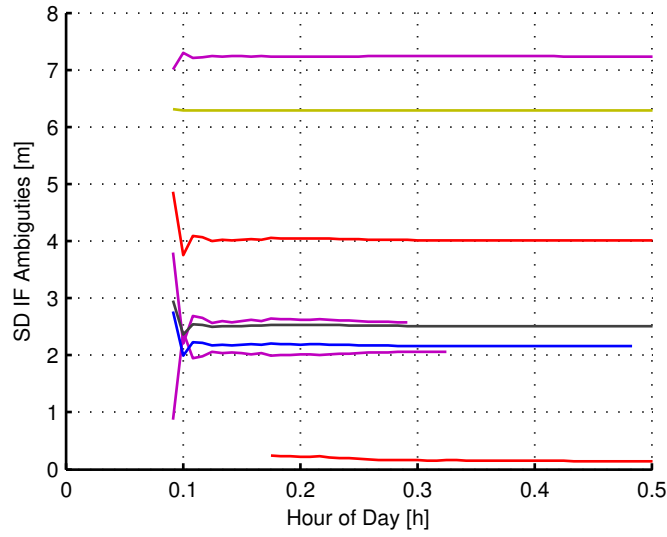


Figure 5.27: Temporal behavior of the SD IF ambiguity parameter at station Belfast

5.3.5.2 Fixing of the SD WL ambiguities

According to Eq. 5.55 the SD PPP solution provides a value for the SD IF float ambiguity B_3^{Ref-j} , which is the first term of the equation. For the estimation of the SD NL UPDs also a value for the second term of the equation \hat{N}_{WL}^{Ref-j} , the integer fixed SD WL ambiguity, is required. This value is obtained by fixing the SD WL ambiguities at each individual station using the previously estimated SD WL UPDs. The fixing of the SD WL ambiguities is performed using a very simple approach. At first the SD WL ambiguities are corrected by means of the corresponding SD WL UPD according to

$$N_{WL}^{Ref-j} = \frac{L_{WL}^{Ref-j}}{\lambda_{WL}} - SD\ WL\ UPD^{Ref-j} \quad (5.66)$$

where N_{WL}^{Ref-j} is the corrected SD WL ambiguity, $\frac{L_{WL}^{Ref-j}}{\lambda_{WL}}$ the SD WL ambiguity and $SD\ WL\ UPD^{Ref-j}$ denotes the corresponding UPD whereby all of these values are given in WL cycles. Afterwards the corrected SD WL ambiguities are rounded to the nearest integer value \tilde{N}_{WL}^{Ref-j} . An ambiguity is fixed, if the requirement given in Eq. 5.67 is fulfilled:

$$|N_{WL}^{Ref-j} - \tilde{N}_{WL}^{Ref-j}| < 0.25 [cycles]. \quad (5.67)$$

This approach represents probably the most simple solution for an ambiguity fixing algorithm. Nevertheless, due to the relatively large wavelength of the WL observation, this approach is sufficient for a successful fixing of most of the WL ambiguities without making too many mistakes. Of course, a change of the reference satellite also affects the fixed SD WL ambiguities. In order to keep the ambiguities consistently fixed, they are corrected according to the already known procedure (see Eq. 5.54).

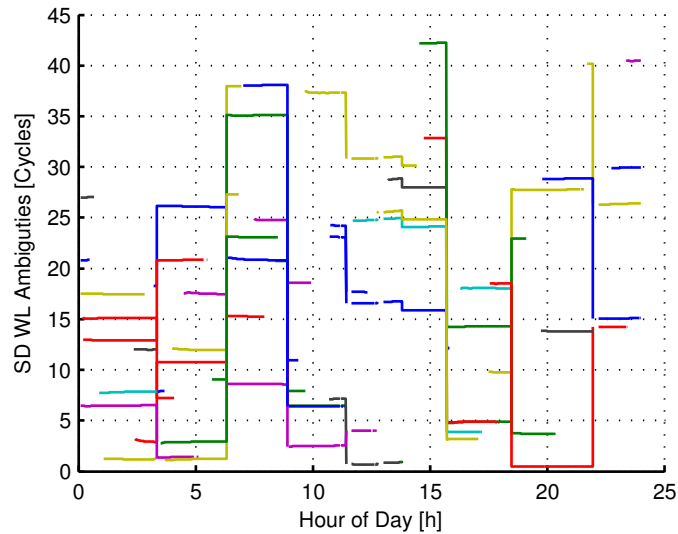


Figure 5.28: Fixed SD WL ambiguities at station Belfast

In Fig. 5.28 the fixed SD WL ambiguities are shown during the first day of GPS Week 1783. In order to make the figure more clear, the absolute values of the ambiguities are shown. It can be seen that the changes of the reference satellite (see Fig. 5.12) result in jumps in the fixed ambiguities. Furthermore, it can be seen that about 6 to 7 SD WL ambiguities are fixed for most of the time, which means that almost every SD WL ambiguity could be fixed.

5.3.5.3 Estimation of the UPDs

In case of a successful fix of the SD WL ambiguities the estimation of the corresponding SD NL UPDs can be carried out. The estimation is based on the combination of the SD NL ambiguities observed at the stations of the reference network, which are calculated according to Eq. 5.55. Like the WL UPDs also the NL UPDs consist of an integer part and a fractional part, whereby the integer part cannot be separated from the integer ambiguity. As we know the fractional part is sufficient to restore the integer nature of the ambiguities. For the calculation of these parts the familiar principle of the positive fractional parts is used again (see Sect. 5.3.4). The estimation of SD NL UPDs itself is performed in the same way as in case of the SD WL UPDs. So the NL UPDs are estimated as parameters within a Kalman filter from the observations of the network solution. Following this, the parameter vector \mathbf{x} just contains the SD NL UPDs of the satellites $1 \dots n$ with respect to the reference satellite Ref , which means that the vector consists of n parameters. In order to ensure a reliable estimation of the NL UPDs, only those UPDs which are observed by more than 20 observations are estimated. The initial values of the parameter vector are calculated by building the median of the positive fractional parts of the $SD\ NL\ UPD_i$ solutions of the different stations i according to:

$$SD\ NL\ UPD = Median \{SD\ NL\ UPD_i\} \quad (5.68)$$

These values are applied to the a priori state vector \mathbf{x}_{k-1} . In addition to that, also the standard deviations are calculated and put into the corresponding entries of the covariance matrix of the a priori states \mathbf{P}_{k-1} . Since the satellites cannot be observed continuously, the length of the parameter vector and the covariance matrix vary with time. If a satellite is not visible any more, the corresponding SD NL UPD parameter is removed from the parameter vector and the covariance matrix. If a new satellite rises and is observed by enough stations, the corresponding SD NL UPD parameter is added to the parameter vector and the covariance matrix must be initialized subsequently.

After the initialization of the filter, the prediction of the parameters and the covariance matrix is carried out using Eqs. 5.39 and 5.40. As for the WL UPDs the prediction of the NL UPDs is based on the assumption that the UPDs are constant. This means that there are no changes between two observation epochs and, therefore, the model can be written as follows:

$$\overline{SD\ NL\ UPD}_k = \widehat{SD\ NL\ UPD}_{k-1}. \quad (5.69)$$

Thus, the transition matrix results in an $n \times n$ identity matrix ($\mathbf{T}_k = \mathbf{1}$).

The prediction of the covariance matrix of the parameters requires the transition matrix that was just determined and the estimated covariances of the previous epoch. Due to an imperfect error modeling the covariance matrix is not a $n \times n$ zero matrix. This is contrary to the estimation of the WL UPDs. Especially small errors have not to be taken into account. According to Sect. 5.2.8, the sum of these errors accounts to 3-5 cm. Some of these errors, like remaining satellite clock corrections or uncertainties in the mapping function, are highly correlated with the UPDs. Due to the high correlation, the estimated UPDs contain parts of these remaining errors. In order to take this fact into account a non-zero value for the disturbances is used. For further calculations, the design matrix \mathbf{H}_k , the covariance matrix of the observations \mathbf{R}_k and the vector \mathbf{l}_k , which is the difference between the observations and the prediction, are needed. The design matrix is obtained by differentiation of the observation equations with respect to the unknown parameters. In case of the SD NL UPDs, the observation equations look as follows.

$$L_k = SD\ NL\ UPD_k \quad (5.70)$$

The number of rows of the design matrix \mathbf{H}_k , which is an identity matrix, is determined by the number of observations, the number of columns by the number of unknown parameters. The values in the design matrix are obtained from a station-by-station differentiation of the observation equations. In a next step, the calculation of the observation vector \mathbf{l}_k is carried out according to Eq. 5.45. According to that, the vector contains just the differences between the observations

and the corresponding predicted parameters.

$$\mathbf{l}_k = \begin{bmatrix} L_{1,k} - \overline{SD\ NL\ UPD}_{1,k} \\ L_{2,k} - \overline{SD\ NL\ UPD}_{2,k} \\ \vdots \\ L_{m,k} - \overline{SD\ NL\ UPD}_{m,k} \end{bmatrix} \quad (5.71)$$

To setup the covariance matrix of the observations \mathbf{R}_k , which are the fractional parts of the SD NL ambiguities, the law of error propagation is applied to Eq. 5.55. However, the second term of the right-hand side of the equation is ignored. The reason for this is, that one can assume that the fixed SD WL ambiguities have no error and, therefore, they do not influence the accuracy of the SD NL ambiguities. As a consequence the equation is simplified and can be written as follows:

$$\sigma_{B_{NL}} = \sqrt{\frac{(f_1 + f_2)^2}{c^2} \cdot (\sigma_{B_3})^2} \quad (5.72)$$

Inserting the standard deviations of the estimated SD IF float ambiguities for σ_{B_3} leads to the accuracy of the corresponding SD NL ambiguities. Assuming that the standard deviation amounts to 1 cm this would lead to a standard deviation of ~ 0.1 NL cycles. For completeness it should be mentioned that, in case of a reference satellite change, the SD NL UPDs are corrected using Eq. 5.54.

In the end, the update phase takes place, where the matrices previously created are linked together and deliver as a result an optimal estimation of the unknown parameters. The estimated SD NL UPDs and the corresponding variances are stored internally and written to a ASCII file.

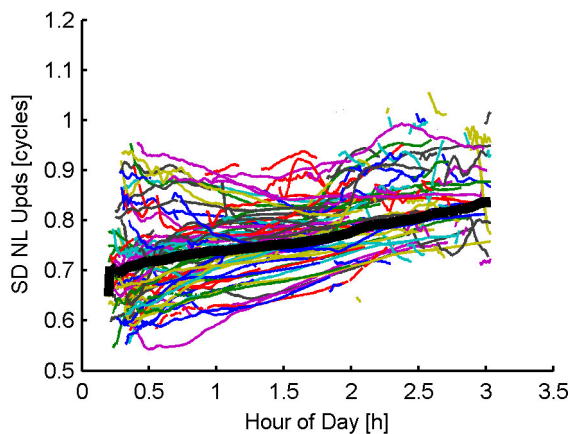


Figure 5.29: SD NL UPD PRN16 - PRN21

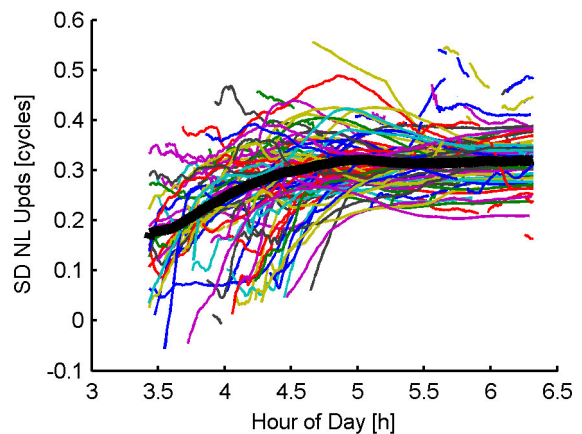


Figure 5.30: SD NL UPD PRN19 - PRN32

Figures 5.29 and 5.30 present the results of the Kalman filter for the satellite pairs PRN16 - PRN21 and PRN19 - PRN32. As for the SD WL UPDs, the observations of the individual stations are illustrated by different colors. In addition to that, the solution of the Kalman filter is illustrated

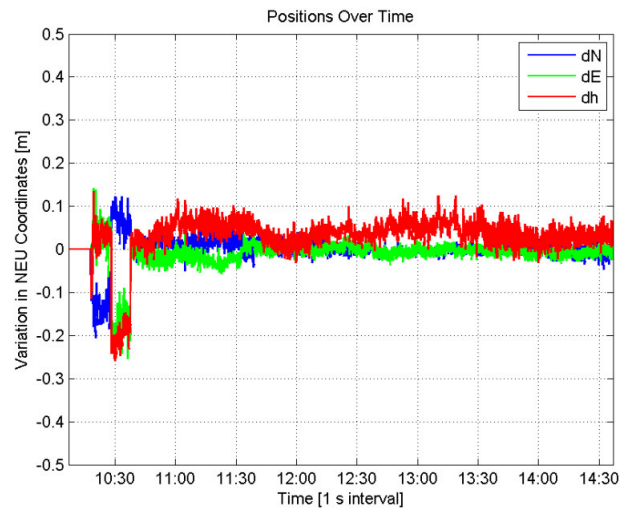


Figure 5.31: PPP solution with ambiguity fixing

by a thick black line. It can be seen, the solution of the Kalman filter corresponds to about the mean value of the observations. Furthermore, it becomes evident that the observations and the estimated SD NL UPD are not completely stable. As discussed earlier in this section, this originates from an imperfect error modeling. However one has to keep in mind that the NL wavelength corresponds to ~ 10 cm, which means that a tenth of a cycle corresponds to ~ 1 cm. Therefore, the observations and the estimated SD NL UPD presented in Fig.5.29 and Fig5.30. are in the range of 1-2 cm, which corresponds to the accuracy of the observations.

5.3.6 Application of the UPDs

At this point a small review about the application of the estimated WL and NL UPDs at the rover-side will be given. This only includes the basic principle and an example of a successful application of the UPDs at a PPP user client. Detailed information on this topic and integer ambiguity fixing at a PPP user client in general can be found in Huber (2015) or Huber et al. (2014), who generously provided the result which will be presented in the following. The application of the UPDs is actually very simple and is realized by adding or subtracting, depending on the definition, the WL and NL UPDs to or from the corresponding float ambiguities, respectively. After this step the ambiguities should be close to integer values and can be fixed using different procedures. A simple procedure for ambiguity fixing was already presented in Sect. 5.3.5.2.

The following figure (Fig. 5.31) shows an integer ambiguity PPP solution which was generated using observation data of the IGS station Graz Lustbühel (GRAZ) of DOY 87 in 2013 together with the precise orbit and clock products of the IGS. In this example the UPDs, which have been estimated with the PPP Post software, were applied to recover the integer nature of the WL and NL ambiguities. As soon as the 4th narrow-lane ambiguity value is fixed to an integer – in the example illustrated in Fig. 5.31 this happens after a couple of minutes – the horizontal position solution stays extremely stable in the surrounding of ± 2 cm of the reference coordinates. In contrast to the

common float PPP solution, the convergence time decreases to a couple of minutes. Furthermore the east-component is as accurate as the north-component, which arises from the fact, that the ambiguities are no unknowns anymore.

Chapter 6

Influence of satellite orbits and clock corrections on the estimation of the WL and NL UPDs

This section is a central element of this thesis and deals with the influence of satellite orbits and clock corrections on the estimation of the WL and NL UPDs. Several investigations have been carried out which are basically concentrated on two issues. The first one is the influence of the accuracy and availability of satellite orbits and clock corrections on the stability and availability of UPDs. The second one is the impact of specific errors in the satellite orbits (in radial, along-track and cross-track direction) and clock corrections (a constant clock offset, clock jumps and a clock drift) on the estimation process and their effect on the numerical results of the UPDs. In further consequence it has been investigated, if and to what extent, these errors are compensated by the UPDs.

6.1 Influence of the accuracy and the availability of satellite orbits and clock corrections

This section contains the results of intensive investigations on the influence of the accuracy as well as the availability of satellite orbits and clock corrections on the stability and availability of the WL and NL UPDs. The influence of the accuracy was studied looking at the stability of the UPDs, which is a parameter of particular interest for two reasons. The first reason is the update rate of the estimation of the UPDs in the Kalman filter as well as the update rate of the transmission of the UPDs to the user. Both should be chosen in such a way that a reliable estimation as well as application of the UPDs is possible. The second reason is that the UPDs, in general, are expected to be stable. This expectation is based on the fact that calibration delays, like the UPDs, should be stable as long as the electron signal chain and the software interface for the generation of the signal do not change. In order to test this hypothesis, the short-term as well as the long-term

stability of the UPDs were investigated. In addition to that, the ZTDs of the SD PPP solutions were compared to the ZTDs of a network solution. Furthermore, the observation residuals were examined as well. Based on these investigations a reliable statement on the influence of the accuracy of the satellite orbits and clock corrections on the stability of the UPDs could be made. In addition, the influence of the availability of the satellite orbit and clock corrections on the availability of the estimated WL and NL UPDs was investigated.

For the investigations WL and NL UPDs were estimated by means of the real-time simulation mode of the PPP Post software. For the estimation daily observations with a temporal resolution of 30 seconds covering GPS weeks 1783-1784 of the chosen network of EPN stations (see Fig. 5.9) have been processed using an elevation cut-off angle of 10° . The estimated parameters included the station specific ZTDs as well as the WL and NL UPDs. The computation was carried out twice, using the precise (IGS) as well as the real-time (IGC01) orbit and clock products of the IGS (IGS (2015)). The solution, which was generated with the precise IGS products served as reference and will be referred to as IGS solution. The solution generated with the real-time product IGC01 will be referred to as IGC solution in the following.

6.1.1 Stability and availability of the satellite WL UPDs

It is expected that the satellite WL UPDs are stable over a couple of days or even weeks. This expectation is based on two different reasons. The first one is that the WL UPDs are estimated based on satellite-to-satellite SD observations of the MW linear combination, which are free of errors except for satellite delays. The second reason is the large wavelength of the WL linear combination, which is large compared to the mismodeling of small errors. The investigations focused on the short-term and long-term stability of the UPDs, as these are the decisive parameters for the update rate of the estimation and the transmission of the UPDs.

IGS solution

To start with, the results of the investigation of the short-term stability of the WL UPDs of the IGS solution are shown over the first day of the investigation period (GPS Week/Day 1783/1) in Fig. 6.1. In order to avoid the overlap of different symbols and to make the figure more clearly to read only six representative satellite pairs, are shown. Each symbol denotes an estimate of a WL UPD at one epoch and each consecutive row of identical symbols corresponds to one pass of a satellite pair. As demonstrated within such a pass, the WL UPDs vary within less than 0.05 cycles.

For a more detailed investigation the mean value and the standard deviation of the estimated UPD series of each single pass of every satellite pair for GPS Week/Day 1783/1 were estimated. As may be imagined, the standard deviation provides information on the stability of the UPDs. In Fig. 6.2 and Fig. 6.3 the mean values and the standard deviations for the first passes of all satellite pairs with respect to two different reference satellites are shown. The mean values are

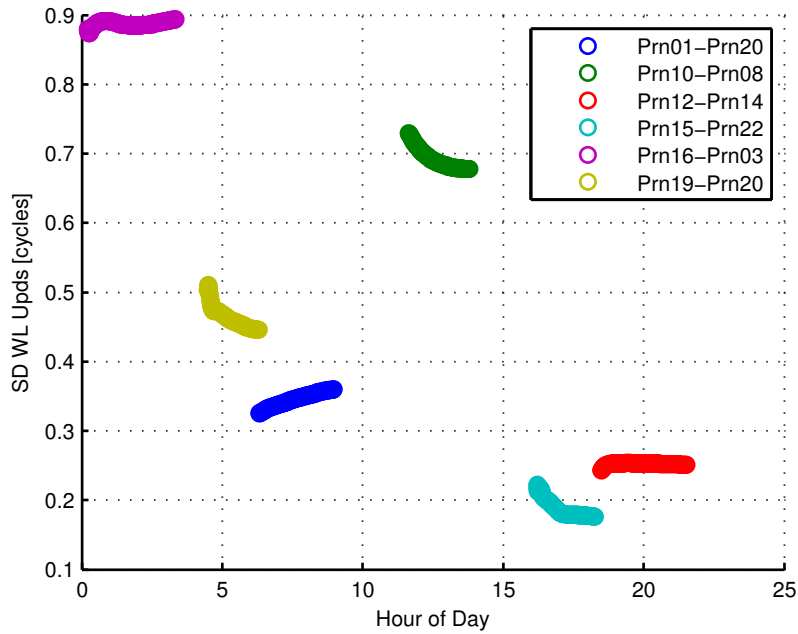


Figure 6.1: SD WL UPDs of six satellite pairs on GPS Week/Day 1783/1 (IGS solution)

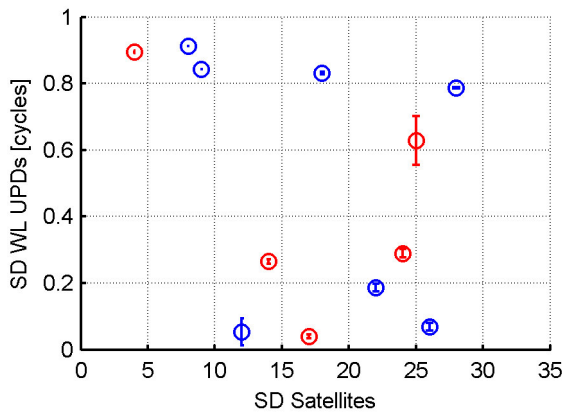


Figure 6.2: Mean values and standard deviations of the SD WL UPDs of the first passes of all satellite pairs related to reference satellite PRN15 on GPS Week/Day 1783/1

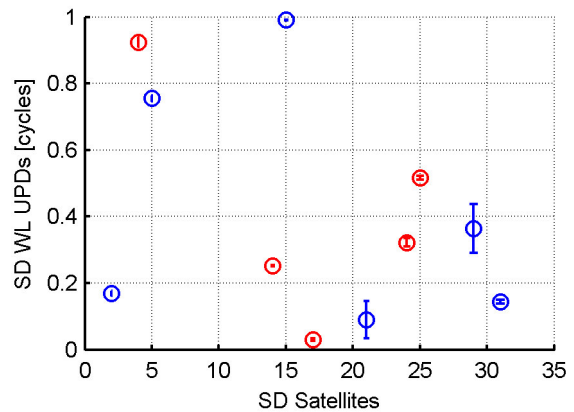


Figure 6.3: Mean values and standard deviations of the SD WL UPDs of the first passes of all satellite pairs related to reference satellite PRN12 on GPS Week/Day 1783/1

illustrated by circles and the corresponding standard deviations as error bars. It can be seen, that the standard deviations are so small that the error bars are hardly visible in most of the cases. The biggest values are related to the WL UPDs of the satellite pairs PRN15 - PRN25, PRN12 - PRN21 and PRN12 - PRN22. They are smaller than 0.1 cycles, however. This reflects the good short-term stability of the WL UPDs within the satellite pair passes. Comparing Fig. 6.2 and Fig. 6.3 it seems that they do not look very similar. First of all the two figures differ with respect to the visible WL UPDs, which is caused by fact that they do not cover the same time period. However, there are five WL UPDs, highlighted by the red circles, which are present in both figures. These WL UPDs should just be shifted by a constant, however, except for PRN25, there seem to be no difference. The constant shift can be estimated using Eq. 5.54. According to that the constant shift is the negative value of the SD WL UPD between the difference of the two reference satellites (PRN15 and PRN12). In Figs. 6.2 and Fig. 6.3 it can be seen that this value is close to zero and one, respectively. The difference of the WL UPDs of PRN25 is caused by a reset of the corresponding parameter in the Kalman filter, which is also indicated by the larger standard deviation visible in Fig. 6.3.

For a precise statement on the stability, a histogram of the standard deviations of all satellite pair passes during the investigation period was created. In total 1578 passes have been observed, which means that a reasonable conclusion on the short-term stability could be made. As shown in Fig. 6.4 the standard deviation of the majority of the passes lies within the range of 0.05 cycles, whereby in most of the cases they are even smaller than 0.0025 cycles. There are only a handful of passes with larger standard deviations, the biggest one corresponding to approximately 0.15 cycles. This means that the WL UPDs can reasonably be assumed to be constant during a pass, which is a first proof that the assumption on the stability of the WL UPDs, at least over a couple of hours, seems to be correct.

However, the presented results did not provide any information on the long-term stability of the UPDs. The long-term stability is of special interest for the update rate of the calculation of the UPDs as well as for the transmission of the UPDs to the user. In case of the UPDs being stable over a couple of days, it would be possible to transmit post-processed WL UPDs. In Fig. 6.5 the mean values of the WL UPD passes of the satellite pairs already known from Fig. 6.1 are shown for the whole investigation period. Only the satellite pair PRN16 - PRN03 has a continuous sequence of passes, while the sequences of the other satellite pairs are interrupted by gaps of different sizes. However, these gaps are not caused by an error of the estimation process but by daily variations of the reference satellite. The reference satellite is selected according to the procedure described in Sect. 5.3.2, which does not guarantee that there is always the same set of reference satellites per day. Of course, this also applies to the WL UPDs related to the reference satellites, which led to the gaps in Fig. 6.1. Apart from the gaps in the solutions, it can be seen that the differences between the daily passes of WL UPDs are smaller than 0.025 cycles. This is even true for the whole investigation period except for the satellite pair PRN16 - PRN03. In this case a drift of approximately 0.05 cycles per week can be identified. In order to determine, if this is an isolated

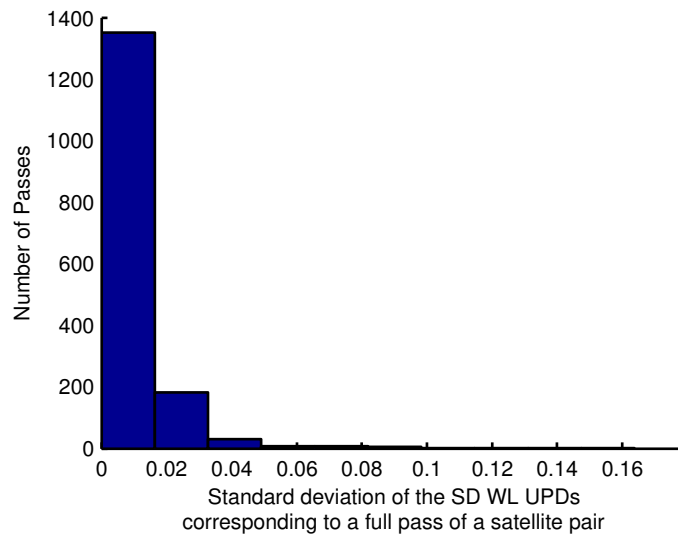


Figure 6.4: Histogram of standard deviations of the WL UPD time series (IGS solution)

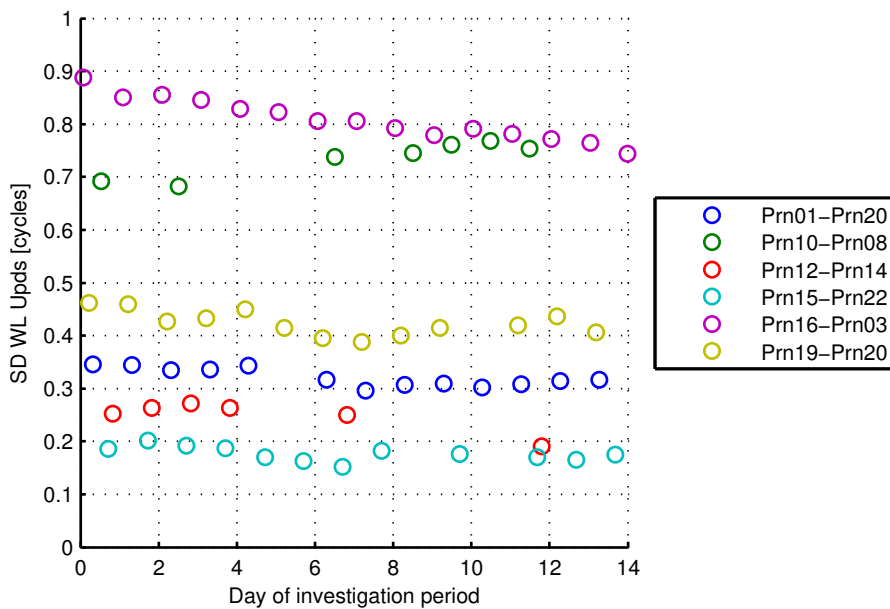


Figure 6.5: Mean values of WL UPD passes during the investigation period (IGS solution)

incident, a more detailed investigation on all series of passes was conducted. At that point, a regression line for every series of satellite pair passes was calculated. Following this, the slopes of the regression lines were determined, which were then used to create the histogram given in Fig. 6.6. As a result, the majority of the UPDs exhibits drifts of less than 0.05 cycles per week, which means that they can be considered to be almost constant. There are only a couple of UPDs, which exhibit drifts greater than 0.05 cycles per week. However, even a drift of 0.1 cycles per week is rather small, since this corresponds to a change of 0.015 cycles per day. The biggest value corresponds to approximately 0.15 cycles per week and can be considered an outlier.

Another approach to investigate the UPD stability is to study the residuals of the estimation process. According to Sect. 5.3.4 the WL UPDs are predicted as constants, assuming that the prediction is free of errors. If this assumption does not apply, this would lead to a continuous increase of the differences between the predicted UPDs and the UPDs observed at the stations. In Fig. 6.7 the histogram of these differences or residuals (30s temporal resolution) for the whole investigation period are shown. The normal distribution has a zero mean value and the standard deviation amounts to about 0.1 WL cycles. This is further proof of that the assumptions made are correct.

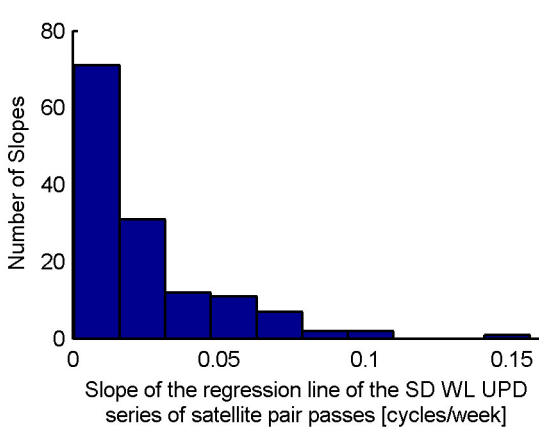


Figure 6.6: Slopes of the regression lines of the SD WL UPD series (IGS solution)

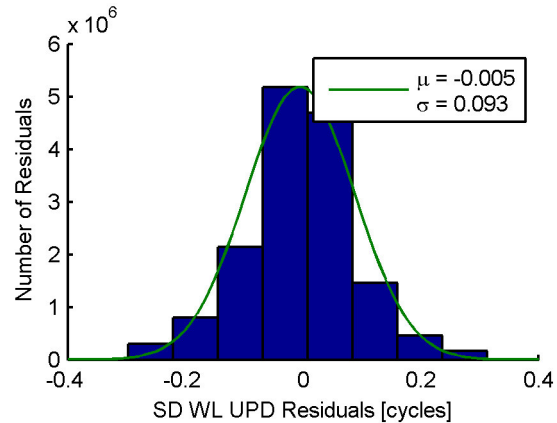


Figure 6.7: Histogram of the absolute WL UPD residuals (IGS solution)

Another very interesting and important aspect, especially for the application of the UPDs at the user side, is the number of estimated WL UPDs. In order to allow for the best possible positioning solution, corrections for every visible satellite should be available. This is of significant importance in case of a restricted field of view, when only a reduced number of satellites is visible.

Fig. 6.8 shows the number of the estimated WL UPDs on the second day of the investigation period (GPS Week/Day 1783/2). Additionally also the number of the satellite pairs, which are observed by more than 30 stations, which is the defined threshold for the estimation of the UPDs, is shown. It can be seen, that there are hardly any differences between the two lines, which means that the WL UPDs are estimated for every satellite pair with enough observations.

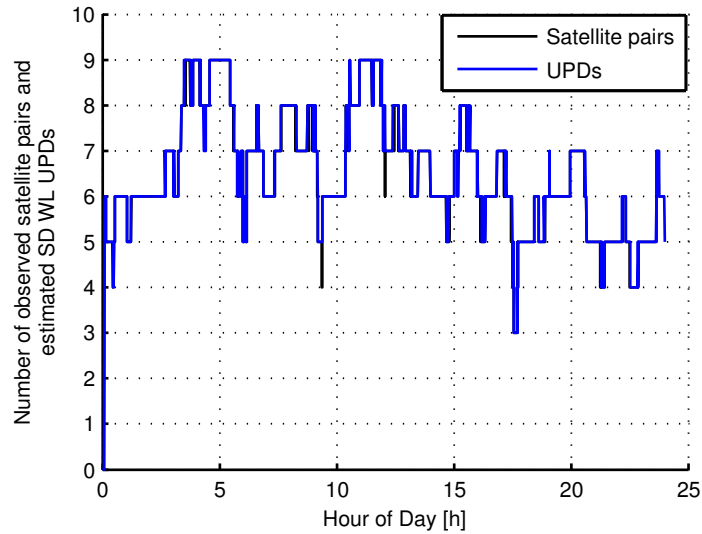


Figure 6.8: WL UPDs on GPS Week/Day 1783/2 (IGS solution)

Summing up, one can say that the WL UPDs exhibit the expected stability. The variations within a pass of a satellite pair are within the range of 0.05 cycles. This also applies for the differences between the daily solutions, which is why the WL UPDs can be considered as constant over these periods. Concerning the stability of periods longer than one day, it is not possible to make a clear statement. Even though most of the UPDs are almost constant for periods longer than one week, a small drift of up to 0.1 cycles per week, can be observed in some cases. Such UPDs cannot be considered as constant. However, regarding the estimation and the transmission of the UPDs, these long-term drifts have no impact. The high stability of the UPDs would allow to use a rather small update rate for the estimation as well as for the transmission of the UPDs. It would be even sufficient to transmit post-processed UPDs of the day before.

IGC solution

According to Sect. 3.1 the precise and the real-time orbit and clock correction products differ with respect to their accuracy and robustness. While the accuracy of the orbits is almost identical, the accuracy of satellite clock corrections differs significantly. It is obvious that this is one of the most critical factors with respect to real-time PPP applications. However, both the orbit errors as well as the satellite clock errors should have no influence on the estimation of the WL UPDs, since both are eliminated in the MW linear combination. In order to examine this, the computation of the WL UPDs was carried out again using the IGC01 product. In Fig. 6.9 the differences between the mean values of the WL UPDs of the daily satellite pair passes of the IGS (see Fig. 6.5) and the IGC solution are shown in terms of a histogram. This graphic confirms that there are hardly any differences between the two solutions. Therefore, the accuracy of the orbit and clock products has obviously no effect on the estimation of the WL UPDs. Hence it is possible to estimate WL UPDs with the highest possible accuracy even in real-time. In Fig. 6.10 the number of estimated

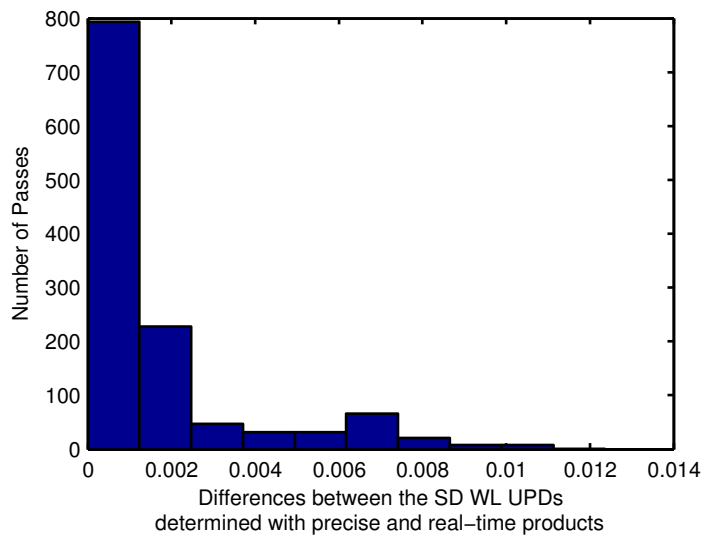


Figure 6.9: Histogram of the differences between the WL UPDs of the IGS and IGC solution

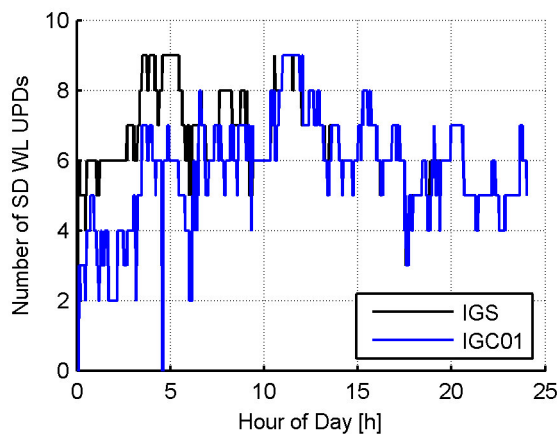


Figure 6.10: Comparison of the number of estimated WL UPDs on GPS Week/Day 1783/2

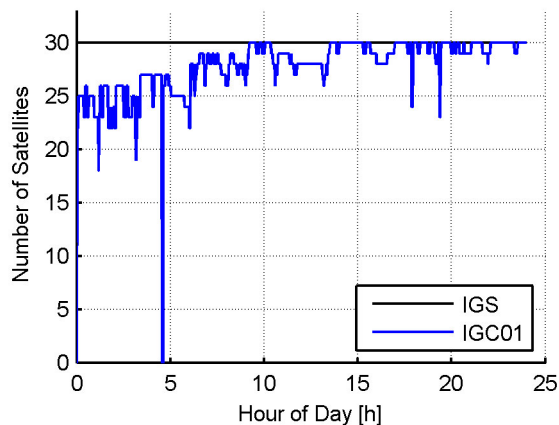


Figure 6.11: Availability of the IGS and IGC01 product on GPS Week/Day 1783/2

WL UPDs is shown in comparison to the solution, which was generated using the precise IGS product. It turns out that, especially at the beginning, there are remarkable differences between the two solutions. Furthermore, there is one period in the IGC solution with even no WL UPD estimates at all. The reason for the differences between the two solutions can be identified in Fig. 6.11, which shows the availability of the IGS and IGC01 product on that day. The IGS product is available for 30 satellites during the whole day, while the availability of the IGC01 product changes continuously. Looking at Fig. 6.10 and Fig. 6.11, it becomes clear that the number of estimated WL UPDs correlates with the availability of the product, which also explains the period with no UPD estimates in the series of the IGC solution. Another disadvantage of the reduced availability of the IGC01 product are more frequent changes of the reference satellite. Missing

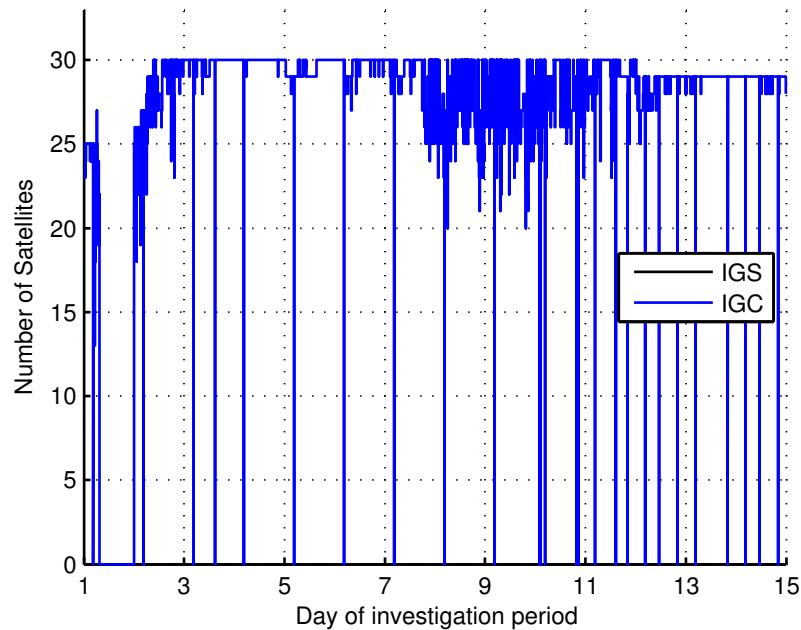


Figure 6.12: Availability of the IGS and IGC01 product during the whole investigation period

ephemerides for the reference satellite requires an immediate reference satellite change according to the procedure described in Sect. 5.3.4.1, or in the worst case, a reset of the filter.

In order to answer the question, whether the reduced availability of the IGC01 product at the beginning of GPS Week/Day 1783/2 is a singular occurrence, the availability of the IGS and IGC01 product during the whole investigation period was plotted as well (see Fig. 6.12). Contrary to the IGS product, the availability of the IGC01 product changes frequently. A slightly reduced number of available satellite orbits and clock corrections has no serious effect on the estimation of the UPDs. Contrary to that, at periods, where the IGC product is completely unavailable, a severe problem comes up, since an estimation of the UPDs is not possible at all. After such a complete outtake it takes up to 15 minutes until it is possible to estimate reasonable UPDs. However, these periods are relatively short, except for the period on the first day of the investigation period, which lasted for several hours. For that reason this day has been ignored in all upcoming investigations.

As noted previously, the estimation of the WL UPDs actually does not require satellite orbit and clock corrections, since they are both eliminated in the MW combination. Nevertheless, in the preprocessing steps of the PPP Post software, observations to satellites without orbit and clock correction data are eliminated. This means that the reduced availability of the WL UPDs is caused by the design of the PPP Post software rather than by the orbit and clock product used.

In conclusion the decreased accuracy of the real-time product has no effect on the estimation of the WL UPDs, since the orbit and clock errors are eliminated in the MW linear combination. Hence it is possible to estimate the WL UPDs with the highest possible accuracy even in real-time.

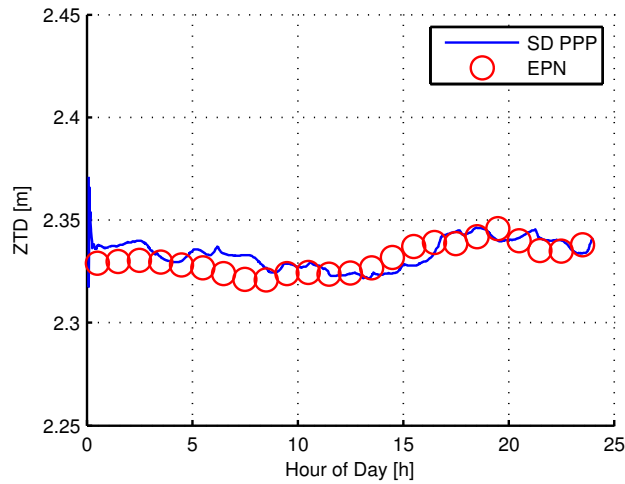


Figure 6.13: Comparison of the ZTDs at station MAN2 on GPS Week/Day 1783/2 (IGS solution)

6.1.2 Stability and availability of the satellite NL UPDs

Contrary to the WL UPDs, the NL UPDs are expected to be less stable (about 0.2 - 0.3 NL cycles). The reason for this is the relatively short wavelength of the NL combination, which amounts to approximately 10 cm. Hence even small range modeling errors map into considerable NL fractional parts. According to Sect. 5.2.8 it is expected, that the applied corrections are accurate at the 3-5 cm level and that the UPDs can be estimated with an accuracy of 3 cm which corresponds to 0.3 NL cycles. As done for the WL UPDs the short-term as well as the long-term stability of the NL UPDs were investigated. The short-term stability is of particular interest for the stability of the Kalman filter. Furthermore, the stability is also the decisive parameter for the update rate of both, the Kalman filter and the transmission of the UPDs to the user. In addition, also the quality of the SD PPP solution has to be evaluated. Again, all investigations were carried out introducing the IGS and IGC product.

6.1.2.1 Quality of the SD PPP solution

IGS solution

To evaluate the accuracy of the SD PPP algorithm, tests focusing on two aspects were performed. First of all the ZTDs, which were estimated within the SD PPP solutions, were compared to ZTDs of a network solution. For comparison, the EPN tropospheric product, which is part of the routinely estimated EPN solutions, was used. This product is available on a weekly basis and contains the zenith troposphere delay estimates for every station of the EPN network with an hourly sampling rate. Furthermore, an investigation of the residuals of the SD PPP solution was conducted. Based on the results an assessment of the accuracy for the SD PPP solution and the corresponding SD IF ambiguities was made.

In Fig. 6.13 the ZTD time series of the SD PPP solution and the EPN solution for the station in Le Mans, which is a representative station, during GPS Week/Day 1783/2 are shown. The ZTDs of the SD PPP solution are available with a temporal resolution of one minute and are illustrated as blue line. An initialization period has to be noted at the start of the displayed interval. The ZTDs of the EPN solution are available with a temporal resolution of one hour and are illustrated as red circles. It can be seen, that the differences are rather small i.e. in the range of only a couple of centimeters.

For a more precise statement, statistics of the ZTD differences between the SD PPP and the EPN solution were created. In Figs. 6.14 and 6.15 the biases and standard deviations of the differences for the whole investigation period are shown for each station of the reference network. The red triangles represent stations with no SD PPP solution during the investigation period, caused by missing observations for that time frame. It can be seen, that all biases are within a range of 2 cm with the majority being close to 1 cm. This is also true for the standard deviations. The mean values of the biases and standard deviations of all stations amounts to about -0.15 cm and 1.0 cm, respectively. This means that the ZTDs of the SD PPP and the EPN solution show a very good agreement during the whole investigation period, independent of the station. However, compared to the EPN solution there is a small systematic offset of about 1.5 mm which indicates that there are still some modeling problems left. Nevertheless, it can be assumed that the SD PPP solution works well under normal conditions and that the accuracy of the ZTDs is in the range of 1 cm only.

Further evidence of this was provided by the investigation of the IF code and phase range observation residuals of the SD PPP solution. In Fig. 6.16 and Fig. 6.17 the values of the IF code and phase observation residuals of the station in Le Mans on the first day of the investigation period are shown. In the outlier detection process of the SD PPP solution, code observations with residuals larger than 4 m and phase observations with residuals larger than 4 cm were removed, which explains the limited value range of the residuals. About 90 percent of the IF code observation residuals are within the range of 2 m, which means that they are rather small. Two jumps in the residuals are caused by the reference satellite, which experienced larger residuals than the other satellites during that time. These jumps are not visible in the phase residuals, as they are captured by the corresponding ambiguities. The IF phase observation residuals are rather small as well, with about 90% being in the region of 2 cm. However, they indicate that there are still some modeling problems left, e.g. satellite clock corrections or errors in the mapping function. In Fig. 6.18 and Fig. 6.19 the histograms for the residuals of all stations during GPS Week/Day 1783/2 are shown. The residuals, which are normally distributed with a zero mean value and standard deviations of about 1.1 m and 1.1 cm, respectively, mimic the residuals observed at the station in Le Mans and are in good agreement with the expected accuracy of the observations (see Sect. 5.2.8). This further proves that the SD PPP solution performs very well under normal circumstances. Combining the earnings of the two investigations, it can be assumed that the accuracy of the estimated SD IF float ambiguities is in the range of 1-2 cm, which allows a reliable

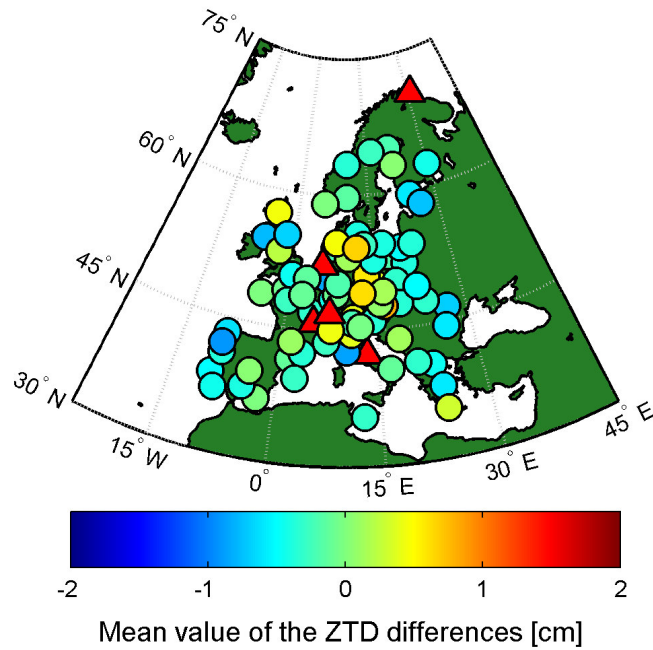


Figure 6.14: Bias of the ZTD differences between the SD PPP solution (IGS) and the EPN solution at each station

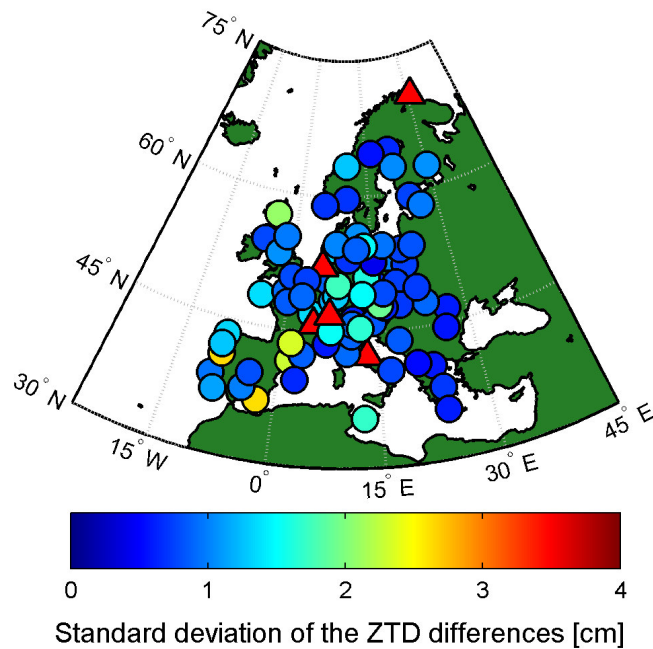


Figure 6.15: Standard deviation of the ZTD differences between the SD PPP solution (IGS) and the EPN solution at each station

estimation of the NL UPDs.

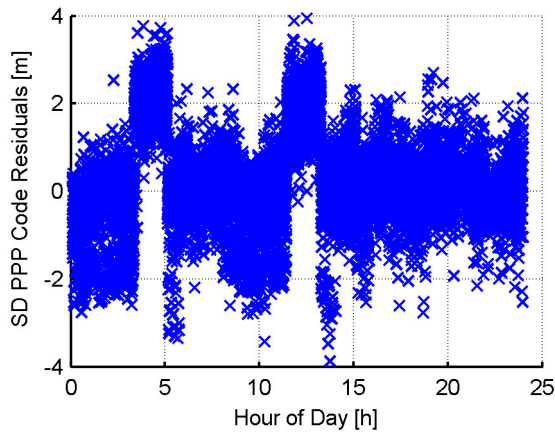


Figure 6.16: IF code observation residuals of the SD PPP algorithm at station MAN2 on GPS Week/Day 1783/2 (IGS solution)

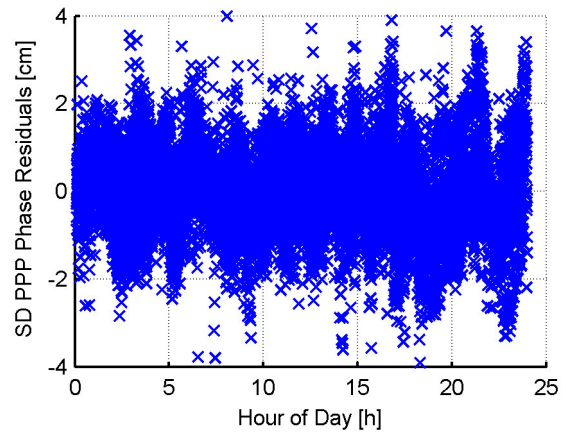


Figure 6.17: IF phase observation residuals of the SD PPP algorithm at station MAN2 on GPS Week/Day 1783/2 (IGS solution)

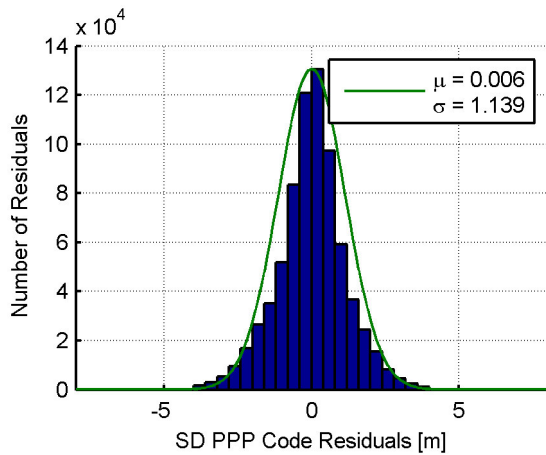


Figure 6.18: Histogram of the absolute IF code observation residuals on GPS Week/Day 1783/2 (IGS solution)

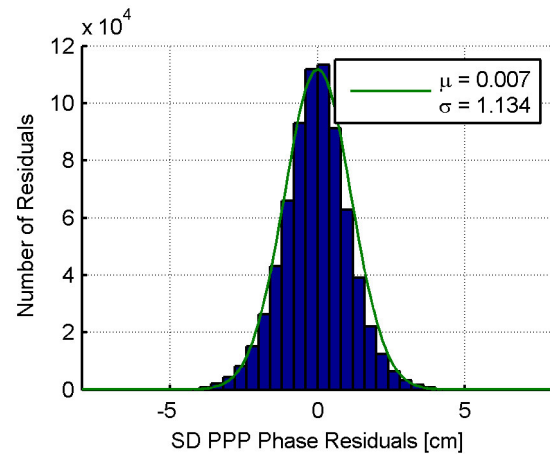


Figure 6.19: Histogram of the absolute IF phase observation residuals on GPS Week/Day 1783/2 (IGS solution)

IGC solution

Contrary to the WL UPDs it is expected, that the accuracy of the satellite orbits and clocks directly effects the estimation of the NL UPDs, since these errors are not eliminated in the estimation process. As it was mentioned before, the estimation of the NL UPDs is based on the SD IF float ambiguities of the SD PPP solutions. Hence it is appropriate to investigate the influence of the satellite orbit and clocks on the SD PPP solutions itself in the first place. In Fig. 6.20 a comparison between the ZTD of the SD PPP using the IGC01 product and the EPN solution for the representative station in Le Mans on the GPS Week/Day 1783/2 is shown. As before, the ZTDs

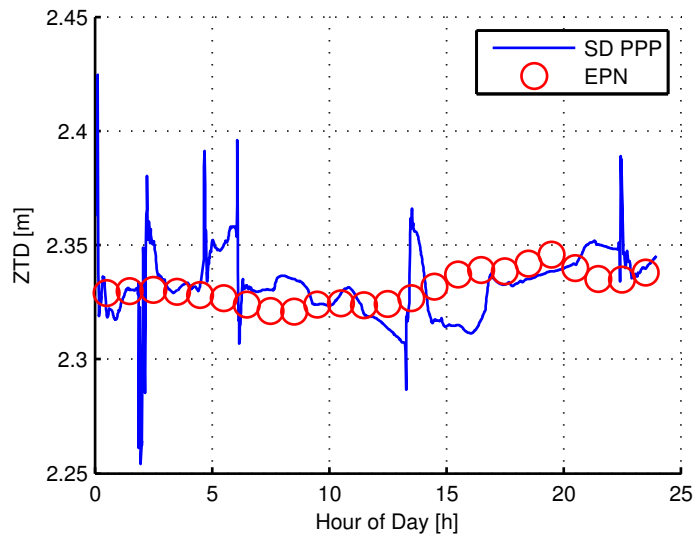


Figure 6.20: Comparison of the ZTDs at station MAN2 of the IGC solution on GPS Week/Day 1783/2

of the SD PPP solution are available with a temporal resolution of one minute and are illustrated as blue line, while the ZTDs of the EPN solution, illustrated as red circles, are available with a temporal resolution of one hour. There is still a good agreement between the two solutions, however in comparison to the IGS solution (see Fig. 6.13), the differences seem to be larger. Furthermore, the SD PPP solution was reset more often, caused by the reduced availability of the IGC01 product (see Fig. 6.11). This reduced availability is especially problematic in view of the SD PPP solution for two reasons. First, the SD PPP solution requires a defined minimum of three SD observations to be successful and, in case of a reduced availability of satellite orbits and clocks, this is not always guaranteed. Furthermore, in case of missing orbit and clock data for the reference satellite, a more frequent change of the reference satellite takes place. Such a change also needs to be considered in the SD PPP solution, which can result in a reset of the filter in the worst case.

As before the statistics of the differences between the SD PPP and the EPN solution were calculated. In Figs. 6.21 and 6.22 the biases and standard deviations of the differences for the whole investigation period are shown for each station of the reference network. Even though the biases and standard deviations are still small they are increased compared to the IGS solution (see Figs 6.14 and 6.15). The mean value of the biases and the standard deviations of all stations amounts to 0.37 cm and 2.19 cm, respectively. This means that using the IGC product led to a degradation of the ZTD estimates, respectively the SD PPP solution. First of all, the systematic offset in the ZTD estimates increased about 2 mm and, furthermore, the standard deviation was increased by about 1 cm. The increase in the standard deviation is caused by two different aspects. The first one is the decreased accuracy of the IGC01 product, especially the accuracy of the clock corrections. The second one is the reduced availability of the IGC01 product, which caused frequent

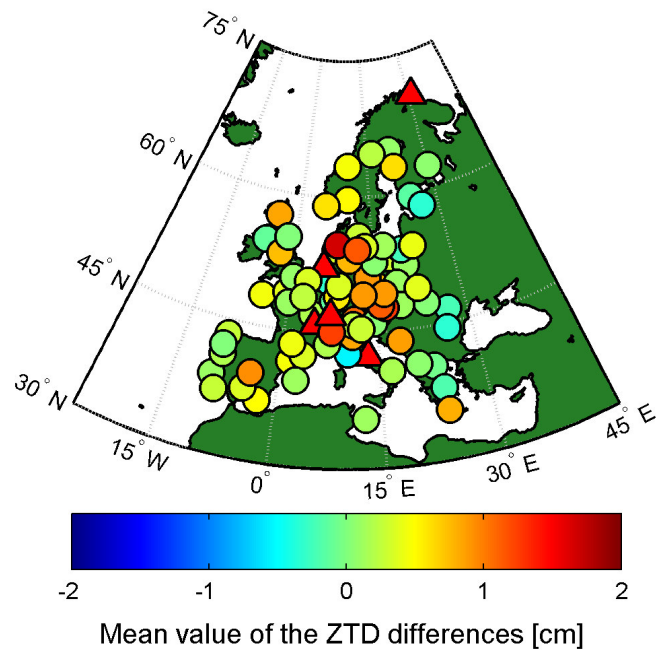


Figure 6.21: Bias of the ZTD differences between the SD PPP solution (IGC) and the EPN solution at each station

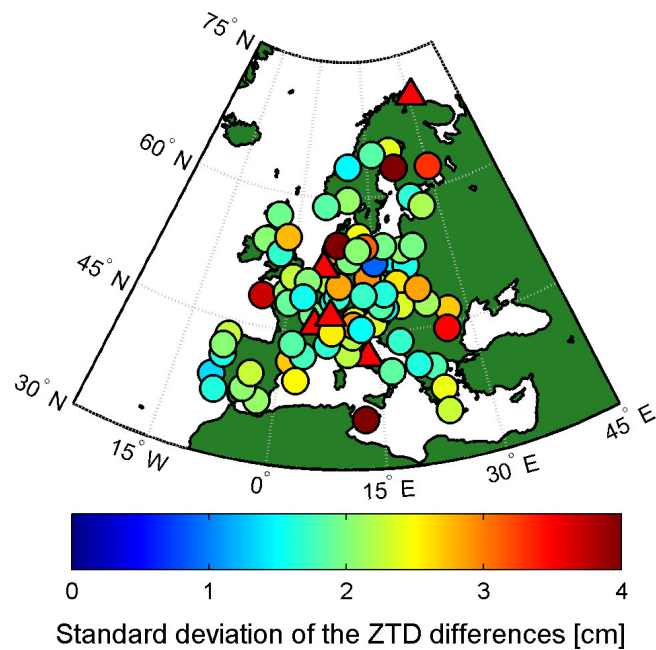


Figure 6.22: Standard deviation of the ZTD differences between the SD PPP solution (IGC) and the EPN solution at each station

resets of the SD PPP solutions. Due to the convergence time of the parameter estimation process this led to a deterioration of the estimated parameters.

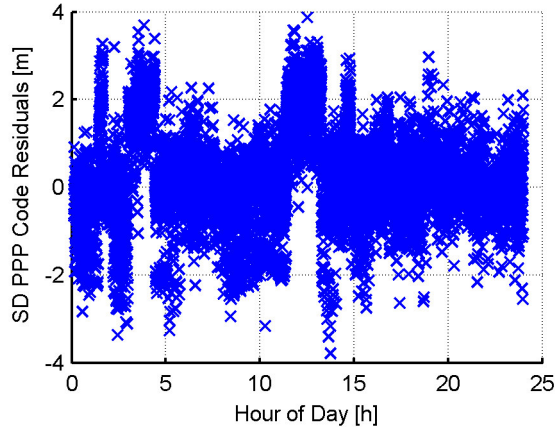


Figure 6.23: IF code observation residuals of the SD PPP solution at station MAN2 on GPS Week/Day 1783/2 (IGC solution)

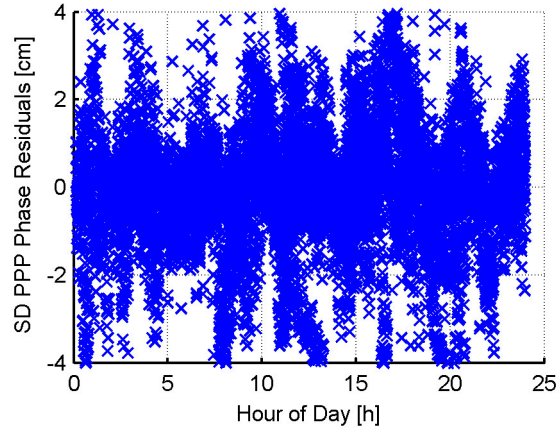


Figure 6.24: IF phase observation residuals of the SD PPP solution at station MAN2 on GPS Week/Day 1783/2 (IGC solution)

Finally, the influence of the satellite orbit and clock corrections on the code and phase observation residuals of the SD PPP solution was investigated as well. In Fig. 6.23 and Fig. 6.24 the IF code and phase residuals of the IGC solution comparable, to Fig. 6.16 and Fig. 6.17, are shown. Obviously the two jumps in the code residuals are also present in the IGC solution, which implies, that they have their origin in a bad tracking of the corresponding reference satellite. Comparing the residuals of the two different solutions shows hardly any differences. For a more precise analysis the histograms of the residuals of all stations during GPS Week/Day 1783/2 have been created as well. In Fig. 6.25 and Fig. 6.26 the histograms for the residuals of all stations during GPS Week/Day 1783/2 are shown. According to the mean values of the normal distributions the residuals are subject of a systematic offset as well. Compared to the IGS solution the mean values of the code and phase residuals are increased by 0.11 m and 0.11 cm, respectively. Contrary to that, the effect on the standard deviations is only marginal as they are only increased by a factor of about 10%. Furthermore, it can be seen that the number of residuals is reduced compared to the IGS solution. This is caused by the limited availability of the IGC01 product.

In conclusion, the reduced availability and accuracy of the satellite orbits and clock corrections of the IGC01 product led to a degradation of the SD PPP solutions. First of all a systematic offset was introduced which was partially absorbed by the ZTD estimates as well as the code and phase residuals. In comparison to the IGS solution the accuracy of the IGC solution was degraded as well. This is indicated by the increased standard deviation of the ZTD estimates of about 2 cm as well as as slightly increased standard deviation of the code and phase residuals. In further consequence, the estimated SD IF ambiguities are not of the same quality as the ambiguities of the IGS solution. In the end, the question arises how the degradation of the SD PPP solution also affects the estimation of the SD NL UPDs. This issue will be subject of the upcoming sections.

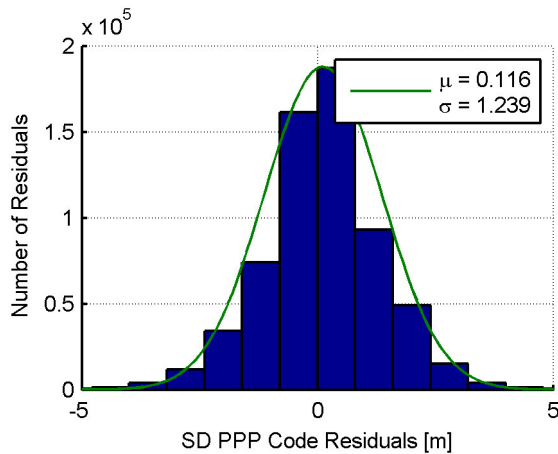


Figure 6.25: Histogram on the IF code observation residuals of GPS Week/Day 1783/2 (IGC solution)

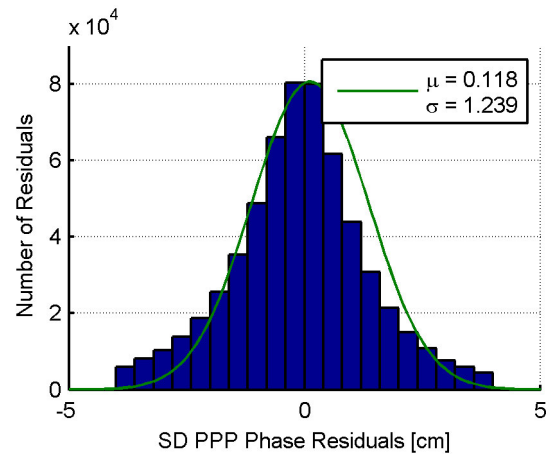


Figure 6.26: Histogram of the IF phase observation residuals on GPS Week/Day 1783/2 (IGC solution)

6.1.2.2 Validation of the fixed SD WL ambiguities

IGS solution

In addition to the IF float ambiguities, the estimation of the NL UPDs also requires fixed SD WL ambiguities. This means that the number of SD NL UPD observations depends on the fixing rates of the SD WL ambiguities. The fixing of the SD WL ambiguities is performed using a very simple approach described in Sect. 5.3.5.2. Since fixing of the SD WL ambiguities takes place with the help of the previously estimated WL UPDs, the fixing rates also allow a conclusion on the quality of the WL UPDs. Table 6.1 shows the fixing rates (FR), the no fix rate (NF) and the no UPD rate (NU) of the SD WL ambiguities at a representative sample of stations, for the whole investigation period. The fixing rate (FR) denotes the percentage of the fixed WL ambiguities w.r.t. the total number of WL ambiguities. On the contrary, the no fix rate and no UPD rate denote the percentage of the WL ambiguities, which could not be fixed w.r.t. the total number of WL ambiguities, whereby a distinction is made, whether the corresponding UPDs have been available (NF) or not (NU). All of the aforementioned rates will be given in percent. For the investigation, only satellite pairs which were observed longer than 10 minutes, have been taken into account. The fixing rate for most of the stations corresponds to about 90 percent. In case of station AQUI the daily observations have not been available and, therefore, the fixing rates could not be estimated. In most cases the reduced fixing rates can be explained by missing UPDs, which particularly affects stations located at the edge of the station network like the stations SUR4, OSLs and VILO. However, there are also some stations which have rather large no fixing rates like HOE2, JOEN, TUC2, DRES and VAAS. In case of HOE2, TUC2 and VAAS these poor rates were probably caused by the receiver types, since the corresponding types do not appear very often in the network. In case of the other stations no correlation between a poor performance and station-specific characteristics could be identified. Summing up, it can be said that the fixing

6.1 Influence of the accuracy and the availability of satellite orbits and clock corrections

Station	FR	NF	NU	Station	FR	NF	NU	Station	FR	NF	NU
ACOR	90.7	0.1	9.1	AQUI	-	-	-	AUTN	94.6	2.2	3.2
BAIA	94.4	0.2	5.4	BELL	93.4	1.5	5.1	BUCU	92.3	0.4	7.3
BYDG	91.0	1.0	8.1	CAEN	91.4	0.8	7.8	CFRM	94.5	0.2	5.2
CPAR	88.9	7.7	3.3	CREU	86.4	7.5	6.2	DRES	77.9	18.3	3.8
ENTZ	96.6	0.7	2.7	GAIA	88.4	1.0	10.6	GRAZ	97.4	1.7	0.9
GWWL	94.3	1.9	3.9	HERT	89.1	2.6	8.3	HOE2	68.6	31.0	0.5
JOEN	77.4	15.3	7.2	KARL	82.7	14.0	3.3	KLOP	94.6	2.6	2.7
LAGO	85.8	1.1	13.1	LAMP	83.9	9.0	7.0	MALL	94.0	0.1	5.9
MATE	96.4	0.0	3.6	MLVL	92.5	1.1	6.4	MOPS	92.3	6.0	1.7
NOA1	76.9	12.9	10.2	OSLS	70.9	10.4	18.8	REDZ	89.4	1.4	9.2
SASS	84.0	14.4	1.6	SONS	92.3	0.2	7.6	SRJV	93.5	2.8	3.7
SUR4	78.6	0.0	21.4	TLSE	91.1	4.7	4.2	TORI	96.9	1.5	1.7
TRF2	97.9	2.1	0.0	TUC2	64.6	23.5	11.9	VAAS	70.8	18.0	11.2
VEN1	98.8	0.1	1.1	VIL0	66.6	9.6	23.7	WTZR	80.5	15.3	4.2

Table 6.1: Fixing rates of the SD WL ambiguities of selected stations of the IGS solution during the investigation period

of the WL UPDs works very well for most of the stations and, therefore, it can be concluded that the estimated WL UPDs are of good quality. Even though there are some stations with poor performance there are enough observations for a reliable subsequent estimation of the NL UPDs.

IGC solution

As shown in the previous section, there are no significant differences between the WL UPDs of the IGS and the IGC solution. Therefore, one can assume that there are also no differences in the fixing rates (given in percent) of the SD WL ambiguities. Nevertheless, the fixing rates of the IGC solution have been calculated as well and the results are presented in Tab. 6.2. Apparently there are no big differences in the rates of the IGS and the IGC solution. The fixing rate of the IGC solution is a little bit worse than that of the IGS solution, which is caused by the reduced number of available UPDs, indicated by the slightly increased no UPD rates. The increased no UPD rate also leads to a slightly reduced no fix rate but one needs to be aware that this is not caused by a decreased accuracy of the estimated UPDs.

6.1.2.3 Satellite NL UPDs

As mentioned in the beginning of this section the NL UPDs are very sensitive even to small errors, caused by the deficiencies in the applied orbits and clock corrections. In the following section, the results of an intense study of the NL UPD of the IGS and IGC solution will be presented which includes investigations of the short-term and long-term stability of the NL UPDs, as well as an investigation of the number of estimated UPDs.

Station	FR	NF	NU	Station	FR	NF	NU	Station	FR	NF	NU
ACOR	88.4	0.1	11.5	AQUI	-	-	-	AUTN	94.0	1.5	4.5
BAIA	92.6	0.2	7.2	BELL	92.0	1.6	6.4	BUCU	87.4	0.1	12.5
BYDG	87.7	0.9	11.4	CAEN	85.1	0.9	14.0	CFRM	90.0	0.2	9.8
CPAR	87.8	6.3	5.9	CREU	84.2	7.5	8.3	DRES	82.8	10.4	6.8
ENTZ	95.6	0.5	3.8	GAIA	85.9	1.2	12.9	GRAZ	94.0	1.1	4.9
GWWL	89.4	0.2	10.4	HERT	88.3	2.3	9.3	HOE2	71.3	27.5	1.2
JOEN	75.6	12.9	11.5	KARL	85.6	11.0	3.4	KLOP	93.9	2.6	3.5
LAGO	82.0	1.3	16.7	LAMP	83.9	8.1	8.1	MALL	93.7	0.0	6.3
MATE	93.9	0.0	6.1	MLVL	90.4	2.1	7.5	MOPS	94.0	3.1	2.8
NOA1	75.4	7.7	16.8	OSLS	66.3	8.8	24.9	REDZ	84.6	1.2	14.2
SASS	85.8	10.1	4.1	SONS	89.9	0.1	10.0	SRJV	89.5	2.4	8.1
SUR4	74.3	0.0	25.7	TLSE	89.5	3.6	6.9	TORI	97.6	0.4	2.0
TRF2	98.4	0.8	0.8	TUC2	64.2	16.4	19.4	VAAS	71.6	14.7	13.7
VEN1	98.4	0.1	1.5	VIL0	62.3	7.4	30.3	WTZR	80.3	11.2	8.5

Table 6.2: Fixing rates of the SD WL ambiguities of selected stations during the investigation period using the IGC product

IGS solution

Initially a survey of the short-term stability was carried out. In Fig. 6.27 the NL UPDs are shown for GPS Week/Day 1783/2. As in the case of the IGS solution only six selected satellite pairs are shown. Each symbol denotes an estimate of an SD NL UPD at one epoch and each consecutive row of identical symbols corresponds to one pass of a satellite pair. The displayed UPDs vary within a maximum of 0.1 cycles over a few hours, which means that in general they can be assumed to be stable during a usual network observation period.

For a more detailed investigation, the mean value and the standard deviation of the estimated UPD time series of each single pass of every satellite pair for GPS Week/Day 1783/2 were estimated. Thereby the standard deviation provides information on the stability of the UPDs. In Fig. 6.28 and Fig. 6.29 the mean values and the standard deviations of the first passes of the satellite pairs, w.r.t. to the reference satellites PRN01 and PRN29, are shown. The mean values are illustrated as blue circles and the corresponding standard deviations as error bars. As the standard deviations are rather small the error bars are hardly visible in most of the cases. This reflects the good short-term stability of the NL UPDs within a satellite pair pass.

For a better overview on the stability, a histogram of the standard deviations of the UPD time series of all satellite pair passes during the investigation period was created. In total more than 1400 passes have been observed, which means that a reasonable conclusion on the short-term stability can be made. As shown in Fig. 6.30, the standard deviation of the majority of the passes lies within the range of 0.05 cycles, whereby in most of the cases it is even smaller than 0.025 cycles. This is also indicated by the average which amounts to about 0.02 cycles. There are only a handful of passes, with standard deviations greater than 0.1 cycles, which can be considered

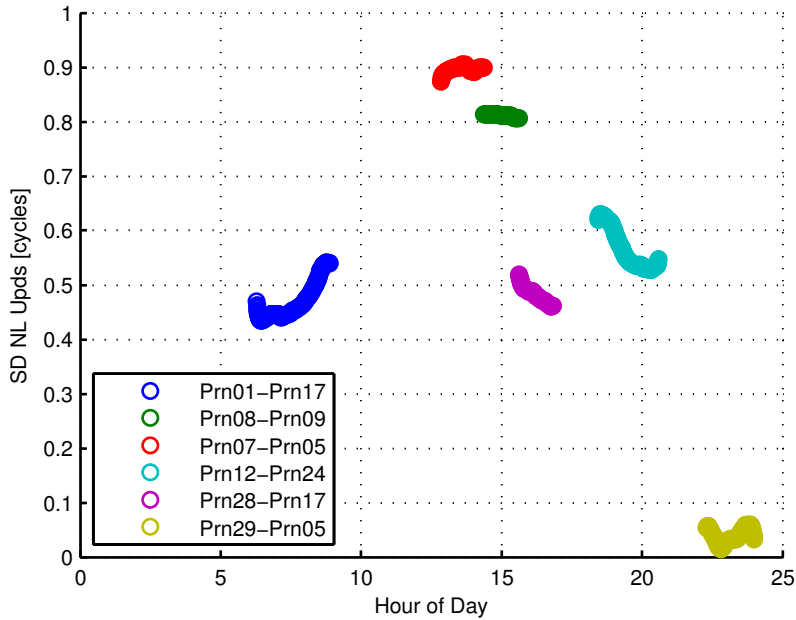


Figure 6.27: NL UPDs on GPS Week/Day 1783/2 (IGS solution)

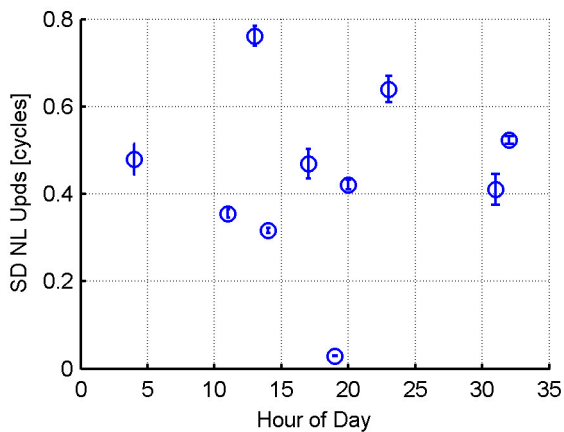


Figure 6.28: Mean values and standard deviations of the NL UPDs of the first passes of all satellite pairs related to reference satellite PRN01 on GPS Week/Day 1783/2

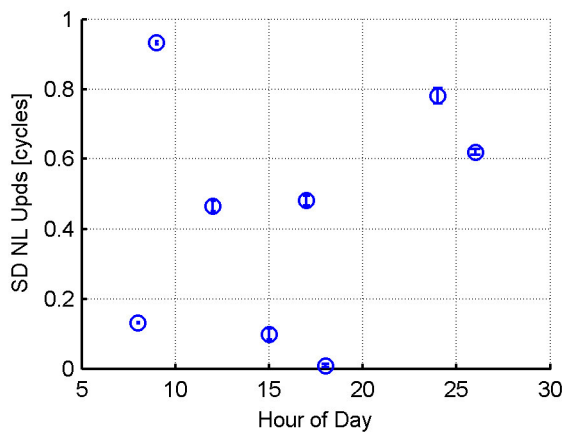


Figure 6.29: Mean values and standard deviations of the NL UPDs of the first passes of all satellite pairs related to reference satellite PRN29 on GPS Week/Day 1783/2

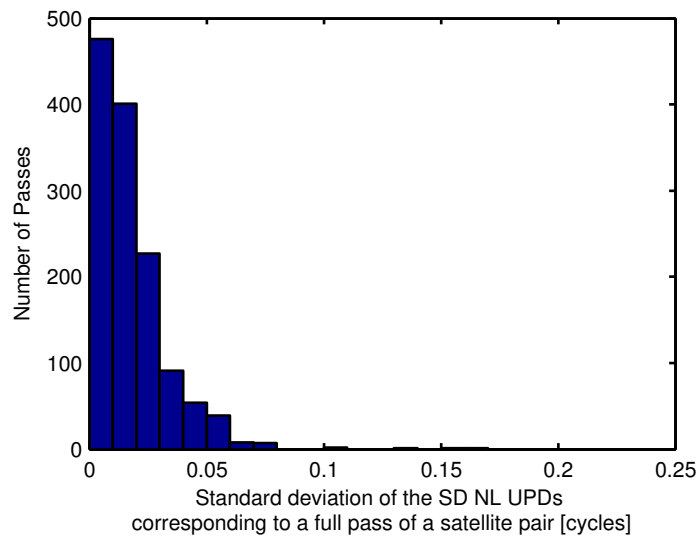


Figure 6.30: Histogram of standard deviations of the NL UPD time series (IGS solution)

as outliers. This validates the previously shown results and confirms that the NL UPDs can be assumed to be almost constant during a pass.

In order to determine whether this also applies to the long-term stability, the progression of the NL UPDs has been investigated as well. In Fig. 6.31 the mean values of the SD NL UPD related to one satellite pair pass are shown for the whole investigation period. It can be seen, that there are significant differences between the passes of the same satellite pair. However, this does not necessarily mean, that there is an error in the estimation of the UPDs. One has to keep in mind that a tenth of a NL cycle corresponds to 1 cm. This means that the variation between the passes corresponds to the expected accuracy of the observations (see Sect. 5.2.8). The variations of the UPDs, which are in the range of a couple of centimeters, are probably caused by remaining in the satellite orbits and clocks, errors introduced by the mapping function, as well as still unknown error sources. Another proof for the good quality of the estimated UPDs is provided by Huber (2015), who has shown that the estimated UPDs can be used to generate an ambiguity-fixed PPP solution at the rover side, which is only possible, if they are of good quality.

A further option to investigate the stability of the UPDs is to analyze the residuals of the estimation process. In Fig. 6.32 a histogram of the residuals for the whole investigation period is shown. The residuals are normally distributed with a zero mean value, which means that the estimation process can be considered to be free of systematic errors. Furthermore, the standard deviation amounts to about 0.1 NL cycles which indicates that the NL UPDs are of high precision.

With respect to their application at the rover side, the number of estimated UPDs is of special interest. In order to allow for the best possible positioning solution, corrections for every visible satellite should be made available. In Fig. 6.33 the number of NL UPDs on GPS Week/Day

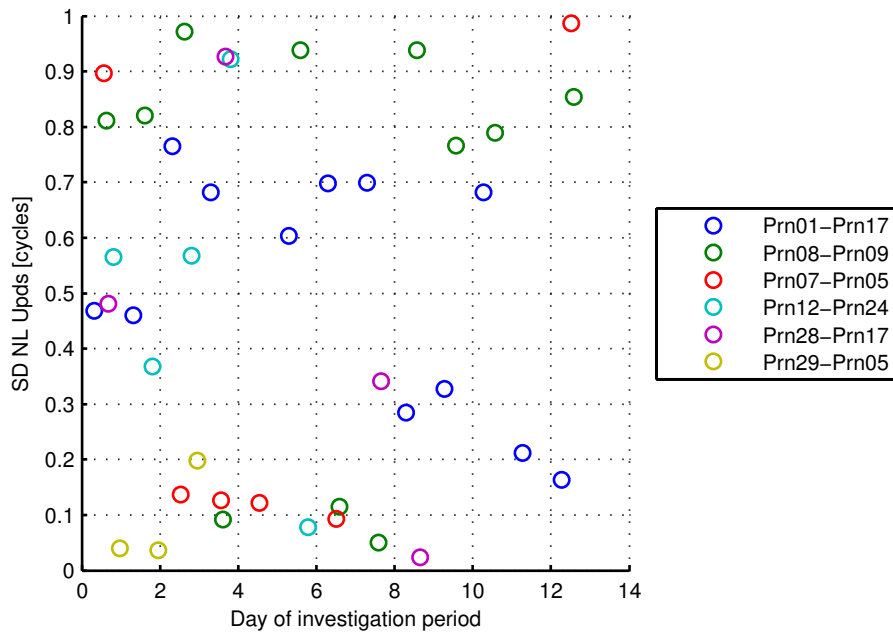


Figure 6.31: Mean values of NL UPD passes during the investigation period (IGS solution)

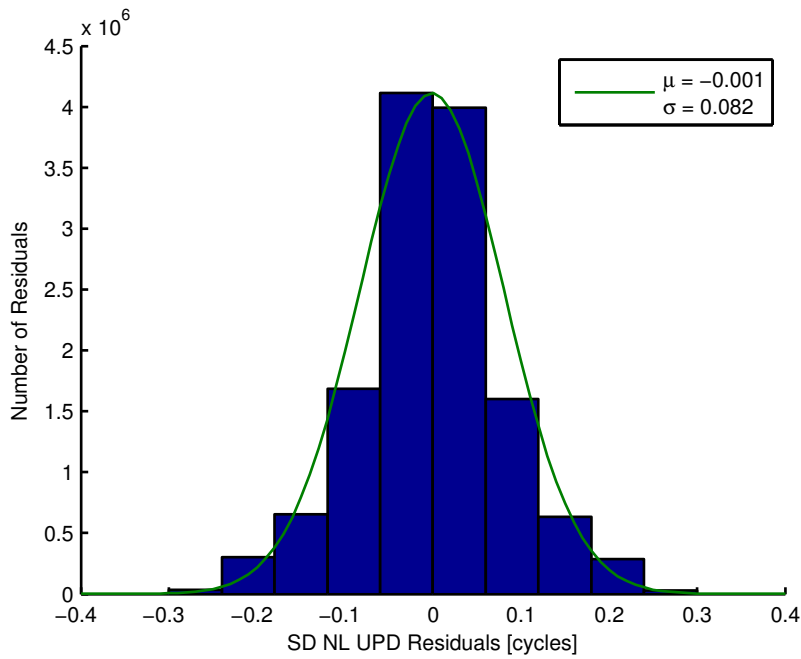


Figure 6.32: Histogram of the NL UPD residuals (IGS solution)

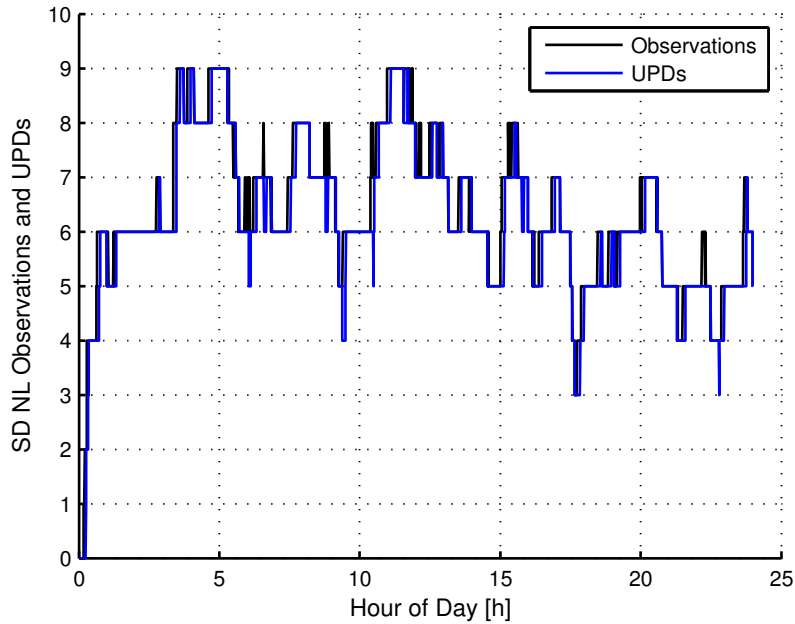


Figure 6.33: NL UPDs on GPS Week/Day 1783/2 (IGS solution)

1783/2 is shown. Additionally, also the number of satellite pairs, which are observed by more than 30 stations, which is the defined threshold for the estimation of the UPDs, is represented. Apparently, there are hardly any differences between the two lines, which means that the NL UPDs are estimated for every visible satellite pair with enough observations.

The investigations have exhibited an interesting behavior in view of the NL UPD stability. While the UPDs are very stable within a pass of a satellite pair, there can be significant differences between the passes. Most likely the reason for this are error model deficiencies. These deficiencies could probably be identified by a global continuous estimation of the NL UPDs. However, this can only be achieved using a global network of reference stations, which is not possible with the current version of the PPP Post software. Nevertheless, the high stability of the NL UPDs within a pass would allow the use of a rather small update rate for the estimation as well as for the transmission of the UPDs. Unfortunately, this high stability does not apply for continuous passes, which means, that it is not possible to use post-processed UPDs as in the case of the WL UPDs.

IGC solution

According to Sect. 4 the estimation of the NL UPDs was carried out by means of the IF float ambiguities and the corresponding fixed WL ambiguities from the SD PPP solutions. While the orbit and clock corrections have hardly any impact on the WL ambiguities, they directly influence the estimation of the IF float ambiguities. The previous investigations have shown that the reduced availability and accuracy of the IGC01 satellite orbits and clocks led to a degradation of the SD PPP solution compared to the IGS solution (see Sect. 6.1.2.1). Using the IGC01 product

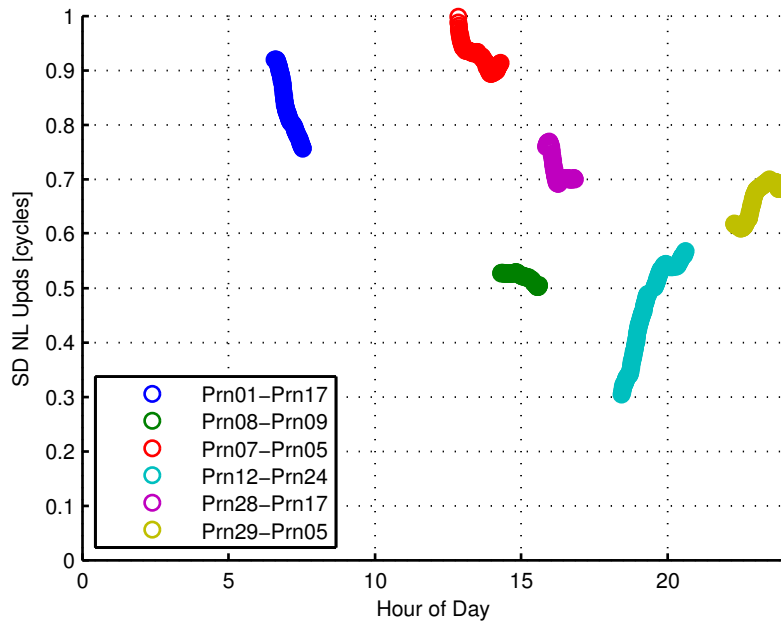


Figure 6.34: NL UPDs of the IGC solution on GPS Week/Day 1783/2

introduced a systematic offset in the ZTD estimates and in the code and phase residuals. Furthermore the accuracy of the ZTD estimates decreased by about 1 cm. Therefore it is expected that the NL UPDs of the IGC solution are not as stable as the NL UPDs of the IGS solution.

As before the short-term stability of the NL UPDs was investigated first. In Fig. 6.34 the NL UPDs of the IGC solution, equivalent to the representative NL UPDs presented in Fig. 6.27, are shown. Again, each symbol denotes an estimate of a NL UPD at one epoch and each consecutive row of identical symbols corresponds to one pass of a satellite pair. Comparing Fig. 6.34 with Fig. 6.27 it becomes obvious that the NL UPDs of the IGC and the IGS solution differ in the mean values of the satellite pair passes as well as in the stability within the passes. The differences in the mean values are caused by the differences of the satellite orbits and clock corrections of the IGC and the IGS product. Even though there are significant differences between the two solutions both of them are correct. However, both solutions can only be used in combination with the orbit and clock products which have been used for the estimation of the UPDs. This means, a user in the field necessarily needs to keep consistency between the satellite orbit and clock corrections and the corresponding NL and WL UPD estimates. Of course, this requirement also applies for all other errors, which have been taken into account in the estimation process. This is probably the most critical factor concerning the application of the UPDs, which must be taken into account carefully by all means.

Contrary to the IGS solution, the NL UPDs of the IGC solution have a higher variability, which is caused by the decreased availability and accuracy of the satellite orbits and clock corrections of the IGC01 product. This especially applies to the NL UPD series of PRN12-PRN24. However,

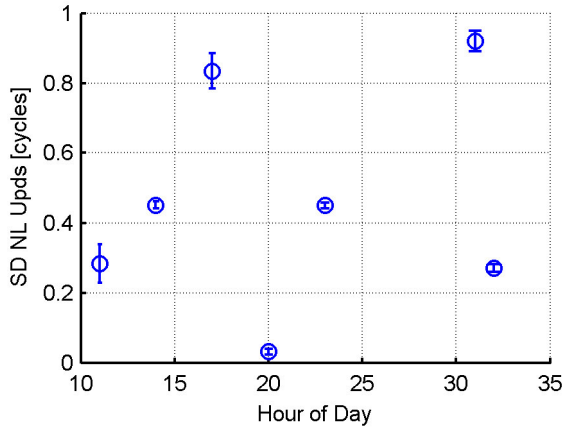


Figure 6.35: Mean values and standard deviations of the NL UPDs of the first passes of all satellite pairs related to reference satellite PRN01 on GPS Week/Day 1783/2

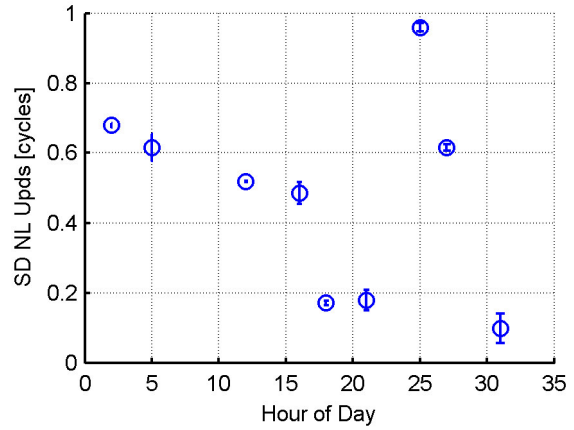


Figure 6.36: Mean values and standard deviations of the NL UPDs of the first passes of all satellite pairs related to reference satellite PRN 29 on GPS Week/Day 1783/2

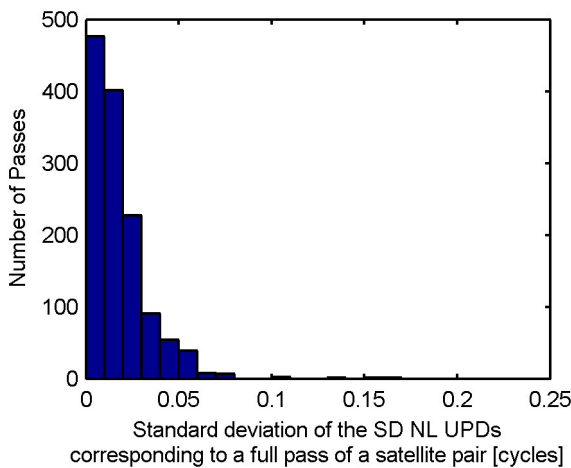


Figure 6.37: Histogram of standard deviations of the NL UPD time series of the IGS solution

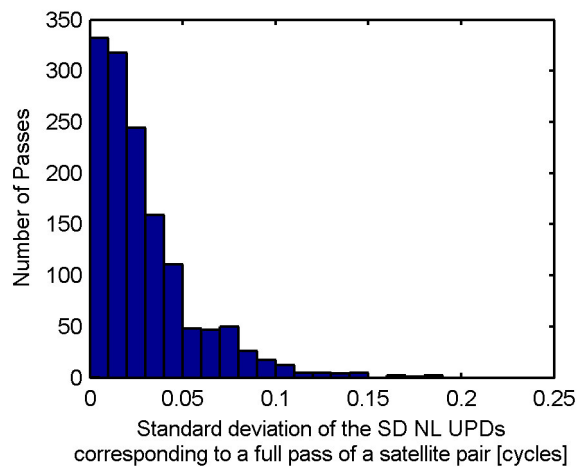


Figure 6.38: Histogram of standard deviations of the NL UPD time series of the IGC solution

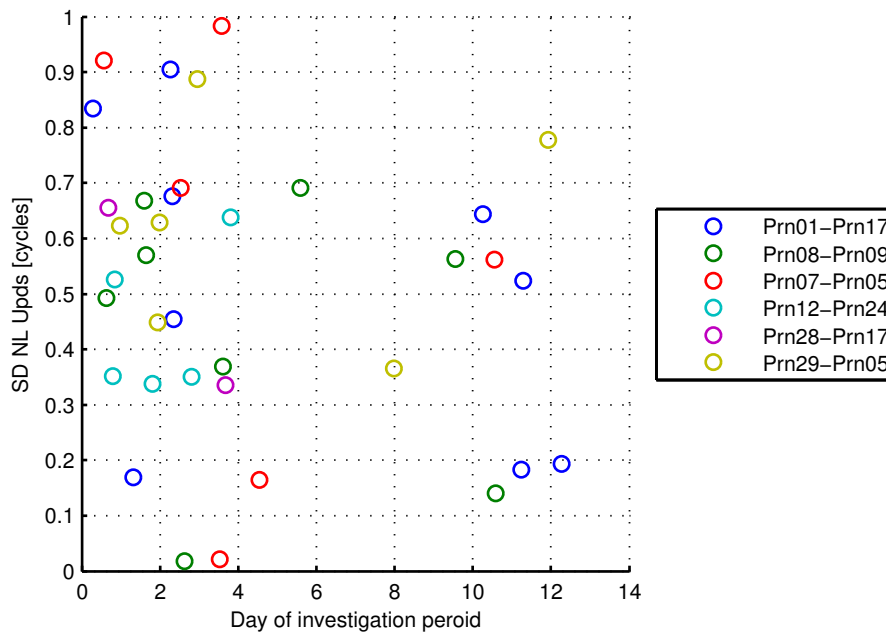


Figure 6.39: Mean values of NL UPD passes during the investigation period (IGC solution)

it should be stressed that the variation is still in the range of 2 cm and is probably caused by the sum of several small errors. Furthermore, only a minority of the NL UPDs experience such effects. In Fig. 6.35 and Fig. 6.36 the mean values and standard deviations of the NL UPDs, equivalent to those of Fig. 6.28 and Fig. 6.29, are shown. Comparing the respective figures, it becomes obvious that the standard deviations of the IGC solution are somewhat larger than those of the IGS solution. This reduced stability also becomes clear in a comparison of the histograms of standard deviations of the IGS solution (see Fig. 6.37) and the IGC solution (see Fig. 6.38). The average of the NL UPD standard deviation of the IGC solutions amounts to about 0.04 cycles, which means that the standard deviation of the IGC solution is increased by a factor of two compared to the IGS solution. Nevertheless, the majority of the passes of the IGC solution still lies within a range of 0.05 cycles, whereby in most of the cases the standard deviations are even smaller than 0.025 cycles. This means that, even though the stability of the NL UPDs of the IGC solution is slightly decreased, the NL UPDs are still quite stable.

The investigation on the long-term stability was carried out by looking at the course of the NL UPDs during the investigation period of 14 days. In Fig. 6.39 the mean values of the SD NL UPD passes, which are equivalent to those in Fig. 6.31, are shown. As in the case of the IGS solution, there can be significant differences between the passes of the same satellite pair. However, the variation between the passes corresponds to the expected accuracy of the observations (see Sect. 5.2.8) and is subject to the imperfect error modeling. Furthermore the IGC solutions suffer from a significantly decreased availability of the SD NL UPDs compared to the IGS solution. These

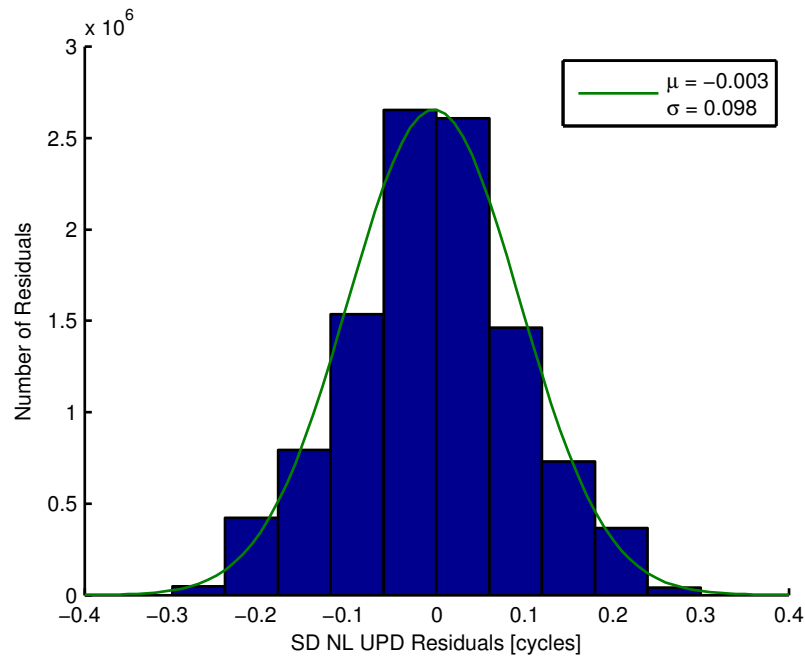


Figure 6.40: Histogram of the NL UPD residuals (IGC solution)

differences originate from differences in the availability of the IGS and IGC products. While the NL UPDs of the IGS solution are continuously available, there is a big gap in the IGC solution on the 6th day of the investigation period, where only one single NL UPD is available. Before this effect will be examined in much more detail a review of the residuals of the estimation process will be carried out.

In Fig. 6.40 the histogram of the residuals for the whole investigation period is shown. As for the IGS solution (see Fig. 6.32) the residuals are normally distributed with a zero mean value. When comparing the two solutions it can also be seen, that the standard deviation of the IGC solution is slightly increased about 0.01 NL cycles. As mentioned before this increase is caused by the decreased accuracy of the IGC01 satellite orbits and clock corrections. Nevertheless, the NL UPDs are still quite stable.

As it was shown throughout this section the reduced availability and accuracy of the IGC01 satellite orbit and clock corrections led to a degradation of the SD PPP solutions. Compared to the IGS solution the systematic offset in the ZTD estimates increased about 2 mm and the accuracy of the ZTD estimates decreased about 1 cm. Contrary to that, the fixing of the WL UPDs was hardly effected. The same applies for the stability of the NL UPDs, which is comparable to the stability of the IGS solution. This is caused by the fact that the ambiguities are estimated as constant values, which damps the influence of errors. Furthermore, the usage of the IGC01 product led to a major change in the availability of the NL UPDs, which will be investigated in the following. In Fig. 6.41 a comparison of the availability of the IGS and the IGC solution is shown for the whole investigation period. Apparently there are significant differences during the

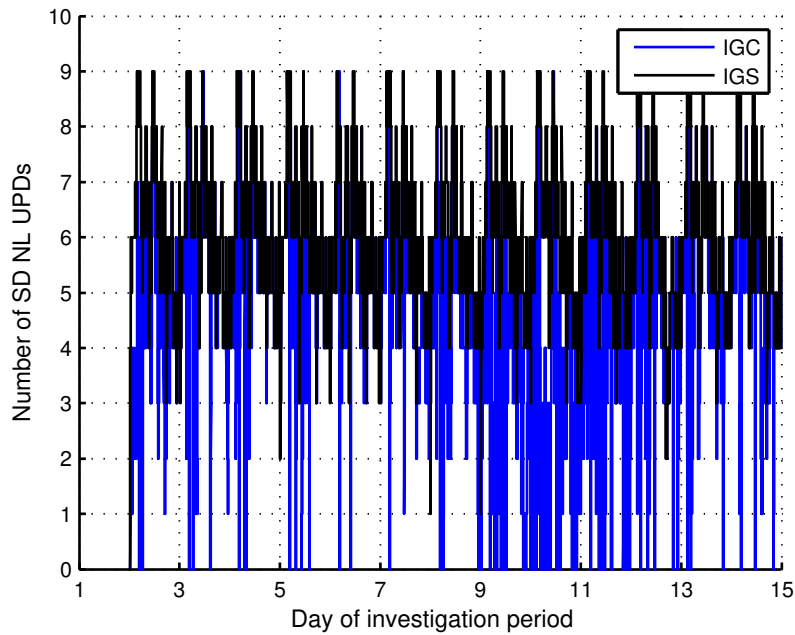


Figure 6.41: Availability of the SD NL UPDs during the investigation period

whole investigation period. Obviously there are a lot of time periods, where the IGC solution is not available. One reason for this phenomenon is the reduced availability of the IGC satellite orbit and clock corrections. However, taking a look at the availability of the IGC product (see Fig. 6.12) it becomes clear that this cannot be the only reason for the significant number of outages. More likely the problem must have its origin in satellite orbit and clock correction deficiencies of the IGC product itself. This will be shown in the following section.

6.2 Impact of errors in the satellite orbits and clock corrections

This section details the impact of specific errors in the satellite orbits and clock corrections on the estimation as well as the numerical results of the NL UPDs. The investigations concentrate on two main points. At first, the orbit and clock corrections are examined in order to find the reason for the outages of the IGC solution. In addition to that, the impact of errors in the satellite orbits and clock corrections on the estimation process and their effect on the numerical results of the NL UPDs have been examined as well. In further consequence it has been investigated if and to what extent these errors are compensated by the NL UPDs. For this purpose, simulated errors have been introduced into the satellite orbits and clock corrections of the IGS product (see Sect. 6.2.2). This modified product (in the following referred to as IGE product) was used to generate additional sets of UPDs, which will be denoted as IGE solution. In the last step, the influence of the introduced errors was investigated by comparing the results to the IGS solution.

6.2.1 Outages of the IGC solution

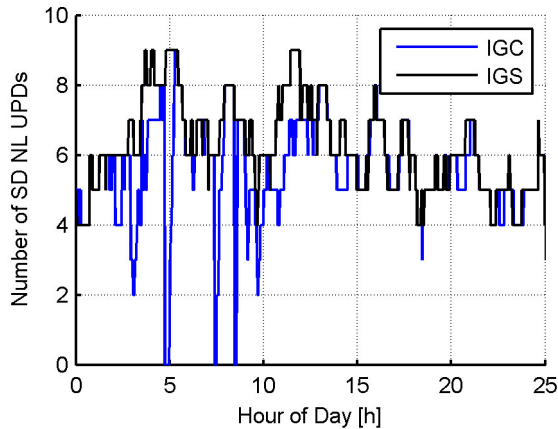


Figure 6.42: Number of NL UPDs of the IGS and IGC solution on GPS Week/Day 1783/4

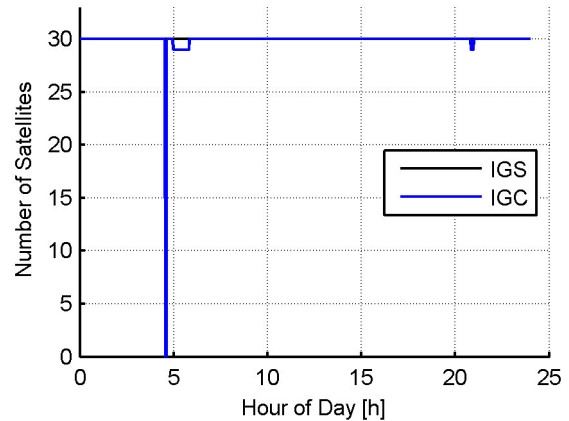


Figure 6.43: Availability of the IGS and IGC product on GPS Week/Day 1783/4

As shown in the previous section, using the IGC satellite orbits and clock corrections leads to a lot of outages in the availability of the NL UPDs. One reason for the outages in the IGC solution is the reduced availability of the IGC product. This is especially a problem during the second week of the investigation period. As shown in Fig. 6.12, most of the time the IGC solution was only available for 25 satellites. Therefore, the number of observations was reduced significantly during that time and at a lot of stations a calculation of the SD PPP solution was not possible. As a consequence the estimation of the NL UPDs was not possible either. However, this does not explain the outages in the course of the first week of the investigation period since there are, except for some outages in the IGC product, no significant differences in the availability of the IGS and IGC product. In order to determine the exact cause of the UPD outages during that time span, a more detailed analysis of the IGC solution on the fourth day of the investigated period (GPS Week/Day 1783/4) (see Fig. 6.42) was performed. This day was chosen because, except for a short outage of the IGC product, there are hardly any differences in the availability of the IGS and IGC product (see Fig. 6.43). Taking a look at Fig. 6.42 and Fig. 6.43, shows that the outage in the NL UPDs of the IGC solution at around five o'clock is caused by an outage of the IGC product. However, there are two more outages in the availability of the NL UPDs at around 7 and 8 o'clock. In order to determine the exact cause for this kind of outages, a comparison of the orbits and satellite clock corrections of the IGS and IGC solution was performed in the first place.

In Fig. 6.44 the differences between the orbits of the IGS and IGC product are shown for every satellite. Obviously the differences change during the course of the day. While they are in the range of one decimeter at the beginning of the day, they reduce to a couple of centimeters at around ten o'clock, which is in good agreement with the comparison of the IGS (see Sect. 3.1). The differences between the satellite clock corrections (converted to range differences) of

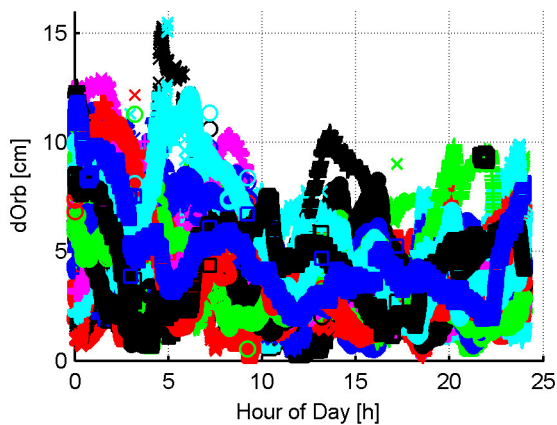


Figure 6.44: Absolute orbit 3D-differences for all available satellites between the IGS and IGC products on GPS Week/Day 1783/4

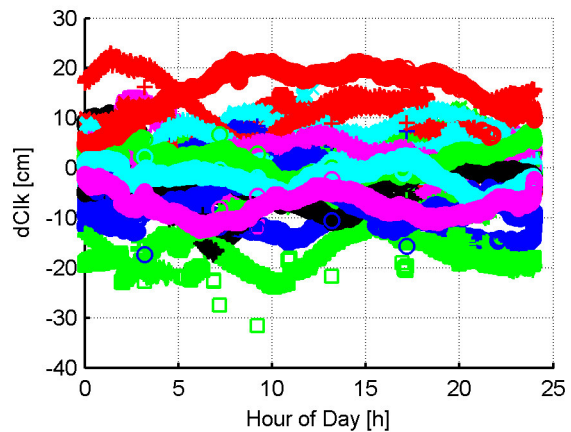


Figure 6.45: Clock correction differences for all available satellites between the IGS and IGC products on GPS Week/Day 1783/4

both products are illustrated in Fig. 6.45. It can be seen that the differences are in the range of two decimeters which is significantly larger than the differences of the satellite orbits. However, an offset of two decimeters in the satellite clock correction is not problematic at all, since it can be compensated by the corresponding ambiguity parameter, as long as it does not change significantly over the period considered. This also applies to the satellite orbits and, therefore the

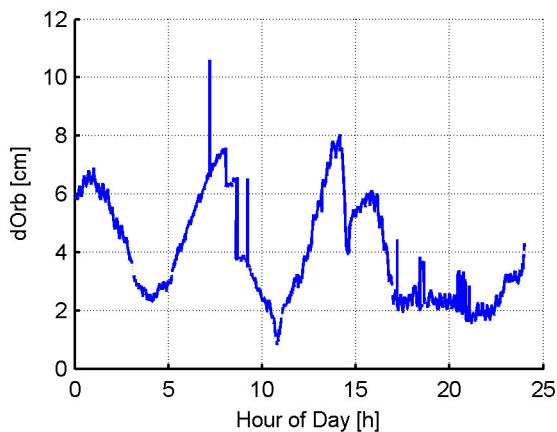


Figure 6.46: Absolute differences between the PRN01 satellite orbits of the IGS and the IGC products on GPS Week/Day 1783/4

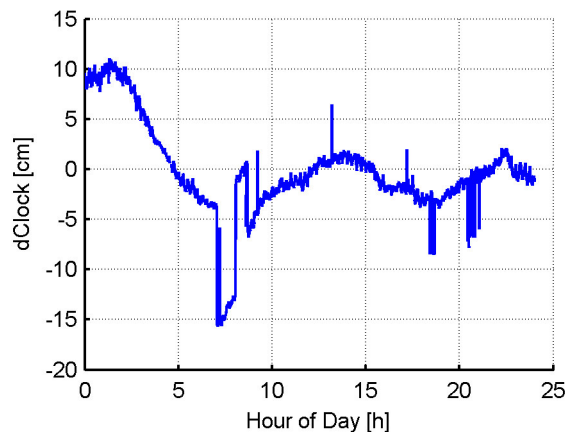


Figure 6.47: Differences between the PRN01 satellite clock corrections of the IGS and the IGC products on GPS Week/Day 1783/4

stability of the satellite orbits and clock corrections was investigated in more detail in the next step. Fig. 6.46 and Fig. 6.47 show the differences between the IGS and IGC satellite orbits and clock corrections of satellite PRN01. Both figures show that there is a long period variation, which is superimposed by a short period variation. The long period variation is in the range of a couple of centimeters and has no serious effect on the estimation process. On the contrary to that there are jumps of different magnitudes in the short period variation. In case of the satellite orbits they

are in the range of one or two centimeters, which is not critical at all. However, the jumps in the satellite clock corrections at the begin of the day reach up to one decimeter which critically affects the estimation process as shown in the following.

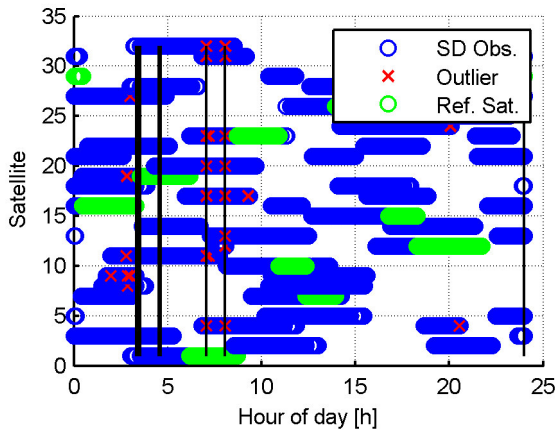


Figure 6.48: SD IF phase observations at station BELF on GPS Week/Day 1783/4. Outliers of the SD PPP solution are indicated by black lines

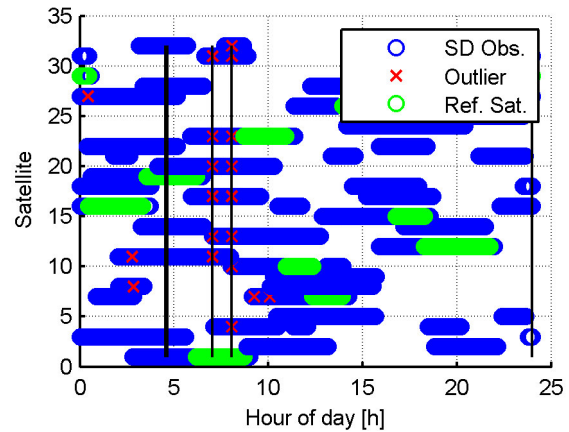


Figure 6.49: SD IF phase observations at station MAN2 on GPS Week/Day 1783/4. Outliers of the SD PPP solution are indicated by black lines

Fig. 6.48 and Fig. 6.49 display the availability of the SD IF phase observations of the SD PPP solutions of the stations BELF and MAN2 for GPS Week/Day 1783/4. The reference satellites of the SD observations are indicated as green circles and the satellites used for the generation of the SD observations are shown as blue circles. The red crosses indicate the SD IF phase observations, which have been detected as outliers and the black lines indicate the outages of the SD PPP solution itself. Obviously there are four outages for station BELF in the course of the SD PPP solution. The first outage of the SD PPP solution is caused by an outage of the observations and the second one by an outage of the IGC product (see Fig. 6.43). The other two outages are much more interesting and the reason for them can be found in the satellite clock corrections of the IGC product. Taking a closer look at Fig. 6.48 shows, that the two outages take place during the time PRN01 was selected as reference satellite. Furthermore, it can be seen that at these two points in time all observations have been detected as outliers, and therefore, no SD PPP solution could be generated. Comparing Fig. 6.48 and Fig. 6.47 suggests that these two points in time perfectly agree with the large jumps in the satellite clock corrections. The same also applies for station MAN2. The first outage corresponds to the second outage of the SD PPP solution at station BELF and is caused by the outage of the IGC product, while the last two outages were caused by the jumps of the satellite clock correction of the reference satellite PRN01. The question how this effect affects the calculation of the NL UPDs still remains to be answered. As already known the calculation of the NL UPDs requires the IF ambiguities of the SD PPP solutions. Since these ambiguities are not available during an outage of the PPP solutions, an estimation of the NL UPDs during that time is not possible either. In conclusion, the non-availability of the NL UPDs (see

Satellite	Error
PRN 01	25 [cm] along track
PRN 03	25 [cm] cross track
PRN 14	5 [cm] radial

Table 6.3: Simulated orbit errors

Fig. 6.42) matches with the outages of the SD PPP solutions (see Fig. 6.48 and Fig. 6.49).

The presented situation is a worst case scenario, as jumps in the satellite clock corrections will not necessarily lead to an outage of the PPP solutions. This only happens, if the jumps take place in the clock corrections of the reference satellite and if they exceed a certain threshold, as it will be shown later on. In case of any other satellite, only the corresponding observation will be removed. As this usually takes place at all stations at the same time, an estimate of the corresponding NL UPD is not possible at that time. This explains the generally reduced availability of the IGC solution, which can be seen at the beginning of the fourth day for instance. A possible solution to overcome this problem would be an algorithm for the detection and correction of clock jumps, which prevent the estimation of the NL UPDs.

6.2.2 Error simulation and compensation

For further detailed investigations, a couple of simulations have been carried out. For these simulations a designated time period of the IGS satellite orbits and clock corrections was modified by applying different types of errors. This modified IGS product (IGE product) was used for the estimation of additional sets of NL UPDs, which will be referred to as IGE solution. Finally, a comparison of the NL UPDs as well as the interim results of the IGS and IGE solution was conducted, which allowed for a detailed investigation of the propagation of the simulated errors into the numerical results of the NL UPDs. The actual goal of these examinations is to determine if and to which extent errors can be compensated by the NL UPDs.

6.2.2.1 Orbit error

In the begin the investigations concentrated on satellite orbits. To get a clear picture, only constant errors were simulated and only one error in along track, cross track and radial direction was applied to one of three designated satellites at the same time. Furthermore, the errors were not applied to any reference satellite. Table 6.3 summarizes the simulated orbit errors. The figures, which will be shown in the following, cover the time period during which satellite PRN19 was the reference satellite. Due to this rather short time period not the complete progress of the errors is shown. However, the examples have been chosen in such a way that all effects of interest are covered.

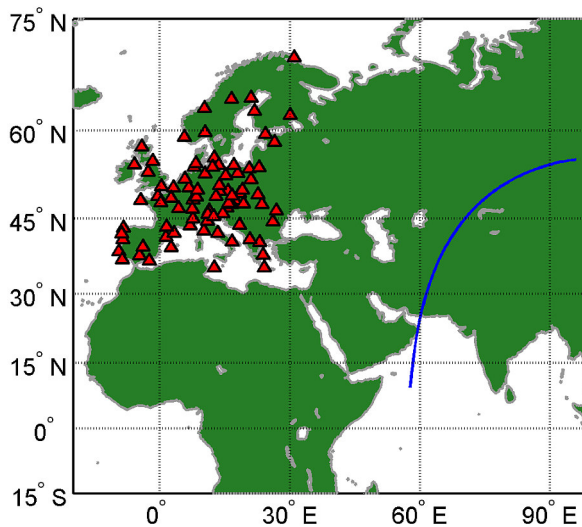


Figure 6.50: Satellite track of PRN14

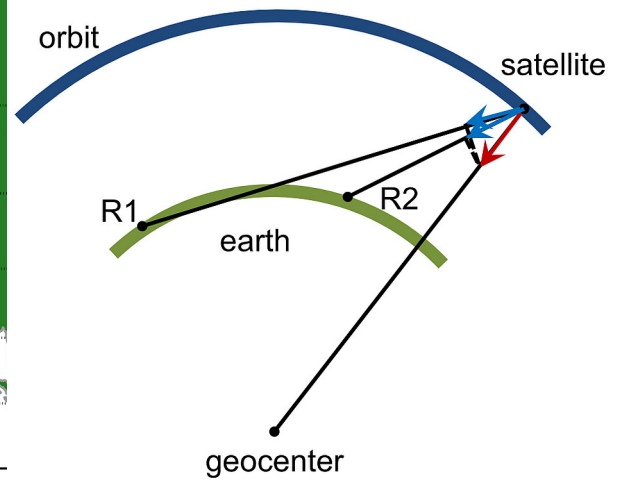


Figure 6.51: Orbit error in radial direction

Radial

Initially the effect of the orbit errors on the observations of the reference station network was examined. The main purpose of this examination was to determine whether the orbit error has a similar effect at all stations. In Fig. 6.50 the satellite track of PRN14 is shown for the investigated time period. The influence of the error can be easily reconstructed from the geometrical situation, which is shown in Fig. 6.51. The figure is a simple illustration of the situation for two different stations R1 and R2. In this scenario the two stations are located in the orbital plane of the satellite and the figure shows a section through this plane. The direction vector from the geocenter to the satellite as well as the direction vectors from the two stations to the satellite are shown as black lines. The error in the radial direction of the satellite orbit is shown as red arrow and the corresponding errors onto the geometric ranges as blue arrows. According to Fig. 6.51 the error in the geometric range is the projection of the radial error onto the direction vector of the corresponding satellite receiver pair and, therefore, it depends on the angle between the two direction vectors. This angle can only vary in the range from 0° (satellite at 90° elevation) to $14,7^\circ$ (satellite at 0° elevation) and, according to this, also the radial error does not vary a lot.

According to Eq. 5.13 the geometric range is subtracted from the IF code and phase ranges which means that the simulated error is directly introduced into them. This can be clearly seen in Fig. 6.52, which shows the differences between the corrected IF phase observations of the IGS and IGE solution of all stations to satellite PRN 14. Thereby each station is illustrated by a different color. The figure shows an offset in the order of 5 centimeters which corresponds to the simulated error of 5 cm in the radial direction. Furthermore, there are small differences in the magnitude of the offset, which originate in the different positions of the stations. In addition to that, it seems that all differences experience small variations in the course of the investigation period, which are caused by the movement of the satellite. Even though both of these two effects

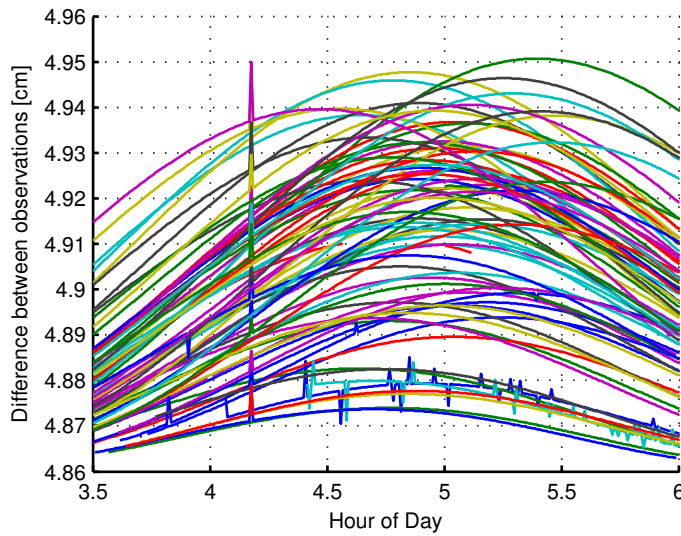


Figure 6.52: Differences between the IF phase ranges of the IGS and IGE solution for all stations to the satellite PRN14 on GPS Week/Day 1783/2. Each station is illustrated by a different color

are very small, they illustrate the influence of the geometry between the station and the satellite on the impact of the satellite orbit error on the ranges. However, the effect on the estimation of the NL UPDs itself is of much more interest.

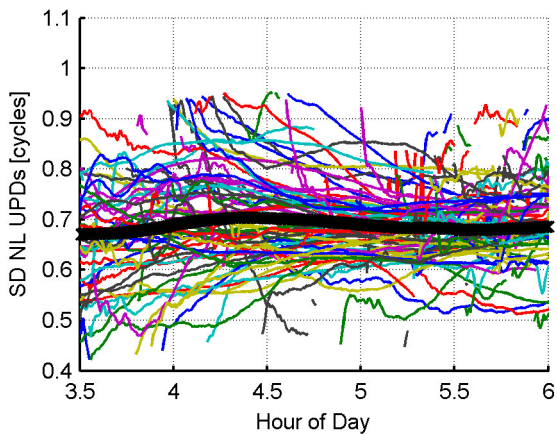


Figure 6.53: SD NL UPDs PRN19 - PRN14 of the IGS solution on GPS Week/Day 1783/2

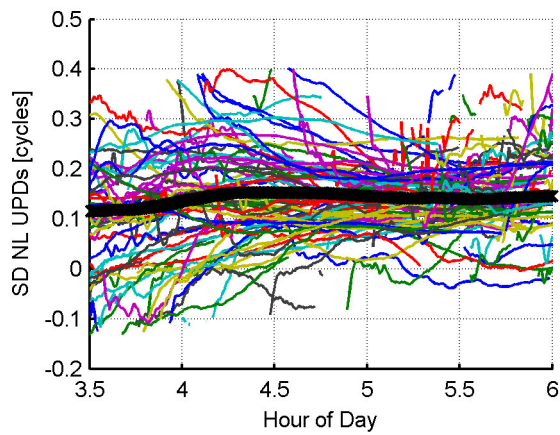


Figure 6.54: SD NL UPDs PRN19 - PRN14 of the IGE solution on GPS Week/Day 1783/2

As shown before, the error in the radial direction results in increased phase ranges. This leads to significant changes in the estimated IF ambiguities as well as the corresponding NL UPDs. In Fig. 6.53 and Fig. 6.54 the NL UPDs, which are observed at the stations, and the NL UPD filter estimates of the IGS and IGE solution are shown. The individual station NL UPDs are illustrated by different colors, while the NL UPD filter estimate is shown as thick black line. The two solutions

differ from each other only by an offset of approximately 0.5 cycles which corresponds to the orbit error of 5 cm. This means that the error in the radial direction is transferred one-to-one to the estimation of the NL UPDs, which leads to the error being compensated by the corresponding UPD value.

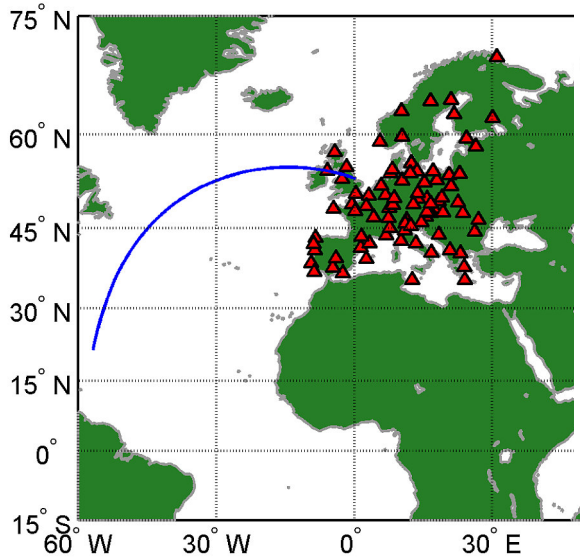


Figure 6.55: Satellite track of PRN01

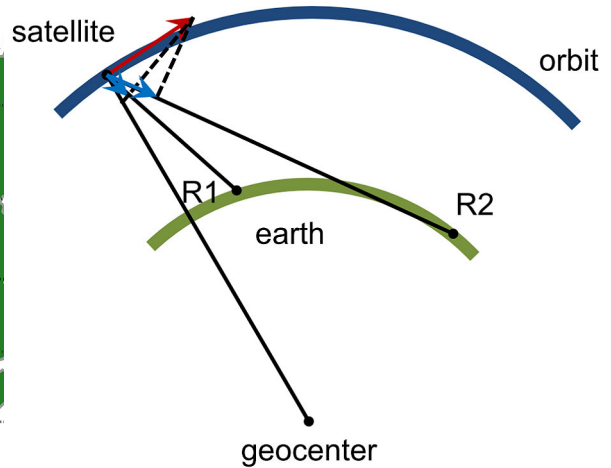


Figure 6.56: Orbit error in along track direction

Along track

Following the error in the radial direction, the error in the along direction (PRN01 / 25 cm) has been examined. As before the influence on the geometric range was investigated first. In Fig. 6.55 the satellite track of PRN01 is shown for the investigated time period. Fig. 6.56 illustrates the corresponding geometric situation. Contrary to the situation in Fig. 6.56 and despite of the fact that the angle between the direction vector from the station to the receiver and the direction vector of the along track component is rather big (it is in the range of 75.3° to 90°), the influence of the error is relatively small. Last but not least it should be mentioned that the station is usually not in the plane of the satellite's orbit as it is shown in Fig. 6.56. For the estimation of the error at a station outside a the plane, also the latitude of the station must be taken into account.

In Fig. 6.57 the differences between the phase ranges of the IGS and IGE solution for all stations to the satellite PRN01 are shown. Similarly to Fig. 6.52 each station is illustrated by a different color. Obviously there is an offset of approximately 5 cm between the IGS and the IGE solution at the beginning of the investigation period. Furthermore, it can be seen that these offsets are not of the same magnitude as in the case of the radial error. Furthermore, the differences undergo a drift of 5 cm during the investigation period and, in addition to that, there are some minor differences between the drifts. The drifts themselves are caused by the movement of the satellite and the differences in the drifts by the position of the stations. Contrary to the previous

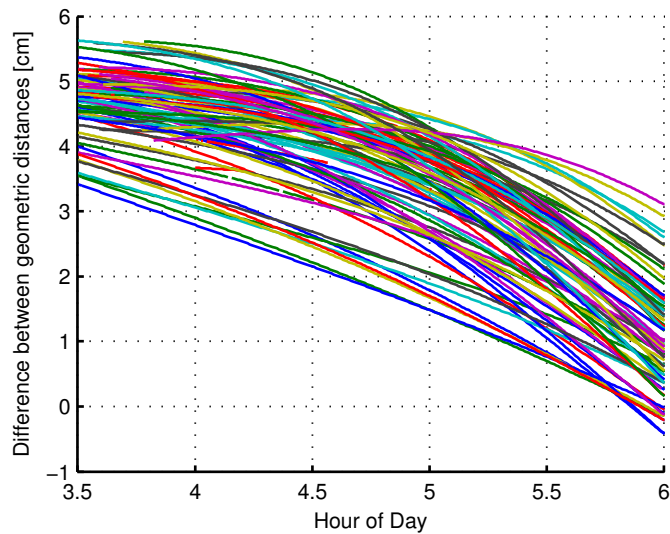


Figure 6.57: Differences between the IF phase ranges of the IGS and IGE solution for all stations to the satellite PRN01 on GPS Week/Day 1783/2. Each station is illustrated by a different color

these differences are rather small due to the extent of the regional network used. In the following the effect of the error on the estimation of the NL UPDs themselves will be presented.

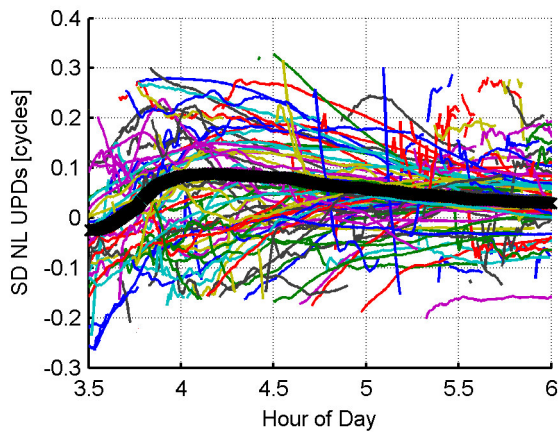


Figure 6.58: SD NL UPDs PRN19 - PRN01 of the IGS solution on GPS Week/Day 1783/2

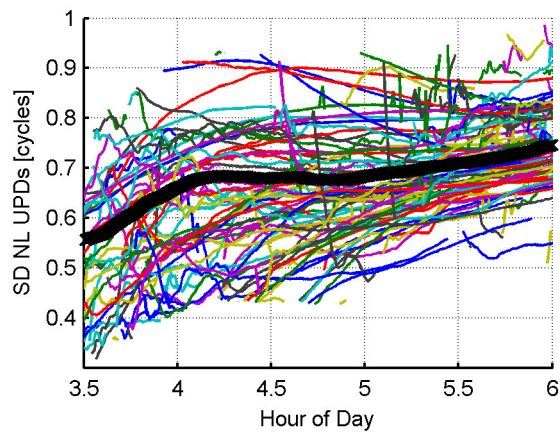


Figure 6.59: SD NL UPDs PRN19 - PRN01 of the IGE solution on GPS Week/Day 1783/2

In Fig. 6.58 and Fig. 6.59 the NL UPDs of the individual stations and the NL UPD filter estimates of the IGS and IGE solution for the satellite pair PRN19-PRN01 are shown. The NL UPDs of the individual stations are illustrated by different colors, while the NL UPD filter estimates are illustrated as thick black lines. When comparing Fig. 6.58 with Fig. 6.59 it can be seen that the error in the along track direction affects the NL UPDs in two respects. On the one hand there is an offset of approximately 0.5 cycles between the IGS and the IGE solution, which corresponds to the difference of 5 cm in the geometric ranges at the beginning of the investigation period. On

the other hand also a discrepancy in the drifts of the NL UPD observations and the estimate of both solutions can be seen. However, this discrepancy does not correspond to the drift, which is visible in the differences of the geometric ranges. The reason for this is that the IF ambiguities are estimated as constant values, which leads to the drift being smoothed. Due to the linear relationship between the IF ambiguities and the NL UPD observations this smoothing is transferred one-to-one.

According to the results shown, the error in the along track direction could be largely compensated by the NL UPDs. Similarly to the radial error the compensation of the offset component was not a problem at all. In addition to the offset the along track error also introduced a drift component, which could be successfully compensated as well. However, the quality of compensation of such a drift depends on the drift rate, which will be shown in Sect. 6.2.2.2.

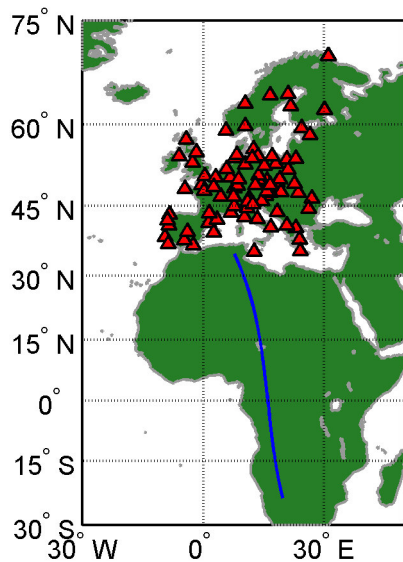


Figure 6.60: Satellite track of PRN03

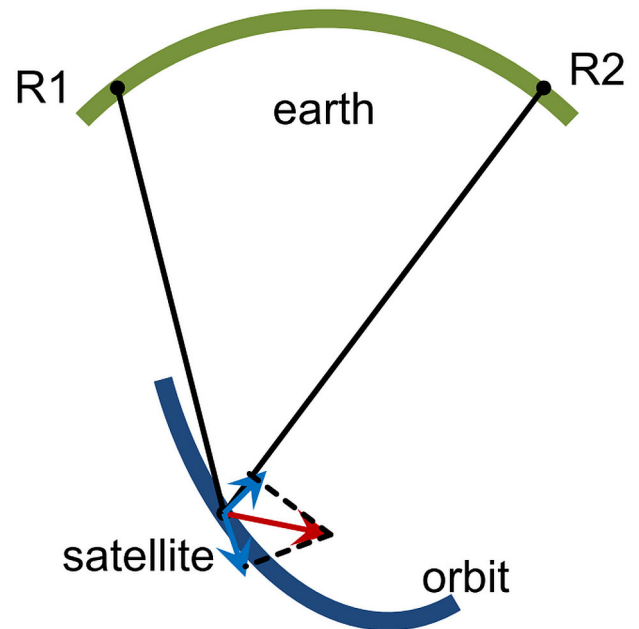


Figure 6.61: Orbit error in across track direction

Across track

As the last step the investigation of the across track error (PRN03 / 25 cm) was carried out. Firstly the examination of the influence on the geometric ranges was conducted. In Fig. 6.60 the satellite track of PRN03 for the investigated time period is shown and Fig. 6.61 depicts a simple approximation of the corresponding geometrical situation. According to Fig. 6.61 the influence of the error varies with the longitude of the station. For stations which are located east of the satellite track the geometric distance increases, while for stations which are located west of the satellite track it decreases.

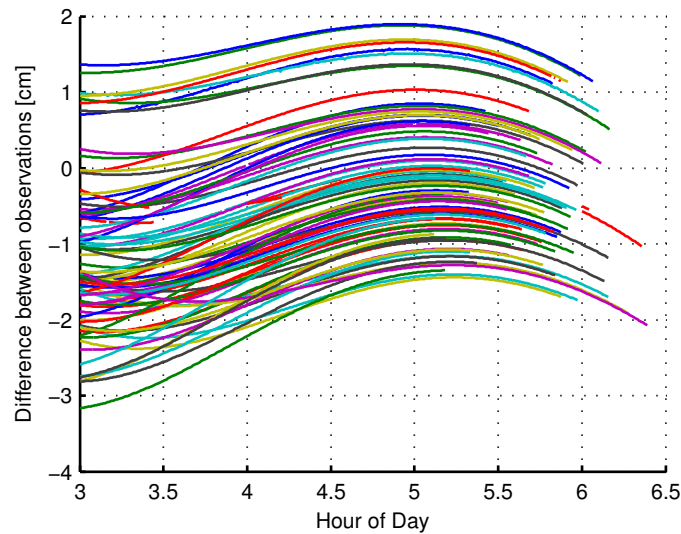


Figure 6.62: Differences between the IF phase ranges of the IGS and IGE solution for all stations to the satellite PRN03 on GPS Week/Day 1783/2. Each station is illustrated by a different color

In Fig. 6.62 the differences between the phase ranges of the IGS and IGE solution for all stations to the satellite PRN03 are shown. As in previous figures each station is illustrated by a different color. It can be seen that the differences vary in the range of 2 centimeters during the investigation period and that there are some minor differences between the variations. These variations are caused by the movement of the satellite and the differences in the variations by the position of the station. Due to the extension of the regional network used, these differences are rather small. Furthermore, it becomes obvious that there are offsets between the observations, which also have their origin in the relative positions of the stations. As opposed to the previous example, the differences between the offsets are rather big, ranging up to 4 cm. Subsequently, it will be shown, how this affects the estimation of the NL UPDs.

In Fig. 6.63 and Fig. 6.64 the NL UPDs of the individual stations and the NL UPD filter estimates of the IGS and IGE solution are shown. The observations of the stations are illustrated by different colors, while the NL UPD filter estimates are shown as thick black lines. When comparing Fig. 6.63 to Fig. 6.64, the influence of the error in the across track direction can be clearly seen. While the NL UPD station observations of the IGS solution almost perfectly match, there are clear offsets between the NL UPD station observations of the IGE solution. These offsets correlate with the offsets of the phase ranges and remain almost stable for the whole investigation period. Compared to the offsets, the variation in the phase ranges cannot be seen in the NL UPD observations. As mentioned before this is caused by the fact that the IF ambiguities are estimated as constant values.

For the estimation of the NL UPDs the constant offsets in the NL UPD observations (see Fig. 6.64) are no problem, as long as enough observations are in the band of 0.3 cycles. In this

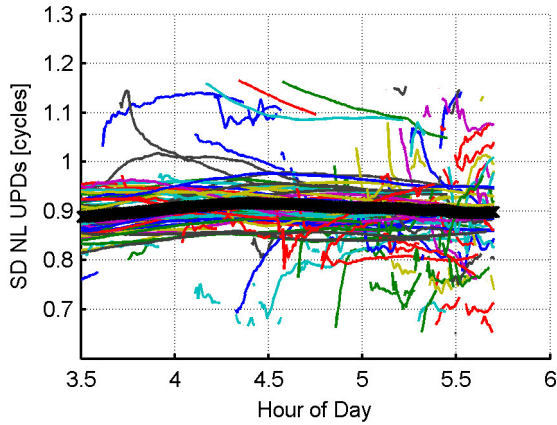


Figure 6.63: SD NL UPDs PRN19 - PRN03 of the IGS solution on GPS Week/Day 1783/2

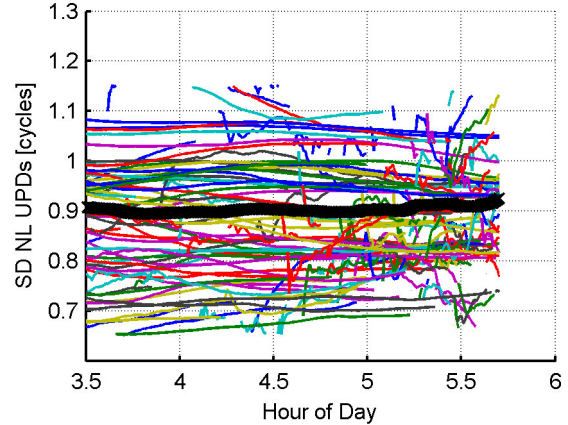


Figure 6.64: SD NL UPDs PRN19 - PRN03 of the IGE solution on GPS Week/Day 1783/2

Satellite	Error
PRN 01	$15 \left[\frac{cm}{h} \right]$ Clock drift
PRN 03	[10 cm every 10 Min.] Clock jumps
PRN 14	-5 [cm] Clock offset
	+5 [cm] radial orbit error

Table 6.4: Simulated clock and orbit errors

particular example this is still the case and the estimated NL UPD even matches the IGS solution, however, this is just a coincidence. As opposed to the estimation, the application of the NL UPDs is more problematic. In case of the IGS solution the majority of the NL UPDs observed at the stations are in the range of less than 0.1 cycles. Applying the estimated NL UPD to one of these observations will result in an observation close to an integer value, which most likely will lead to a successful ambiguity fix. In contrast to that, the observations of the IGE solution vary within 0.4 cycles. This means that utilizing this NL UPDs at the rover site does not necessarily result in an SD observation very close to an integer value, which makes it much harder to fix the corresponding ambiguity.

6.2.2.2 Satellite clock correction error

Following the satellite orbits the investigations on satellite clock correction errors have been carried out. Three different types of errors have been simulated. A constant offset, a drift as well as regular jumps have been introduced to the satellite clock corrections of the satellites PRN01, PRN03 and PRN14. For the simulation the same satellites and the same time period as in the previous investigations have been used (see Tab. 6.4). In case of satellite PRN14, a constant offset in the satellite clock correction was simulated together with a constant radial orbit shift, which has already been investigated previously.

Clock offset

In the course of studying the impact of satellite clock errors on the phase ranges their similarity with radial orbit errors can be emphasized. The significant difference between these two error types is that an error in the satellite's clock correction affects all observations from a station network exactly the same way, while a range error caused by satellite orbit errors always depends on the geometry between station and satellite. This phenomenon becomes obvious when comparing Fig. 6.65 to Fig. 6.52, which show the differences between the phase ranges of the IGS and IGE solution of all stations to satellite PRN14. In both figures each station is illustrated by a different color, but due to the rather small differences in Fig. 6.52 only a few of them are visible. The differences between the observations presented in Fig. 6.65 are constant at the 0.1 mm level. The minimal variations in the differences are introduced by the movement of the satellite. Comparing Fig. 6.65 with Fig. 6.52, the high correlation, over 90%, between the two errors can be seen. Furthermore, it can be seen that both errors have different algebraic signs. Since they have the same magnitude, they almost cancel each other.

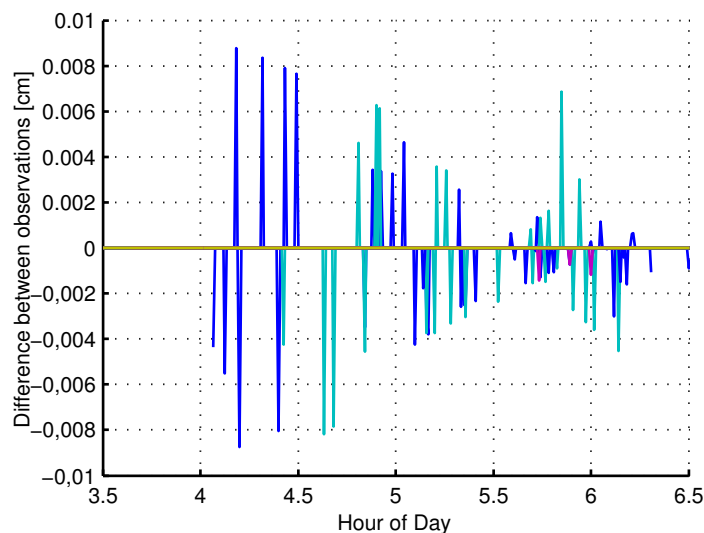


Figure 6.65: Differences between the IF phase ranges of the IGS and IGE solution for all stations to the satellite PRN14 on GPS Week/Day 1783/2. Each station is illustrated by a different color

In Fig. 6.66 and Fig. 6.67 the NL UPDs of the individual stations and the NL UPD filter estimates of the IGS and IGE solution are shown. Obviously there are hardly any differences between the two solutions, even though the IGE solution includes errors in the satellite orbits as well as in the satellite clock corrections (see Tab. 6.4). As mentioned before, both errors have the same effect but different algebraic signs and, therefore, are almost canceling each other. If they point into the same direction this would result in a shift of the UPDs in the order of the sum of both errors. Of course such scenarios are not very likely, but the example should illustrate that it is very hard to separate these two types of errors.

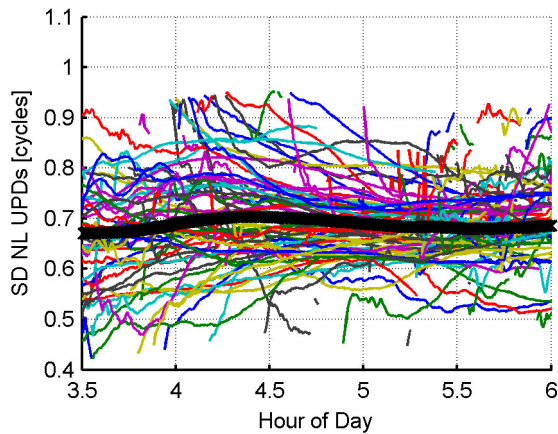


Figure 6.66: SD NL UPDs PRN19 - PRN14 of the IGS solution on GPS Week/Day 1783/2

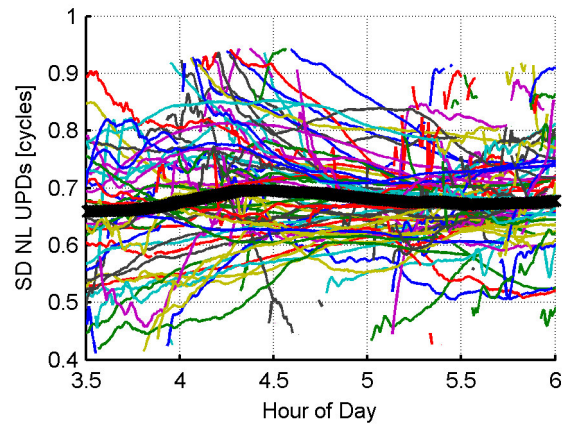


Figure 6.67: SD NL UPDs PRN19 - PRN14 of the IGE solution on GPS Week/Day 1783/2

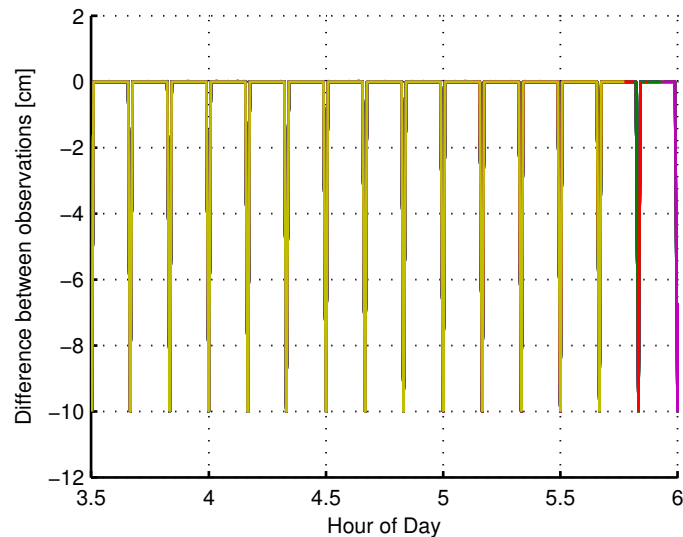


Figure 6.68: Differences between the IF phase ranges of the IGS and IGE solution of satellite PRN03 on GPS Week/Day 1783/2. Each station is illustrated by a different color

Clock jumps

The effect of jumps in the satellite clock corrections has already been presented in the course of Sect. 6.2.1. Nevertheless, simulations concerning this error have been carried out as well in order to highlight the effect of such jumps in the satellite clock corrections on the estimation process. As shown in Fig. 6.68, the jumps in the clock errors are directly transferred to the phase ranges observed by the stations. Each station is illustrated by a different color but, as they overlap, only a few stations can be seen.

In Fig. 6.69 and Fig. 6.70 the NL UPDs of the individual stations and the NL UPD filter

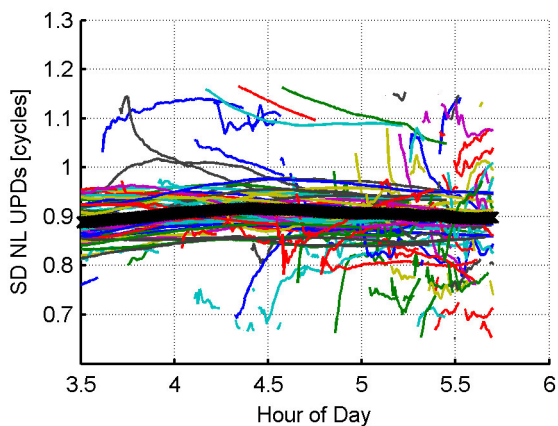


Figure 6.69: SD NL UPDs PRN19 - PRN03 of the IGS solution on GPS Week/Day 1783/2

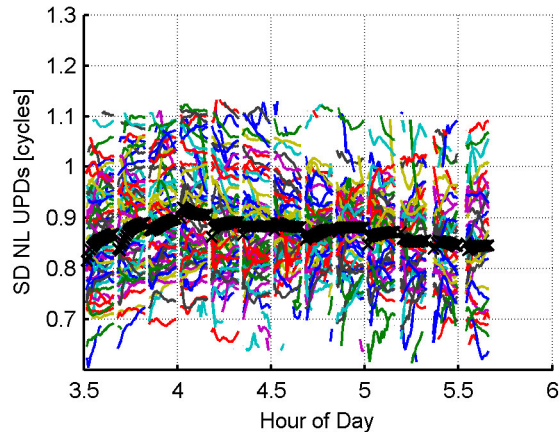


Figure 6.70: SD NL UPDs PRN19 - PRN03 of the IGE solution on GPS Week/Day 1783/2

estimates of the IGS and IGE solution are shown. According to Fig. 6.70 the jumps in the satellite clock corrections lead to a loss of the IF ambiguities, which were needed for the estimation of the NL UPDs. When comparing Fig. 6.69 and Fig. 6.70, also significant differences between the observations appear. While the NL UPDs of the individual stations of the IGS solution are almost perfectly aligned, those of the IGE solution vary in a band of 0.4 cycles. The reason for this can be traced back to the resets of the corresponding ambiguity parameters in the SD PPP solutions. Every time a jump in the satellite clock correction took place, the corresponding ambiguity parameters were detected as outliers. As a consequence the parameters could not converge, which led to the increased variability of the IGE solution. However, comparing the IGS and the IGE solution shows that the estimated NL UPDs are very consistent even though the accuracy of the NL UPDs of the individual stations of the IGE solution is much worse.

Clock drift

When considering satellite clock corrections, also drifts are of interest, since this is a common type of error. The effect of a drift in the phase ranges was already visible in case of the along track error. In this particular example the drift could be compensated very well, nevertheless the influence of a drift strongly depends on the drift rate, which will become evident throughout this section. For this investigation a clock drift of 15 centimeters per hour has been applied to satellite PRN01. Due to the linear relationship between the satellite clock error and the phase ranges, this drift is directly transferred to the differences between the phase ranges of the IGS and IGE solution, which can be perfectly seen in Fig. 6.71.

In Fig. 6.72 and Fig. 6.73 the NL UPDs of the individual stations and the NL UPD filter estimates of the IGS and IGE solution are shown. In Fig. 6.73 the drift in the satellite clock correction of PRN01 and its effect are clearly visible. As opposed to the drift introduced by the along track error, the simulated drift in the satellite clock corrections led to severe problems.

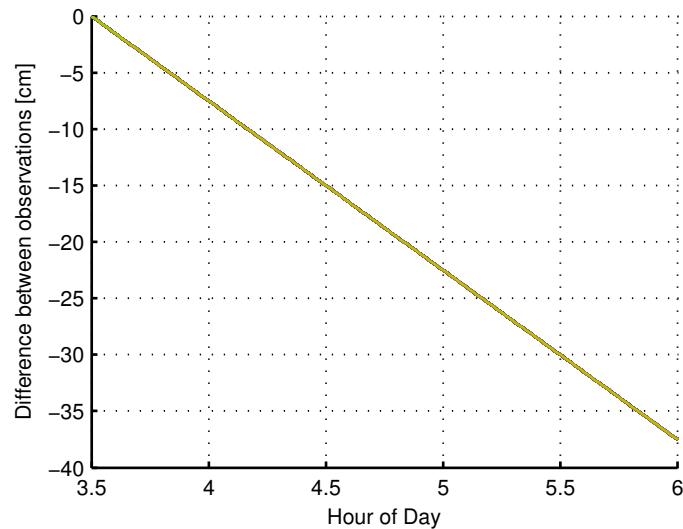


Figure 6.71: Differences between the IF phase ranges of the IGS and IGE solution of satellite PRN01 on GPS Week/Day 1783/2. Each station is illustrated by a different color

The major problem is the fact that the IF ambiguities were assumed to be stable. This led to repeated resets of the ambiguity parameter of satellite PRN01 in the SD PPP solutions of the station network, every time the difference between the prediction and the observation values exceeded a defined threshold. The red vertical lines in Fig. 6.73 highlight the epochs at which such resets took place at a high number of stations. It might be surprising that the resets at the stations do not take place at exactly the same time, but there are several reasons, why this is not the case. Firstly, satellite PRN01 did not become visible at all stations at the same time and, therefore, the estimation of the corresponding ambiguity parameters started sooner or later. In addition to that, the estimation of the ambiguity parameter itself also depends on many factors like number of parameters, noise of the phase observations etc., which vary from station to station. Last but not least, the simulated drift is superimposed by the drift introduced by other unknown error sources. This drift is even visible in the IGS solution (see Fig. 6.72) and, it can be seen, that there are stations and also time dependent variations. The sum of all the aforementioned effects led to the fact that the resets did not take place at all stations at the same time, but at certain epochs a high quantity of stations was affected. After such resets the ambiguities were initialized again, which led to the jumps in the time series of the observations illustrated in Fig. 6.73. Concerning the estimation of the NL UPDs, this led to the same problem as for the SD PPP solution. This means that in case of jumps in the NL UPD observations, the difference between the prediction and the observations became too large, which finally led to a reset of the NL UPD parameter, see Fig. 6.73.

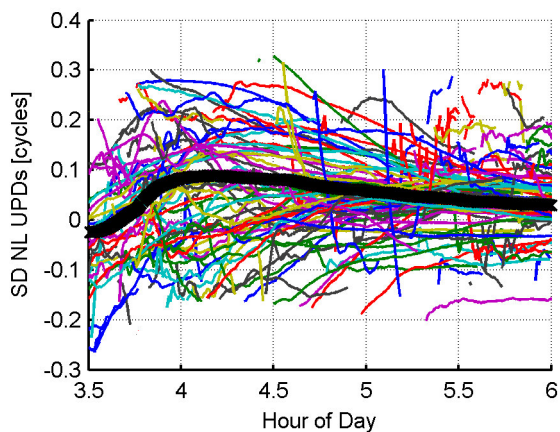


Figure 6.72: SD NL UPDs PRN19 - PRN01 of the IGS solution on GPS Week/Day 1783/2

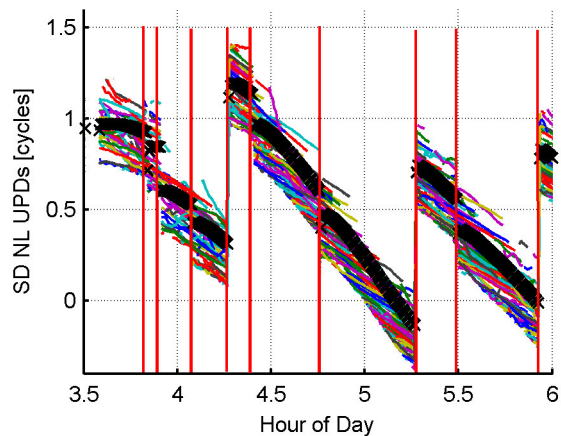


Figure 6.73: SD NL UPDs PRN19 - PRN01 of the IGE solution on GPS Week/Day 1783/2

Summary

In the previous sections the effects of errors in the satellite orbits and satellite clock corrections were shown. Even though the simulated errors did not cover the whole spectrum of possible errors and only a regional station network was used, some founded statements on the effects can be made.

Instead of distinguishing between the individual error sources and types the summary will be conducted based on the phase ranges. As it was shown in the course of this section, all errors led to errors in the phase ranges at first instance. The errors in the phase ranges directly affect the estimation of the NL UPDs. Considering the types of errors in the phase ranges, a distinction between the three following types can be made:

- Offsets
- Jumps
- Drifts

Of course also a combination of these effects is possible, however it is much easier to consider them separately. By means of the previous investigations the following conclusions for the aforementioned effects can be made.

Offsets: A common offset in the phase ranges can be easily compensated by the NL UPDs and has no considerable effect, neither on the estimation nor on the application of them.

Jumps: The influence of jumps in the phase ranges strongly depends on their magnitude. If they exceed a defined threshold, this leads to the corresponding observations being detected as outliers, which makes it impossible to estimate the related NL UPD in further consequence. Of course, the same also applies for the application of the NL UPDs. This is especially

critical, if the reference satellite is concerned. In such a case the estimation as well as the application of the NL UPDs is not possible at all (see Sect. 6.2.1). Another problem, which comes along with jumps, is the slightly reduced accuracy of the ambiguity estimates after they have been detected as outliers. Which affects the estimation as well as the application of the NL UPDs.

Drifts: The influence of the drifts strongly depends on the drift rate. In dependency of the drift rate, irregular losses of the observations take place, which can lead to a loss of the corresponding NL UPD. The frequency of these losses increases with a higher drift rate. Furthermore, high drift rates can not be totally compensated by the NL UPDs as they are assumed to be stable. Such uncompensated errors are especially critical for the application of the NL UPDs, as they decrease the chance for successfully fixing the ambiguities.

A critical aspect with respect to errors in the satellite orbits and clock corrections is the use of SD observations, as errors in the observations of the reference satellite affect every observation. As it was shown, depending on the type and magnitude of the error, this can even prevent an estimation of the NL UPDs in the worst case.

In the case of errors in the satellite orbits, another important element, which needs to be considered, is that the errors vary depending on the positions of the stations and the satellites. This means that the aforementioned effects vary from station to station and that they also change over time, which maps to an increased difference between the phase ranges observed at the stations. Dependent on the differences, the estimation as well as the application of the NL UPDs becomes harder. In the worst case a successful estimation or application is not possible at all.

Chapter 7

Summary and conclusions

The work presented in this thesis deals with the estimation of uncalibrated phase delays (UPDs) which are the missing link for a phase ambiguity-fixed PPP solution. PPP is a technique which is especially used for a lot of real-time applications and, therefore, the UPDs are needed in real-time as well. However, an estimation in real-time comes along with some disadvantages. Probably, the most significant disadvantage is the reduced accuracy of the real-time orbits and clock corrections, which are required for the estimation of the UPDs. On the basis of this problem the software PPP Post was developed which allows for the estimation of UPDs in a real-time simulation mode. This real-time simulation mode is a powerful tool to test the influence of different models, algorithms and corrections and was used to investigate the influence of the satellite orbits and clock corrections. According to the progress of this studies, this thesis is centered on two primary issues. The first one is a detailed description of the functional design and the processing scheme of the PPP Post software. The second one are detailed investigations of the influence of the satellite orbit and clock corrections on the estimation of the UPDs.

At the beginning of the thesis a short introduction to the principles of GNSS point positioning and the IGS as well as its services were given. After that the basic principles of PPP were discussed and the problem of integer ambiguity resolution in PPP was introduced. Subsequently an overview of the methods for PPP integer ambiguity resolution was given. Thereby a strong emphasis was placed on the detailed explanation of the method “Phase recovery from fractional parts”, which served as fundamental basis for the development of the PPP Post software.

The description of the PPP Post software itself is one of the major parts of this thesis. At the beginning the functional design of the software was introduced and an overview of all required data sources was given. Afterwards the PPP observation model including all necessary corrections of effects affecting the GPS satellites, the receiver and the propagation of the signal were discussed. These corrections include the application of satellite orbit and clock corrections in post-processing and in real-time. Furthermore the treatment of atmospheric effects, relativistic effects, satellite and receiver antenna phase center offsets as well as several corrections was described. Finally an assessment of the accuracy of the corrected observations and the expected accuracy of the UPDs

was made. Subsequently a detailed description of the estimation of the UPDs, which is the centerpiece of the PPP Post software, was given. The realized approach allows for the estimation of satellite-specific wide-lane WL and narrow-lane NL UPDs by satellite-to-satellite single difference (SD) observations of a regional station network. Using SD observations requires the determination of a reference satellite, which takes place according to a simple procedure. The estimation of the UPDs is carried out separately. In the first step the WL UPDs are estimated by means of the MW linear combination. Following this the estimation of the NL UPDs takes place which are calculated by subtracting fixed WL ambiguities from IF float ambiguities. The IF float ambiguities are obtained from the PPP solutions of the station network. The WL ambiguities can be fixed with the help of the previously estimated WL UPDs. Finally the PPP Post software has been utilized to investigate the influence of the satellite orbits and clock corrections on the estimation of the UPDs. These investigations were divided into two major parts.

7.1 Discussion of the influence of satellite orbit and clock corrections on the estimation of WL and NL UPDs

The investigations, which have been carried out in the context of this thesis are basically concentrated on two main points. The first one is the influence of the accuracy and availability of satellite orbits and clock corrections on the stability and availability of UPDs. The second one is the impact of specific errors in the satellite orbits and clock corrections on the UPD estimation process and their effect on the numerical results of the UPDs. Last but not it has been investigated, if and to which extent errors can be compensated by the UPDs.

7.1.1 Stability and availability of the UPDs

For the investigations two weeks of daily observations of a network of carefully selected stations located in Europe have been used. The computation was carried out twice using the precise (IGS solution) as well as the real-time (IGC solution) orbit and clock products from the IGS. Thereafter a rigorous comparison of these two solutions has been made which allowed for drawing a conclusion about the influence of satellite orbits and clock corrections on the stability and availability of WL and NL UPDs.

The comparison of the WL UPDs has shown that their stability is not affected by the accuracy of the satellite orbits and clock corrections. This meets the expectations as the MW combination, which is used for the estimation of the WL UPDs, is free of geometric errors which also includes the satellite position and clock. Furthermore, it was shown that the WL UPDs of both, the IGS and the IGC solution are very stable. The reason for the high stability of the WL UPDs is the large wavelength of the WL linear combination, which is insensitive to mismodelings of small errors. The variations between the daily solutions are in the range of a couple of centimeters. This is the reason why they can be considered as constant over such periods. However, this is not true

for longer periods, since small drifts in the range of up to 10 cm per week have been observed in some cases. Furthermore, it was shown that the availability of the WL UPDs correlates with the availability of the orbit and clock correction product. However, this correlation is caused by the functional design of the PPP Post software, as it would be possible to estimate the WL UPDs without information on the satellite orbit and clock corrections.

Contrary to the WL UPDs, using the real-time IGS orbit and clock corrections led to a degradation of the SD PPP solutions. Compared to the IGS solution the systematic offset in the ZTD estimates increased about 2 mm and the accuracy of the ZTD estimates decreased about 1 cm. Furthermore, a constant offset of 0.11 m and 0.11 cm was introduced to the code and phase residuals, respectively. In addition to that the stability of the NL UPDs have been affected as well. However, there are only minimal differences between the short-term stability of the IGS and the IGC solution even though the IGC clock corrections are less accurate than the IGS corrections. The reason for this is that the IF ambiguities, which are used for the estimation of the NL UPDs, are estimated as constant parameters within the PPP solutions. This damps the influence of the satellite orbits and clock corrections. With regard to the stability itself, it was shown that the NL UPDs are very stable within one satellite pair pass. However, this does not apply to the long-term stability, where differences of several centimeters between consecutive NL UPD estimates have been shown. These differences are probably caused by remaining errors like errors introduced by satellite orbit and clocks as well as the mapping function. However it was not possible to determine the origin of this effect. Even though the accuracy of the IGS and IGC product has no significant influence on the stability of the UPDs great differences between the numerical results of the NL UPDs of both solutions were observed. These differences are caused by differences between the orbit and clock corrections of the IGS and IGC solution. As a consequence, a successful ambiguity fixed PPP solution can only be achieved by the user in the field if NL UPDs are used together with consistent satellite orbits and clock corrections already used for their generation. This also applies for all other errors which are taken into account in the estimation process. Concerning the availability, it was shown that an estimation of the NL UPDs is only possible, if the corresponding satellite orbits and clock corrections are available. This means that the availability of the NL UPDs correlates with the availability of the orbit and clock correction product.

7.1.2 Impact on the estimation and the numerical results of the NL UPDs

The influence of satellite orbit and clock correction errors was studied in two steps. The first one concentrated on outages of the NL UPD solution which was estimated based on the IGC satellite orbits and clock corrections. It was shown that these outages are caused by jumps in the satellite clock corrections. Furthermore, it was shown that this is especially critical, if such jumps affect the reference satellite. In such a case an estimation of the NL UPDs is not possible at all. The second investigation concentrated on the propagation of satellite orbit and clock errors on the numerical results of the UPDs. Furthermore, it was determined if and to which extent it is possible to compensate these errors by means of the NL UPDs. Therefore, satellite orbit errors

in along track, cross track and radial direction as well as three different types of clock correction errors were introduced to the IGS product. This modified product was used for the estimation of a third set of NL UPDs (IGE solution). By means of a comparison of the NL UPDs and the interim results of the IGS and IGE solution, the impact of the errors was investigated. It was shown that the effects on the errors strongly depend on the type. An error, which introduces a common offset in the phase ranges can easily be compensated and has no considerable effect on the estimation of the NL UPDs. Contrary to that, the effect of errors, which introduce jumps in the phase ranges, strongly depends on the magnitude of the jumps. If a certain threshold is exceeded an estimation of the corresponding NL UPD is not possible at all, as the corresponding observation will be detected as an outlier. The effect of errors which introduce a drift in the phase ranges strongly depend on the drift rate. While small drifts can easily be compensated, large drifts lead to outages in the estimation process. Thereby the frequency of these losses increases with higher drift rates. With respect to errors in the satellite orbits, another effect was observed. It was shown that the effect of satellite orbit errors varies depending on the position of the station and the satellite. This means that the effect on the phase ranges varies from station to station and changes over time. Depending on the differences between the phase ranges, the estimation of the NL UPDs is exacerbated, with a successful estimation not being possible in the worst case.

7.2 Outlook

The presented thesis has shown that the satellite orbits and clock corrections hardly affect the estimation of the WL UPDs, while they play an important role in the estimation of the NL UPDs. This is especially true for possible applications in real-time, when only real-time orbit and clock corrections are available. While satellite orbits and clock corrections of poor accuracy have no considerable effect on the estimation of the UPDs, possible errors in the satellite orbits and clock corrections can lead to substantial problems. It was shown that errors in the satellite orbits and clock corrections are especially critical, if they affect the reference satellite, which is a serious disadvantage of using SD observations. A possible solution to overcome this problem would be an algorithm for the detection and correction of such errors which prevent the estimation of the NL UPDs.

The current status of the PPP Post software does not allow for a continuous estimation of the UPDs as only regional reference station networks can be used. However a continuous estimation of the UPDs would be especially interesting with respect to the long-term stability of the NL UPDs. Furthermore, it would also allow for a more detailed analysis of the errors, which affect the estimation. So a future task, especially supporting the investigations of the UPDs, could be to extend the software for the use of global reference station networks.

The most recent and probably also most interesting and challenging aspect concerning the estimation of UPDs are the modernization of the current GNSS as well as the upcoming new GNSS, which will provide new signals on additional frequencies. The presented approach is

limited to the dual frequency case, as it relies on a specific linear combination. In case of a third frequency, there are a lot of possible combinations in addition to that. This is tricky, as it is desired that the UPDs should be used to keep the integer nature of the phase ambiguities of every linear combination, which is especially critical for linear combinations that were not used in the estimation of the UPDs. A simple solution would be the identification of an additional UPD using a linear combination, which includes the third frequency (Laurichesse (2016)).

With respect to the realization of an operational service, the presented approach has a significant drawback. The current method relies on the estimation of UPDs for specific linear combinations. Thus the user side must implement the same method for the application of the UPDs as the one on the server side used for the estimation. This is especially critical for a standardization of the bias messages and also for the implementation of new signals due to additional frequencies as discussed before. Under consideration of these problems, the RTCM Special Committee 104 SSR working group for phase bias messages proposed a model, which is based on the idea that the UPDs are inherent to their respective frequencies. This means that, instead of UPDs related to specific linear combinations, one UPD per phase observable needs to be identified (Laurichesse (2016)).

Appendix A

GPS satellites coordinates and clock correction computation

Table 5.1 provides the GPS broadcast ephemerides to compute the satellite positions and clock corrections using the algorithm provided by the DoD (1995). The satellite coordinates at the epoch t can be computed according to the following algorithm.

Computation of the time difference t_k to the ephemerides reference epoch t_e expressed in seconds of the GPS week:

$$t_k = t - t_e \quad (7.1)$$

If $t_k > 302400$ sec, subtract 604800 sec from t_k . If $t_k < -302400$ sec, add 604800 sec. Computation of the mean anomaly for t :

$$M = M_0 + \left(\frac{\sqrt{\mu}}{\sqrt{a^3}} + \Delta n \right) t. \quad (7.2)$$

Solving (iteratively) the Kepler equation for the eccentric anomaly E :

$$M = E - e \cdot \sin(E). \quad (7.3)$$

Computation of the true anomaly ν :

$$\nu = \arctan \left(\frac{\sqrt{1-e^2} \sin(E)}{\cos(E) - e} \right). \quad (7.4)$$

Computation of the argument of latitude u from the argument of perigee ω , true anomaly ν and corrections C_{uc} and C_{us} :

$$u = \omega + \nu + C_{uc} \cdot \cos 2(\omega + \nu) + C_{us} \cdot \sin 2(\omega + \nu). \quad (7.5)$$

Computation of the radial distance r , considering the corrections C_{rc} and C_{rs} :

$$r = a(1 - e \cdot \cos(E)) + C_{rc} \cdot \cos 2(\omega + \nu) + C_{rs} \cdot \sin 2(\omega + \nu). \quad (7.6)$$

Computation of the inclination i of the orbital plane from the inclination i_0 , considering the

corrections C_{ic} and C_{is} :

$$i = i_o + \dot{i}t + C_{ic} \cdot \cos 2(\omega + \nu) + C_{is} \cdot \cos 2(\omega + \nu). \quad (7.7)$$

Computation of the longitude of the ascending node λ according to:

$$\lambda = \Omega_0 + (\dot{\Omega} - \omega) \cdot t - \omega \cdot t_e. \quad (7.8)$$

Computation of the coordinates in the TRS system, by applying three rotations:

$$\begin{bmatrix} X \\ Y \\ Z \end{bmatrix} = R_3(-\lambda) \cdot R_1(-i) \cdot R_3(-u) \cdot \begin{bmatrix} r \\ 0 \\ 0 \end{bmatrix}. \quad (7.9)$$

The individual satellite clock t_{sv} is corrected to GPS time t according to:

$$t = t_{sv} - \Delta t_{sv} \quad (7.10)$$

where

$$\Delta t_{sv} = a_0 + a_1(t - t_e) + a_2(t - t_e)^2. \quad (7.11)$$

Bibliography

- N. Ashby (2003). 'Relativity in the Global Positioning System'. *Living Rev. Relativity* **6**. Online; accessed 23 March 2016.
- J. Böhm, et al. (2009). 'Forecast Vienna Mapping Functions 1 for real-time analysis of space geodetic observations'. *Journal of Geodesy* **86(5)**:397–401.
- J. Böhm & H. Schuh (2013). *Atmospheric Effects in Space Geodesy*. Springer.
- G. Blewitt (1990). 'An automatic editing Algorithms for GPS data'. *Geophysical Research Letters* **17(3)**:199–202.
- M. Caissy, et al. (2012). 'The International GNSS Real-Time Service'. <http://gpsworld.com/gnss-systemaugmentation-assistanceinnovation-coming-soon-13044/>.
- P. Collins, et al. (2010). 'Undifferenced GPS Ambiguity Resolution Using the Decoupled Clock Model and Ambiguity Datum Fixing'. *Journal of the Institute of Navigation* **57(2)**.
- U. DoD (1995). *Global Positioning System Standard Positioning Service Performance Standard*. 2 edn.
- M. Ge, et al. (2008). 'Resolution of GPS carrier-phase ambiguities in precise point positioning (PPP) with daily observations'. *Journal of Geodesy* **82**:389–399.
- J. Geng, et al. (2010). 'Integer ambiguity resolution in precise point positioning: method comparison'. *Journal of Geodesy* **84**:569–581.
- Gov. GPS (2015). 'Official U.S. Government information about the Global Positioning System (GPS) and related topics'. www.gps.gov. Online; accessed 20 December 2015.
- W. Gurtner & L. Estey (2007). *RINEX: The Receiver Independent Exchange Format Version 2.11*. Astronomical Institute, University of Berne and UNAVCO, Boulder, Co.
- W. Gurtner & L. Estey (2009). *RINEX: The Receiver Independent Exchange Format Version 3.01*. Astronomical Institute, University of Berne and UNAVCO, Boulder, Co.
- F. Hinterberger, et al. (2015). 'Ambiguity fixing in real-time PPP - Determination of uncalibrated phase delays using a regional network'. *Österreichische Zeitschrift für Vermessung und Geoinformation (VGI)* **1**:130 – 137.

- B. Hofmann-Wellenhof, et al. (2008). *GNSS Global Navigation Satellite Systems. GPS, GLONASS, Galileo and more*. SpringerWienNewYork, 1 edn.
- K. Huber (2015). *Precise Point Positioning with Ambiguity Resolution for real-time Applications*. Ph.D. thesis, Technische Universität Graz.
- K. Huber, et al. (2014). 'Real-time PPP with Ambiguity Resolution - Determination and Application of Uncalibrated Phase Delays'. *Proceedings of the 27th International Technical Meeting of the Satellite Division of the Institute of Navigation* 1:976 – 985.
- IERS Conventions (2010). 'G. Petit and B. Luzum (eds.)'. IERS Technical Note; 36, Frankfurt am Main: Verlag des Bundesamtes für Kartographie und Geodäsie.
- IGS (2002). 'Towards Real-Time Network, Data, and Analysis Centre 2002 Workshop'. *Proceedings, Ottawa, Canada, April 8-11 2002* .
- IGS (2015). 'Main Page — IGS'. <http://www.igs.org/>. Online; accessed 20 December 2015.
- A. Karabatić (2011). *Precise Point Positioning (PPP) - an alternative technique for ground based GNSS troposphere monitoring*. Ph.D. thesis, Faculty of Mathematics and Geoinformation, Vienna University of Technology,.
- J. Kouba (2009). 'A guide to using International GNSS Service (IGS) products'. <http://igs.cb.jpl.nasa.gov/components/usage.html> .
- J. Kouba & P. Héroux (2001). 'Precise Point Positioning Using IGS Orbit and Clock Products'. *GPS Solutions* 5(2):12–28.
- D. Laurichesse (2016). 'Handling the Biases for Improved Triple-Frequency PPP Convergence'. <http://gpsworld.com/innovation-carrier-phase-ambiguity-resolution/> .
- D. Laurichesse, et al. (2009). 'Integer Ambiguity Resolution on Undifferenced GPS Phase Measurements and its Application to PPP and Satellite Precise Orbit Determination'. *Journal of the Institute of Navigation* 56(2).
- L. Mervart (1995). *Ambiguity Resolution Techniques in Geodetic and Geodynamic Applications of the Global Positioning System*. Ph.D. thesis, University of Bern, Philosophisch-naturwissenschaftlichen Fakultät.
- Natural Resources Canada (2015). 'CSRS-PPP Canadian Spatial Reference System' Online; accessed 4-December-2015.
- Navipedia (2013). 'Main Page — Navipedia'. http://www.navipedia.net/index.php?title=Main_Page&oldid=12478. Online, accessed 10 January 2016.
- A. Niell (1996). 'Global mapping functions for the atmosphere delay at radio wavelengths'. *Journal of Geophysical Research* (101):3227–3246.

- R. S. Radovanovic (2002). *Adjustment of Satellite-Based Ranging Observations for Precise Positioning and Deformation Monitoring*. Ph.D. thesis, University of Calgary, Department of Geomatic Engineering.
- C. Rizos (2008). "The Research Challenges of IAG Commission 4 "Positioning & Applications"". *International Association of Geodesy Symposia* **132**:126–132.
- RTCM Special Committee No. 104 (2011). *RTCM 10410.1 Standard for Networked Transport of RTCM via Internet Protocol (Ntrip) - Version 2.0 with Amendment 1*. Radio Technical Commission for Maritime Services, 1611 N. Kent Str., Suite 605, Arlington, Virginia 22209-2134, U.S.A.
- RTCM Special Committee No. 104 (2013). *RTCM 10403.2, Differential GNSS (Global Navigation Satellite Systems) Services - Version 3*. Radio Technical Commission for Maritime Services, 1611 N. Kent Str., Suite 605, Arlington, Virginia 22209-2134, U.S.A.
- S. Schaer & P. Steigenberger (2006). 'Determination and use of GPS Differential Code Bias Values'. IGS Workshop 2006, Darmstadt, Germany.
- H. Schildt (2004). *C++ Die professionelle Referenz*. mitp, 4 edn.
- G. Seeber (2003). *Satellite Geodesy*. Walter de Gruyter & Co., 2 edn.
- J. Shi & Y. Gao (2014). 'A comparison of three PPP integer ambiguity resolution methods'. *GPS Solutions* **18**:519–528.
- J. S. Subirana, et al. (2013). *Global Navigation Satellite Systems: Volume I: Fundamentals and Algorithms*. ESA Communications.
- G. Thaler (2011). *Echtzeit Bahn- und Uhrenberechnung der GPS-Satellitenkonstellation basierend auf Echtzeit-Beobachtungsdaten des RTIGS-Stationsnetzwerks*. Ph.D. thesis, Vienna University of Technology.
- University of New Brunswick (2015). 'GAPS GPS Analysis And Positioning Software'. <http://gaps.gge.unb.ca/index.html>. Online, accessed 4 December 2015.
- G. Weber & L. Mervart (2014). *BKG Ntrip Client (BNC), Version 2.11.0, Manual*. Federal Agency for Cartography and Geodesy and Czech Technical University.
- J. Wu, et al. (1993). 'Effects of Antenna Orientation on GPS Carrier Phase Measurements'. *Manuscripta Geodaetica* **18**:91–98.
- G. Xu (2003). *GPS Theory, Algorithms and Applications*. Springer.
- J. Zumberge, et al. (1997). 'Precise point positioning for the efficient and robust analysis of GPS data from large networks'. *Journal of Geophysical Research* **102**:5005–5017.

LEBENS LAUF

ZUR PERSON



DIPL. ING. FABIAN HINTERBERGER

fabian.hinterberger@gmail.com

Geburtsdatum 10. APRIL 1984
Geburtsort LINZ
Staatsangehörigkeit ÖSTERREICH

BERUFSERFAHRUNG

- DERZEIT / SEIT APRIL 2010 **PROJEKASSISTENT**
TU Wien, Department für Geodäsie und Geoinformation, Forschungsgruppe Höhere Geodäsie
- Technischer Assistent bei Drittmittelprojekten (Schwerpunkt GNSS/RTK und Navigation)
 - Softwareentwicklung (Matlab, C, C++)
 - Betreuung von Vorlesungen und Übungen
- SEPTEMBER 2013 **AUSLANDSAUFENTHALT**
BIS OKTOBER 2013 GFZ Potsdam, Department für Geodäsie
- Wissenschaftliche Vertiefung für die Dissertation
- OKTOBER 2008 **TECHNISCHER MITARBEITER**
BIS JUNI 2009 Vermessung Reichhart
- Vermessung im Außendienst
 - Technische Tätigkeiten im Büro

SCHUL- UND BERUFSBILDUNG / PRÄSENZDIENST

- MÄRZ 2011 **DOKTORATSTUDIUM**
BIS NOVEMBER 2016 TU Wien, Arbeitstitel: „Einfluss von GPS Satellitenorbits und Satellitenuhrkorrekturen auf die Berechnung von einfach differenzierten unkalibrierten Phasenverzögerungen“
- März 2010 **GRADUIERUNG ZUM DIPL. ING.**
TU Wien, Arbeitstitel: „Automatisierte Berücksichtigung von Netzspannungen und Geoidundulationen in der RTK-Vermessung“
- OKTOBER 2003 **STUDIUM FÜR GEODÄSIE UND GEOPHYSIK**
BIS MÄRZ 2016 TU Wien
- 2002 BIS 2003 **ZIVILDienst**
ST. PIUSHEIM / PEUERBACH
- 1994 BIS 2002 **AHS**
BRG, Fadingerstraße, Linz

GEOWISSENSCHAFTLICHE MITTEILUNGEN

Bisher erschienen:

- Heft 1 Kolloquium der Assistenten der Studienrichtung Vermessungswesen. 1970 - 1973, Dezember 1973.
- Heft 2 EGGER-PERDICH-PLACH-WAGENSOMMERER, Taschenrechner HP 45 und HP 65, Programme und Anwendungen im Vermessungswesen. 1. Auflage, März 1974, Special Edition in English, Juli 1974, 2. verbesserte Auflage, November 1974.
- Heft 3 Kolloquium der Assistenten der Studienrichtung Vermessungswesen 1973 - 1974, September 1974.
- Heft 4 EGGER-PALFINGER-PERDICH-PLACH-WAGENSOMMERER, Tektronix-Tischrechner TEK 31, Programmbibliothek für den Einsatz im Vermessungswesen, November 1974.
- Heft 5 K. LEDERSTEGGER, Die horizontale Isostasie und das isostatische Geoid, Februar 1975.
- Heft 6 F. REINHART, Katalog von FK4 Horrebow-Paaren für Breiten von +30 bis +60, Oktober 1975.
- Heft 7 Arbeiten aus dem Institut für Höhere Geodäsie, Wien, Dezember 1975.
- Heft 8 Veröffentlichungen des Instituts für Photogrammetrie zum XIII. Internationalen Kongreß für Photogrammetrie in Helsinki 1976, Wien, Juli 1976.
- Heft 9 W. PILLEWIZER, Felsdarstellung aus Orthophotos, Wien, Juni 1976.
- Heft 10 PERDICH-PLACH-WAGENSOMMERER, Der Einsatz des programmierbaren Taschenrechners Texas Instruments SR-52 mit Drucker PC100 in ingenieurgeodätischen Rechen-technik, Wien, Mai 1976.
- Heft 11 Kolloquium der Assistenten der Studienrichtung Vermessungswesen 1974 - 1976, November 1976.
- Heft 12 Kartographische Vorträge der Geodätischen Informationstage 1976, Wien, Mai 1977.
- Heft 13 Veröffentlichung des Instituts für Photogrammetrie anlässlich des 80. Geburtstages von Prof. Dr.h.c. K. Neumaier, Wien, Januar 1978.
- Heft 14 L. MOLNAR, Self Checking Analytical Relative Orientation and Strip Formation, Wien, Dezember 1978.
- Heft 15 Veröffentlichung des Instituts für Landesvermessung anlässlich des 80. Geburtstages von Prof. Dr. Alois Bavir, Wien, Januar 1979.
- Heft 16 Kolloquium der Assistenten der Studienrichtung Vermessungswesen 1976 - 1978, Wien, November 1979.
- Heft 17 E. VOZIKIS, Die photographische Differentialumbildung gekrümmter Flächen mit Beispielen aus der Architekturbildmessung, Wien, Dezember 1979.
- Heft 18 Veröffentlichung des Instituts für Allgemeine Geodäsie anlässlich des 75. Geburtstages von Prof. Dipl.-Ing. Dr. F. Hauer, Die Höhe des Großglockners, Wien, 1981.
- Heft 19 H. KAGER, Bündeltriangulation mit indirekt beobachteten Kreiszentren, Wien, April 1981.

- Heft 20 Kartographische Vorträge der Geodätischen Informationstage 1980, Wien, Mai 1982.
- Heft 21 Veröffentlichung des Instituts für Kartographie anlässlich des 70. Geburtstages von Prof. Dr. Wolfgang Pillewizer: Glaziologie und Kartographie, Wien, Dezember 1982.
- Heft 22 K. TEMPFLI, Genauigkeitsschätzung digitaler Höhenmodelle mittels Spektralanalyse, Wien, Mai 1982.
- Heft 23 E. CSAPLOVICS, Interpretation von Farbinfrarotbildern, Wien, November 1982.
- Heft 24 J. JANSKA, Rektifizierung von Multispektral-Scanneraufnahmen - Entwicklung und Erprobung eines EDV-Programms, Wien, Mai 1983.
- Heft 25 Zusammenfassung der Diplomarbeiten, Dissertationen und Habilitationen an den geodätischen Instituten der TU Wien, Wien, November 1984.
- Heft 26 T. WUNDERLICH, Die voraussetzungsfree Bestimmung von Refraktionswinkeln, Wien, August 1985.
- Heft 27 G. GERSTBACH (Hrsg.), Geowissenschaftliche/geotechnische Daten in Landinformationssystemen - Bedarf und Möglichkeiten in Österreich, Juni 1986.
- Heft 28 K. NOVAK, Orientierung von Amateuraufnahmen ohne Paßpunkte, Wien, August 1986.
- Heft 29 Veröffentlichung des Instituts für Landesvermessung und Ingenieurgeodäsie, Abt. Ingenieurgeodäsie, anlässlich des 80. Geburtstages von Prof. Dipl.-Ing. Dr. F. Hauer, Wien, Oktober 1986.
- Heft 30 K.-H. ROCH, Über die Bedeutung dynamisch ermittelter Parameter für die Bestimmung von Gesteins- und Gebirgseigenschaften, Wien, Februar 1987.
- Heft 31 G. HE, Bildverbesserung mittels digitaler Filterung, Wien, April 1989.
- Heft 32 F. SCHLÖGELHOFER, Qualitäts- und Wirtschaftlichkeitsmodelle für die Ingenieurphotogrammetrie, Wien, April 1989.
- Heft 33 G. GERSTBACH (Hrsg.), Geowissenschaftliche/geotechnische Daten in Landinformationssystemen - Datenbestände und Datenaustausch in Österreich, Wien, Juni 1989.
- Heft 34 F. HOCHSTÖGER, Ein Beitrag zur Anwendung und Visualisierung digitaler Geländemodelle, Wien, Dezember 1989.
- Heft 35 R. WEBER, Lokale Schwerefeldmodellierung unter Berücksichtigung spektraler Methoden zur Geländereduktion, Wien, April 1990.
- Heft 36 o.Prof. Dr. Hans Schmid zum 70. Geburtstag. Veröffentlichung der Abteilung für Landesvermessung, Wien, Oktober 1990.
- Heft 37 G. GERSTBACH, H. P. HÖLLRIEGL und R. WEBER, Geowissenschaftliche Informationsbörse - Eine Nachlese zu GeoLIS II, Wien, Oktober 1990.
- Heft 38 R. ECKER, Rastergraphische Visualisierungen mittels digitaler Geländemodelle, Wien, August 1991.

- Heft 39 Kartographische Forschungen und Anwendungsorientierte Entwicklungen, herausgegeben von W. Stams und F. Kelnhofer zum 80. Geburtstag von Prof. Dr. W. Pillewizer, Wien, Juli 1991.
- Heft 39a W. RIEGER, Hydrologische Anwendungen des digitalen Geländemodelles, Wien, Juli 1992.
- Heft 40 K. STEINNOCHER, Methodische Erweiterungen der Landnutzungsklassifikation und Implementierung auf einem Transputernetzwerk, Wien, Juli 1994.
- Heft 41 G. FORKERT, Die Lösung photogrammetrischer Orientierungs- und Rekonstruktionsaufgaben mittels allgemeiner kurvenförmiger Elemente, Wien, Juli 1994.
- Heft 42 M. SCHÖNER, W. SCHÖNER, Photogrammetrische und glaziologische Untersuchungen am Gäsbre (Ergebnisse der Spitzbergenexpedition 1991), Wien, Mai 1996.
- Heft 43 M. ROIC. Erfassung von nicht signalisierten 3D-Strukturen mit Videotheodoliten, Wien, April 1996.
- Heft 44 G. RETSCHER, 3D-Gleiserfassung mit einem Multisensorsystem und linearen Filterverfahren, Wien, April 1996.
- Heft 45 W. DAXINGER, Astrogravimetrische Geoidbestimmung für Ingenieurprojekte, Wien, Juli 1996.
- Heft 46 M. PLONER, CCD-Astrometrie von Objekten des geostationären Ringes, Wien, November 1996.
- Heft 47 Zum Gedenken an Karl Killian "Ingenieur" und "Geodät" 1903-1991, Veröffentlichung der Fachgruppe Geowissenschaften, Wien, Februar 1997.
- Heft 48 A. SINDHUBER, Ergänzung und Fortführung eines digitalen Landschaftsmodelles mit multispektralen und hochauflösenden Fernerkundungsaufnahmen, Wien, Mai 1998.
- Heft 49 W. WAGNER, Soil Moisture Retrieval from ERS Scatterometer Data, Wien, Dezember 1998.
- Heft 50 R. WEBER, E. FRAGNER (Editoren), Prof. Bretterbauer, Festschrift zum 70. Geburtstag, Wien, Juli 1999.
- Heft 51 Ch. ÖHRENER, A Similarity Measure for Global Image Matching Based on The Forward Modeling Principle, Wien, April 1999.
- Heft 52 M. LECHTHALER, G. GARTNER, Per Aspera ad Astra, Festschrift für Fritz Kelnhofer zum 60. Geburtstag, Wien, Jänner 2000.
- Heft 53 F. KELNHOFER, M. LECHTHALER, Interaktive Karten (Atlanten) und Multimedia – Applikationen, Wien, März 2000.
- Heft 54 A. MISCHKE, Entwicklung eines Videotheodlit-Meßsystems zur automatischen Richtungsmessung von nicht signalisierten Objektpunkten, Wien, Mai 2000.
- Heft 55 Veröffentlichung des I.P.F. anlässlich der Emeritierung von Prof. Dr. Peter Waldhäusl, Wien.
- Heft 56 F. ROTTENSTEINER, Semi-automatic Extraction of Buildings Based on Hybrid Adjustment Using 3D Surface Models and Management of Building Data in a TIS, Wien, Juni 2001.

- Heft 57 D. LEGENSTEIN, Objektrekonstruktion aus perspektiven Bildern unter Einbeziehung von Umrisslinien, Wien, Mai 2001.
- Heft 58 F. KELNHOFER, M. LECHTHALER und K. BRUNNER (Hrsg.), Telekartographie und Location Based Services, Wien, Jänner 2002.
- Heft 59 K. BRETTERBAUER, Die runde Erde eben dargestellt: Abbildungslehre und sphärische Kartennetzentwürfe, Wien, 2002.
- Heft 60 G. GARTNER, Maps and the Internet 2002, Wien 2002.
- Heft 61 L. DORFFNER, Erzeugung von qualitativ hochwertigen 3D Photomodellen für Internetbasierte Anwendungen mit besonderem Augenmerk auf Objekte der Nahbereichsphotogrammetrie, Wien, Jänner 2002.
- Heft 62 K. CHMELINA, Wissensbasierte Analyse von Verschiebungsdaten im Tunnelbau, Wien 2002.
- Heft 63 A. NIESSNER, Qualitative Deformationsanalyse unter Ausnutzung der Farbinformation, Wien 2002.
- Heft 64 K. BRETTERBAUER, R. WEBER, A Primer of Geodesy for GIS-Users, Wien 2003.
- Heft 65 N. PFEIFER, 3D Terrain Models on the basis of a triangulation, Wien, Jänner 2002.
- Heft 66 G. GARTNER (Hrsg), Location Based Services & Telecartography, Wien 2004.
- Heft 67 I. KABASHI, Gleichzeitig-gegenseitige Zenitwinkelmessung über größere Entfernungen mit automatischen Zielsystemen, Wien 2004.
- Heft 68 J. BÖHM, Troposphärische Laufzeitverzögerungen in der VLBI, Wien 2004.
- Heft 69 R. WEBER, W. SCHLÜTER, U. SCHREIBER, O. TITOV Evolving Space Geodesy Techniques (EGS XXVII General Assembly, Nice, France, 2002), Wien 2004.
- Heft 70 G. WEINWURM, Amalthea's Gravity Field and its Impact on a Spacecraft Trajectory, Wien 2004.
- Heft 71 Forschungsgruppe Ingenieurgeodäsie, Festschrift anlässlich des 65. Geburtstages von Herrn o.Univ. Prof. Dr.-Ing. Heribert Kahmen, Wien 2005.
- Heft 72 A. REITERER, A Knowledge-Based Decision System for an On-Line Video-Theodolite-Based Multisensor System, Wien 2005.
- Heft 73 M. HABERLER, Einsatz von Fuzzy Methoden zur Detektion konsistenter Punktbewegungen, Wien 2005.
- Heft 74 G. GARTNER, Location Based Services & Telecartography, Proceedings of the Symposium 2005, Wien 2005.
- Heft 75 Th. HOBIGER, VLBI as a tool to probe the ionosphere, Wien 2006.
- Heft 76 E. KLAFFENBÖCK, Troposphärische Laufzeitverzögerung von GNSS-Signalen – Nutzen aktiver Referenzstationsnetze für die Meteorologie, Wien 2006.
- Heft 76a P. J. MENDES-CERVEIRA, Tidal and non-tidal contributions to surface loading processes on station coordinates, Wien 2006.

- Heft 78 G. KOSTOV, G. BOURDA, L. FERNANDEZ, T. KONDO, Research Projects at IGG Reports, Wien 2007.
- Heft 79 J. BÖHM, A. PANY, H. SCHUH (Editors), Proceedings of the 18th European VLBI for Geodesy and Astrometry Working Meeting, 12-13 April 2007, Wien 2007.
- Heft 80 J. BÖHM, Tropospheric Delay Modelling at Radio Wavelengths for Space Geodetic Techniques, Wien 2007.
- Heft 81 G. Retscher, Mobile Multi-sensor Systems for Personal Navigation and Location-based Services, Wien 2007.
- Heft 82 R. HEINKELMANN, Bestimmung des atmosphärischen Wasserdampfes mittels VLBI als Beitrag zur Klimaforschung, Wien 2008.
- Heft 83 F. ROTTENSTEINER, Automatic extraction of buildings from airborne laserscanner data and aerial images, Wien 2008.
- Heft 84 S. TODOROVA, Kombination geodätischer Weltraumverfahren für globale Karten der Ionosphäre, Wien 2009.
- Heft 85 J. WRESNIK, Simulationen für die neue Generation von VLBI-Systemen, Wien 2009.
- Heft 86 A. KARABATIC, Precise Point Positioning (PPP). An alternative technique for ground based GNSS troposphere monitoring, Wien 2011.
- Heft 87 K. TEKE, Sub-daily Parameter Estimation in VLBI Data Analysis, Wien 2011.
- Heft 88 G. THALER, Echtzeit Bahn- und Uhrberechnung der GPS-Satellitenkonstellation basierend auf Beobachtungsdaten des RTIGS-Stationsnetzwerkes, Wien.
- Heft 89 P. SWATSCHINA, Dynamic and Reduced-Dynamic Precise Orbit Determination of Satellites in Low Earth Orbits, Wien 2012.
- Heft 90 S. BÖHM, Tidal excitation of Earth rotation observed by VLBI and GNSS, Wien 2012.
- Heft 91 H. KRÁSNÁ, Estimation of solid Earth tidal parameters and FCN with VLBI, Wien 2013.
- Heft 92 J. SUN, VLBI scheduling strategies with respect to VLBI2010, Wien 2013.
- Heft 93 M.M. ALIZADEH ELIZEI, Multi-Dimensional modeling of the ionospheric parameters, using space geodetic techniques, Wien 2013.
- Heft 94 M. KARBON, Atmospheric effects on measurements of the Earth gravity field, Wien 2013.
- Heft 95 L. PLANK, VLBI satellite tracking for the realization of frame ties, Wien 2014.
- Heft 96 M. SCHINDELEGGGER, Atmosphere-induced short period variations of Earth rotation, Wien 2014.
- Heft 97 M. MADZAK, Short period ocean tidal variations in Earth rotation, Wien 2016.
- Heft 98 A. HOFMEISTER, Determination of path delays in the atmosphere for geodetic VLBI by means of ray-tracing, Wien 2016.
- Heft 99 F. HINTERBERGER, Influence of GPS satellite orbits and clock corrections on the estimation of single difference uncalibrated phase delays, Wien 2016.